University of Milano-Bicocca
Department Biotechnology and Biosciences
PhD program in Converging Technologies for Biomolecular Systems (TeCSBI) Cycle XXXIV

Multifunctional three-dimensional hydrogel architectures for biomedical applications

Sofia Magli
Matr. 767377

Tutor: Prof. Francesco Nicotra
Supervisor: Laura Russo

Anno Accademico 2020-2021

SCUOLA DI DOTTORATO

UNIVERSITÀ DEGLI STUDI MILANO-BICOCCA

Department of Biotechnology and Biosciences

PhD program in Converging Technologies for Biomolecular Systems

(TeCSBI)

Cycle XXXIV

Multifunctional three-dimensional hydrogel architectures for biomedical applications

Surname: Magli

Name: Sofia

Registration number: 767377

Tutor: Prof. Francesco Nicotra

Supervisor: Dr. Laura Russo

Coordinator: Prof. Paola Branduardi

ACADEMIC YEAR 2020/2021

CONTENTS

ABSTRACT

ECM-mimicking biomaterial research has driven numerous advances in tissue engineering in recent years, bringing novelties in polymer chemistry and cell-material interactions. New 3D biomaterial platforms can provide pivotal insights for bioengineering, allowing the investigation of cell fate, drug delivery, or novel translational applications in regenerative medicine. Recently, hydrogels have received a considerable interest as leading candidates for engineered tissue scaffolds due to their unique compositional and structural similarities to the natural extracellular matrix. This research topic aims to implement recent advances in the areas that focus on developing next-generation biomaterials and biotechnologies with controlled material composition, defined structural architectures, dynamic functionality, and biological complexity targeted toward various applications in regenerative engineering and translational medicine.

In this thesis the functionalization of gelatin and chitosan with methylfuran is reported. The obtained polymers were combined with a maleimide PEG through Diels-Alder reaction, formulating GelChiDA (GELatin, CHitosan, Diels-Alder), an enhanced 3D hybrid hydrogel platform. The click chemistry-based hydrogel is formed spontaneously by mixing reactive compounds, and occurs in mild conditions without further purifications, catalysts or UV irradiation. The starting materials and the resulting hybrid biomaterial were characterized in terms of physical-chemical properties. The proposed analytical strategy guarantees a global view of the complex biomaterials properties and

can be applied to characterize all platforms of this nature. GelChiDA showed interesting rheological properties, including self-healing characteristics and promising preliminary biocompatibility tests. GelChiDa was formulized as bioink to be used with pneumatic 3D bioprinters, and the protocol was optimized by assessing the optimal timing to perform bioprinting at low pressure into grid-like structure, without affecting cell viability. Moreover GelChiDA was investigated as construct for *in vitro* tumor model spheroids, proving to be a stable platform for future pharmacological tests as pathological models.

The ability to control the shape, porosity and surface morphology of scaffolds has created new opportunities to overcome various challenges in tissue engineering such as vascularization and complex architecture. In this context, a novel application of Ice Binding Proteins is proposed: the use of these proteins allows to tune the biomaterial according to the endmost need without affecting cellular vitality. Starting from GelChiDA construct, elastin, identified as a potential scaffold that renders extensibility and elasticity to tissues, was included as component to a new hybrid construct. The multimodal three component GELCHEL (GELatin, CHitosan, ELastin) hydrogel conceived and studied in our work, combines the various properties and advantages that each component provides and lends itself to future massive variety of biomedical applications. After chemical and physical deep characterization, GELCHEL hydrogel has been formulated and bioprinted with U87 glioblastoma cell line and cytotoxicity tests highlight a great biocompatibility. Moreover, antibacterial property of chitosan in the construct is maintained in the network, giving a relevant advantage to the platform.

Project perspective is to expand the Diels-Alder based hydrogel library to other materials and composition. The final aim is to create an extensive standardized library of formulations that includes all features that are required and could be used as a versatile material for a wide range of bioapplications.

U87 spheroids were employed as tumor models to evaluate the inhibitory effect of sodium hyaluronate functionalized with matrix metalloproteinases (MMPs) inhibitor molecules. Spheroids were included into the functionalized platform and the specific inhibition of membrane metalloproteins was evaluated by immunofluorescent quantification assay, opening doors to future application in biomedical field.

1. INTRODUCTION

Modern medicine, as scientific discipline based on the experimental method, is the result of continuous progress since the beginning of the last century.[1] Despite the developments and sophistications introduced in the biomedical field, nowadays the replacement of tissues and organs damaged by trauma or diseases still represents a crucial problem. In fact, organ transplantation is confined by the limited availability of donors and incompatibility or rejection problems.[2] To overcome these limitations, the multidisciplinary field of artificial organs or regenerative medicine strategies aim to reproduce functions and structures of human tissues taking inspiration from organs features and tissues micro- and macroenvironments.[3] Artificial organs employed for clinic applications, include a variety of medical devices of different nature and with different functionalities. Animal derived medical devices opportunely modified are currently employed as implantable heart valves subtitutes.[4] Engineered artificial retina or visual devices are used as functional implantable devices displaying different functional and structural features.[5] However, these systems are usually connected to external devices for the functionality control. Other examples that include also extracorporeal implantable devices (i.e. lung, pancreas, heart) with functional properties, still limiting patients' life–style and representing temporary solutions to resolve organ and tissues failure.[6] Thus, we are not still able to replace with artificial

devices the functional complex organs besides substantial simplifications.[3] Globally there are a large number of constraints, often unfortunately not completely known.[7]

In this panorama, great expectations are placed in regenerative medicine and tissue engineering that aim to repair and regenerate tissues and organs damaged from trauma or pathologies, taking advantage of intrinsic self-renewal properties of cells and tissues of human body.[8]

In fact, by increasing the knowledge of how different cell populations and the surrounding acellular components interact within the tissue microenvironments, many researchers are studying new solutions to induce in a controlled way tissue morphogenesis.[9]

1.2 Tissue Engineering

The term Tissue Engineering (TE) was coined by the Washington National Science foundation in the 1987 meeting and today represents a rapidly evolving science with publications that over the years have become more and more numerous and extensive.[10–12]

Tissue engineering was defined by its founders, Prof. Langer and Dr. Vacanti, as follows:

"Tissue engineering is an interdisciplinary science that applies the principles and methods of engineering and biological sciences with the aim of understanding the fundamental relationships between structure and function in healthy and diseased mammalian tissues and to develop biological substituteable to restore, maintain or improve the functions of damaged organs or tissues ". [13]

The main purpose of this new discipline is to recreate various human tissues (epithelial, vascular, nervous, bone, cartilage...) by developing engineered systems that allows the replacement of human damaged tissues ex vivo or in vivo.[3]

It involves the cooperation of many professional figures as it requires several disciplines: the areas concerned are basic sciences, biomaterials science, biotechnologies, bioengineering, regenerative medicine and cell biology. Among these, cell biology assumes significant importance: it is increasingly necessary to study and understand in detail the mechanisms that regulate the growth,

proliferation, differentiation of cells and the methods through which components of the extracellular matrix (ECM) interact and control cellular functions.[14]

The design of these tissues arises through the combined use of materials, cells, biochemical mediators and innovative culture systems through two types of approach:

- *in vitro*: the biomaterial is seeded with the cells and placed in a bioreactor that simulates the biological environment, creating optimal culture conditions for tissue growth. Once completed, the tissue will then be implanted in the patient.[15] *In vitro* tissue engineering approaches make it possible to recapitulate physiological and pathological conditions outside the body; these approaches also enable the development of tissue-on-the-chip and organ-on-the-chip platforms for cell biology studies or drug screening. However, the *in vitro* tissue engineering approach still faces technical and regulatory obstacles prior to in vivo translation. Translational concerns include immune-acceptable cell sources, challenges with off-the-shelf availability and scaling up capability, cost effectiveness, as well as preservation and handling issues.[16] Furthermore, even if the production of tissues able to replicate the damaged structural tissue has been already applied in clinic (i.e. cartilage transplant), the production of functional tissue is still challenging.

- in vivo (tissue guided regeneration): in this approach engineered biomaterials are implanted in damaged tissues taking advantage of

native regenerative potential of human body and inducing *in situ* tissue repair.[17,18] While cells can be transplanted for *in situ* tissue regeneration, *in situ* tissue engineering approaches often focus on the recruitment of endogenous stem cells to the site of injury by using biomaterial or growth factor based cues in order to enhance healing.[19–21] A distinctive feature of *in situ* tissue engineering is that any engineered constructs that are implanted are not functionally mature. In contrast, *in vitro* tissue engineering focuses on the functional development of a tissue prior to implantation. The *in situ* approach has several advantages: *in situ* tissue-engineered products offer improved off-the-shelf availability of the finalized products, because *in situ* tissue engineering often does not involve extensive manipulation of cells and materials outside of the body to create functionalized tissue. Because *in situ* tissue engineering often relies on extracellular components to stimulate native regeneration, this approach offers the opportunity to bypass some (but not all) of the regulatory issues inherent *in vitro* tissue engineering-based approaches.[16]

The fundamental elements for the realization of biological tissues are:

- Cells: the choice of the correct cellular source is a crucial point for the engineering of a tissue. The cells used can be of various type:
    - autologous, taken by the same individual on whom the implant will be performed. This type of cells drastically

reduces the problems of rejection and transmission of diseases

  - allogeneic, coming from a donor of the same species
  - xenogenic, obtained from a donor of another species
  - stem cells: undifferentiated cells that have the ability, as they grow, to divide into specialized cells of various types.

- Scaffold: constitutes the support on which the cells are implanted. It can be natural or synthetic, permanent or biodegradable, but always and necessarily biocompatible with the natural environment in which it will be implanted. Besides the support function, it must allow the adhesion and movement of cells and act as a carrier of biochemical factors (e.g. growth factors) and substances necessary for cell development. The scaffold in tissue engineering is therefore the analogue of the extracellular matrix in the physiological environment.[12]
- Bioreactor: *in vitro* approach need a device designed and built to stimulate cultured cells, and in particular biophysical and mechanical conditions, in order to reproduce in a biomimetic way the environment that regulate the processes of tissue generation and growth in living organisms.[22,23]

1.3 Extracellular Matrix And Cell Environment

In the field of bioengineering and tissue engineering, in addition to the tools and techniques, the materials used are of fundamental importance. Traditional materials are not suitable because, operating in the biological field, particular properties are required. Thus, biomaterials are employed, since they are capable to mimic the extracellular matrix complexity in order to give the right structural support and biochemical signals during 3D cell culturing.[24]

A substantial part of the tissue volume is made up of the extracellular space, largely filled by an intricate network of macromolecules and soluble factors that establish the ECM, where cells live, proliferate and migrate.[25,26] It includes a variety of locally secreted proteins and polysaccharides, which aggregate in a network organized in a compact manner and connected directly to the surface of the cell that produced it.[27]

The relative quantity variations of macromolecules constituting the ECM and the way in which they assemble, give rise to a diversity of morphologies, each adapted to the functional requirements of a different tissue (Figure 1).[28]

Originally it was thought that the ECM of vertebrates performed mainly as a relatively inert scaffold, able to stabilize the physical structure of the tissues. By now, it is widely demonstrated that the matrix plays a much more active and complex role in cells behavior

regulation, influencing their development, migration, proliferation and metabolic function.[29–31]

The ECM has a complex molecular conformation. The three main classes of macromolecules that establish the matrix are fibrous proteins, glycoproteins, proteoglycans.

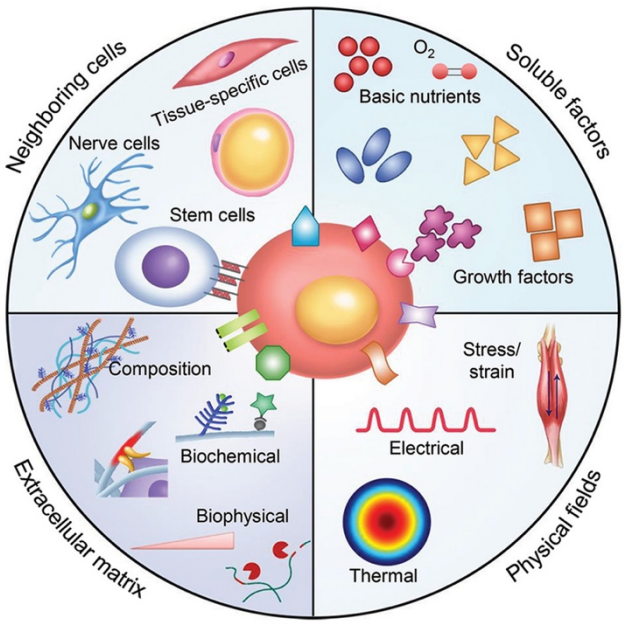

Figure 1: Schematic illustration of the main components of the cell microenvironment. Key components of the cell microenvironment include neighboring cells, soluble factors, the ECM, and biophysical fields (e.g., stress and stain, electrical, and thermal fields). Reprinted (adapted) with permission from Huang at al.[32] Copyright 2017 American Chemical Society.

Among all the fibrous proteins, the main component of the animal extracellular matrix is collagen. It is the most abundant protein in mammals (30% of the protein mass) and sequentially organizes in helices of three chains, fibrils and fibers. Generally, regardless of the collagen types, they provide tensile strength and stiffness, regulate cell

adhesion, support chemotaxis and migration, and direct tissue development.[33,34] Another abundant protein in the extracellular matrix is elastin, which gives elasticity to tissues, such as blood vessels, skin and lung tissue.[35]

Proteoglycans are given by the combination of proteins and glycosaminoglycans (GAGs). GAGs are linear polysaccharide chains formed by repeating disaccharide units, where one is an amino sugar (i.e. N-acetyl glucosamine). The most common GAGs are chondroitin, keratin, and dermatan, which are sulfated, and hyaluronan. Another class, the heparans, are mainly associated with cells and basement membranes.[36] Except for hyaluronan, all GAGs can be associated to a protein backbone and give rise to the proteoglycans, another fundamental component of ECM. Proteoglycans are large macromolecules, weighting millions of Daltons, mainly with the appearance of "bottle brush**",** capable to attract a lot of water, occupying space and giving compressive strength to the matrix.[37] The proteoglycan molecules form a viscous and highly hydrated substance in the connective tissues, where the fibrous proteins are engaged: the polysaccharide gel resists the compressive forces exerted on the matrix, while the collagen fibers ensure tensile strength.

Cells adhere to the extracellularmatrix through interaction with adhesive extracellular matrix glycoproteins, including fibronectin (FN) and laminins.[38] FN exists in two main forms: a soluble form, called plasma FN (pFN), non-reactive with adhesion receptors and present in

the blood, and another insoluble multimeric form, called cellular FN (cFN), highly adhesive. cFN is deposited as fibrils in the ECM by fibroblasts, epithelial cells and other cell types (i.e. chondrocytes, synovial cells and myocytes).[39] Both forms have similar, but not identical precursors, which consist of a dimer of about 450 kDa composed of two identical subunits of 225 kDa, linked by a disulfide bridge. Each subunit contains approximately 2300 amino acids and is highly glycosylated.[40] FN is involved in a wide variety of cellular events, such as cell adhesion, morphology, organization of the cytoskeleton, migration, differentiation, oncogenic transformation, phagocytosis and hemostasis.[41] The polymerization of FN in the ECM is strongly regulated to ensure that the adhesive information in the ECM is appropriate. The adhesive information of the FN is due to the presence, in its amino acid sequence, of particular repeating units of three amino acids, Arg-Gly-Asp (RGD), motif in common with other protein specifically recognized by the integrins.[41,42] Laminins are a family of glycoproteins consisting of homo and heterodimers of α, β and γ chains with molecular weight between 140-400 kDa encoded by eleven genes related to each other and variously combined together to form numerous isoforms.[43,44] From a functional point of view, they are involved in the binding of cells to the basement membrane and have binding domains for integrins, dystroglycans, proteoglycans and other receptors for the maintenance of the phenotype and tissue survival. Laminins regulate cell migration, proliferation and differentiation during embryonic development; they also influence cell adhesion, migration and differentiation in adult life and in numerous pathological conditions.[45,46]

From what has been explained, the importance of the cell-matrix interaction in the regulation of all cellular functions is evident. For this reason, biomaterials science is trying to properly engineer materials to meet the most common needs of biomedical applications. Nowadays, there are a plethora of approaches used for the design of increasingly innovative biomaterials. Until recent past, the only two characteristics that a biomaterial had to possess were biocompatibility (the material must not be cytotoxic or immunogenic) and biodegradability (degradation during ECM remodeling). In the modern meaning of biomaterial, however, among its characteristics, we must consider the ability of the biomaterial to interface with the biological environment and modulate the cellular response in a desired way. Therefore, the biomaterial becomes not only a support for the regeneration of a tissue or a vehicle for the transport of a drug, but an active part in the regulation of cellular functions. In the design of a biomaterial, it is necessary to consider the multiple factors that can influence the cell-material interaction. These parameters represent the chemical characteristics of the material, such as the nature of the material and the presence of biochemical signals, and the physical features, such as the mechanical properties, shape and dimensions.

1.4 3D Cell Cultures

Cell cultures are laboratory methods that allow cells growth under controlled conditions *in vitro*, through the supply of basic nutrients contained in proper culture media. Thanks to artificial environments that allow to regulate temperature, humidity and gas concentration, cells can grow, proliferate, differentiate, migrate, and perform all the various mechanisms underlying their natural behavior. In 2D cultures, used since the early 1900s, cells are seeded on adhesion substrates, typically coated plastic plates, on which they exhibit a planar growth pattern.[47] The 2D method is consolidated, relatively inexpensive and has the great advantage to have a lot of comparative literature. However, it is far from reproducing accurately physiological circumstances. 2D cultures are still widely used and convenient for many routinely employments but result inappropriate for more advanced applications: growing on a flat surface is not a good way to understand how cells grow and function in a human body, where they surrounded by other cells in a 3D complex environment. Furthermore, cells arranged on two-dimensional surfaces receive equal amount of nutrients, growth factors and drugs, giving a not reliable predictive testing system. Moreover, abnormal cell morphology, flatter and stretched in 2D culture than in vivo, influences many cellular processes including cell proliferation, differentiation, apoptosis, gene and protein expression.[48] For these reasons, in recent years, three-dimensional

culture systems have been increasingly the subject of studies and use. Research has shown that 3D methods more accurately represent the microenvironment in which cells naturally live as they are able to reproduce cell-cell and cell-ECM interactions, allow the co-culture of heterogeneous cell types and display cells in different life stages (proliferating, quiescent, necrotic, etc.) (Figure 2).

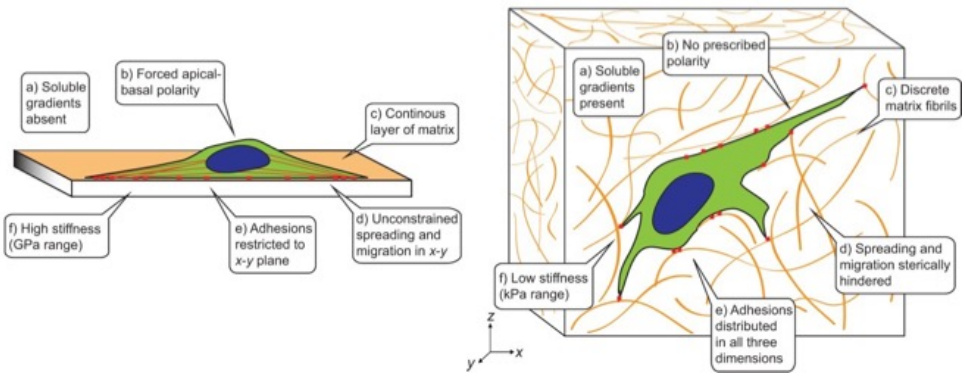

Figure 2: Schematics shows the difference of cells growing in 2D and 3D environment.[49]

3D culture systems are generally divided into two classes: scaffold-free and scaffold-based. Among the scaffold-free methods, spheroids and organoids are the most employed models. They resemble the 3D organization of cell aggregates mimicking cell-cell communications and, in case of spheroid co-cultures or organoids the crosstalk between different cell components. However, lack of ECM and scaffold to support cell populations and to induce cell-ECM interactions, does not allow to obtain homogeneous tissues.[50]

Alternatively, other advanced systems can be developed through a 3D matrix support or scaffolds, a construct able to support the initial attachment and/or proliferation of cells, facilitating formation of functional 3D cultures.[51] Therefore, the principles of tissue engineering can also be used for the development of 3D models for drug testing or biological studies.

There are no scaffolds universally suitable for every cell type and application. Indeed different types of them are available, and a variety of manufacturing techniques have been developed to fabricate new ones, tuning their properties as needed.[52] Scaffolds-based system has the advantage of guarantee various predefined biochemical (cytokines, growth factors, cell adhesion peptides, etc) and biophysical (structures, stiffness, degradation, etc) cues for cell fate control and tissue formation.

1.5 Biomaterials

A first definition of biomaterial was given during the Consensus Development Conference on the Clinical Application of Biomaterials in 1982 at the NHI (National Institute of Health, Bethesda, USA):

"Any substance or combination of substances, other than a drug, of synthetic or natural origin, that can be used for any period of time, alone or as part of a system that treats, augments or replaces any tissue, organ or function of the body." [53]

This definition is certainly general as it includes transplanted tissues and organs, materials used for the construction of biomedical equipment that are not used in direct contact with the tissues and included the concept of temporary implant.[54]

In 1986, during a second Consesus Development Conference held in Chester, the definition of biomaterial was changed as follows: *"A non-living materials used in medical device intended that has an interface with biological systems."* [55]

The contact between the material and the living tissue is pivotal for this definition, even if it is not intended to be necessarily lifetime enduring. Living materials such as transplanted organs are excluded from the definition, which includes instead treated and no longer living tissues of biological origin.

Given the heterogeneity and vastness of biomaterials, it is appropriate to classify them. A possible classification is based on

structural and chemical features, and according to it biomaterials are grouped into five categories: metals, polymers, ceramics, composites and biological materials.

Most used biomaterials in tissue engineering are polymers thanks to their greater resemblance to body tissues and their ease of processing and formulating. They are used in particular in the construction of supports (scaffolds) where cells are implanted and guided in their organization and arranged with each ther, thus creating the desired tissue. [11,53,56]

With the advent of 3D Bioprinting, biomaterials suitable for biofabrication using this technology are often referred to as bioinks and have become an important area of research within the field. A definition of bioink has been proposed to clarify its distinction from classical biomaterials:

"a formulation of cells suitable for processing by an automated biofabrication technology that may also contain biologically active components and biomaterials".[57]

1.5.1 Properties of Biomaterials

Some essential properties of biomaterials must be evaluated in employed in tissue engineering applications:

- Biocompatibility: The ability of a material to determine, by a living system, a favorable reaction to its presence in a specific application;

- Biodegradation: Each implanted material causes and undergo to a reaction by the organism. The materials can therefore be divided into biostable and biodegradable materials with respect to their application as permanent or temporary implant materials. The biostable ones resist the action of the biological environment while preserving their characteristics; biodegradable materials on the other hand, undergo progressive degradation or chemical transformation as a result of specific actions by the cells. The residues due to the biomaterial degradation can produce unwanted inflammatory reactions. Polymeric biomaterials are generally biodegradable;

- Bioactivity: bioactivity indicates the ability of the material to trigger specific biological pathways in the body. This type of material allows the formation of direct interactions with biological tissue, which can grow on the surface following certain stimuli. All this allows the integration, from a mechanical point of view, between the natural tissue and the implanted biomaterial.[58,59]

1.5.2 Synthetic Polymer Biomaterials

Synthetic polymeric materials have significant advantages: they can be industrially reproduced on a large scale with fine control over certain parameters such as molecular weight, degradation times, shape and

porosity of the structure.[60,61] The main disadvantage is due to the lack of bioactive residues to allow cellular recognition.

Polymeric materials for biomedical applications differ in the requirements asked for traditional applications: they must contain very limited quantities of additives and monomeric residues that could be released into the tissues.

The most used biomaterials in tissue engineering are degradable polyesters, in particular polylactic acid (PLA), polyglycolic acid (PGA) and γ-polycaprolactone (γ PCL) (Figure 3).

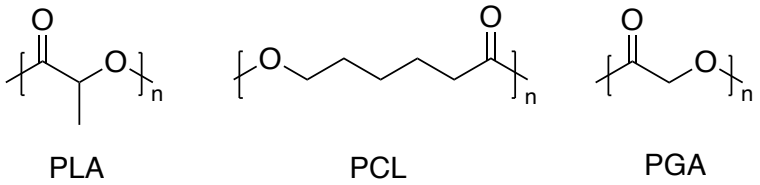

Figure 3: Chemical structure of PLA, PCL and PGA

Their success was mainly determined by the fact of being known and approved for use in the production of sutures and systems for the controlled delivery of drugs.[62]

PGA is a rigid thermoplastic polyester with high crystallinity (about 50%), characterized by a high melting point (225 °C). The interest in this type of polyester comes from the fact that the degradation products are natural metabolites. The hydrolytic cleavage of the ester bond leads to the formation of glycolic acid, which can then be degraded to CO_2 and H_2O, similarly to what happens for polylactic acid, or follow a

different path that involves enzymatic oxidation to glyoxylate and subsequent conversion into glycine by the action of glycine transaminase.[63,64]

Due to its hydrophilic nature, PGA tends to lose its mechanical strength rapidly, 50% in two weeks, and is reabsorbed about 4 weeks after implantation.

Like PGA, PLA is also a thermoplastic polyester, whose hydrolytic degradation leads to the formation of acid lactic, a natural metabolite. The L isomer of lactic acid is preferentially metabolized in the human body. The lower hydrophilicity of polylactic acid compared to polyglycolic acid determines a slower hydrolysis.

Both PGA and PLA have also been used in the manufacture of nails, screws and plates for orthopedic implants where, instead of being removed when they have exhausted their stabilizing function, they are absorbed and metabolized by the host organism.[65] PCL is a biodegradable synthetic semi-crystalline polyester. Being endowed with good characteristics of biocompatibility and a high thermal stability, it has received attention for the realization of implantable devices.[66] In particular, it is used for the construction of long-lasting plants since the degradation of PCL is much slower than PGA and PLA: it is of the order of 2-3 years.[67]

1.5.3 Natural Polymer Biomaterials With Protein Structure

1.5.3.1 Collagen and Gelatin

Collagen is the main component of the extracellular matrix and represents the most abundant protein in mammals: about 25% of the total protein mass and about 6% of humans body weight.[33]

There are different collagen types and they are able to form fibers in the skin, tendons, bones, cartilages and cardiovascular tissues. Collagen fibers have the purpose of limiting tissue deformations and preventing mechanical breakage.

The primary structure of the individual chains is composed of over 1400 amino acids and is characterized by the repetition of numerous sequence triplets: glycine, proline, hydroxyproline (Gly-Pro-Hyp). Pro-Hyp sequence is responsible for the secondary structure of the molecule due to the steric hindrance between the two aforementioned amino acids. Linear collagen polymers interact with each other to form a triple helix. Collagen is made up of polypeptide chains that are resistant to stretching and tightly intertwined in such a way to form a compact superhelix. Each single filament assumes a left-handed helical tertiary structure providing a high traction force due to its rigidity; filaments are then arranged in a right-handed superhelix forming the quaternary structure of tropocollagen, which is the structural unit of

collagen whose organization modulates the strength and stiffness of the entire tissue. Glycine, being the smallest amino acid with a hydrogen as R-group, is placed inside the triple helix while proline and hydroxyproline favor the spiral winding of the chains.[68]

The stabilization factors of the collagen molecules are the interactions between the three helices constituting the superhelix which are represented by hydrogen bonds, ionic bonds or by cross-links. These interactions contribute to mechanically stabilize the fibers and increase the tensile strength of the tissue. The particular structure of collagen fibers is responsible for its mechanical behavior: indeed, when subjected to traction, the fibers rotate and flex, modifying their spatial geometry from helical to linear shape. When the protein chains are stretched, the mechanical properties increase depending on intra and intermolecular bonds.[68]

Collagen is also very chemically stable and is used as a support for tissue regeneration as it facilitates proliferation and cellular metabolism; however, it is difficult to regulate its biodegradability and mechanical properties.

Gelatin, a high molecular weight polypeptide, is produced from the denaturation and / or physico-chemical degradation of collagen. The mechanical properties of gelatin-based products depend on the physical and chemical characteristics of the raw material.[69] Collagen and Gelatin interact with cells throught different way: in Collagen, cell binding motifs include the high affinity triple-helical GxOGER

sequences (where G is glycine; O is hydroxyproline; R is arginine, and x is hydrophobic, exemplified by phenylalanine, F). By contrast Gelatin contains the linear RGD cell adhesive motif.[70] Gelatin is available at low cost from bovine dermis, porcine skin or their bones. The resulting protein is biocompatible, biodegradable, and is water soluble. Gelatin-based gels have low mechanical properties and low stability, which can be improved with chemical functionalizations. Combining gelatin with other materials enhances its physical, mechanical and structural properties.

1.5.3.2 Elastin

Many animal tissues, such as skin, blood vessels, ligament cartilages, lungs, bladder, require resistance and elasticity to perform their functions in the best possible way. These properties are guaranteed by a dense network of elastic fibers, present in the ECM, which allow the relaxation of these tissues after deformation due to stretching or contractions.[29] Elastic fibers consist mainly of two elements: amorphous elastin, which forms the central core, and a sheath of microfibrils, the latter has a diameter of around 10 nm and is mainly composed of glycoproteins.[71]

Elastin, together with collagen, is a fibrous protein present in the extracellular matrix of most vertebrate organisms and represent the

longest structures of the ECM. It represents more than 50% of the extracellular component of the great arteries (aorta), 30% of the lungs and 2-3% of the skin.[71–73] The main characteristic of this protein, hence the name, is to give elasticity to the organs and tissues in which it is present.

Elastin is composed of considerable quantities of Proline and Glycine, which, unlike collagen, are distributed randomly, and is almost totally free of Hydroxyproline. There are also other amino acids, such as Desmosine and Isodesmosine: it is believed that these particular amino acids cause cross-links between molecules, forming a three-dimensional network of randomly wound chains, which would be responsible for its elastic properties. In fact, the elastic fibers stretch easily and return to their original length when the deformation force is removed.[74]

These mechanical characteristics are also due to the tertiary structure of the elastin, which adopts a spiral shape with disordered winding (random coil). This protein is synthesized by fibroblasts and smooth muscle cells, in the form of tropoelastin, a soluble precursor.[75] The tropoelastin molecules, once secreted in the intercellular spaces, undergo a process of aggregation, transforming themselves into elastin, a highly hydrophobic and insoluble protein.[75]

1.5.4 Natural Polymer Biomaterials With Polysaccharidic Structure

1.5.4.1 Hyaluronic Acid

Hyaluronic acid (HA) is a high molecular weight polysaccharide belonging to the glycosaminoglycan family. HA is a linear polysaccharide consisting of disaccharide units repetitions of D-glucuronic acid and N-acetyl glucosamine joined by β (1,4) and β (1,3) glycosidic bonds (Figure 4).[76] Under physiological conditions it forms a sodium salt, with the carboxylic residue negatively charged (sodium hyaluronate): it is highly hydrophilic, surrounded by water molecules linked by hydrogen bonds.

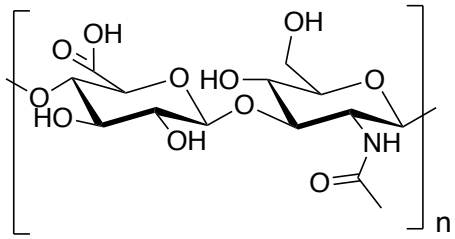

Figure 4: Hyaluronic acid chemical structure

The chemical-physical properties of HA have been the subject of in-depth studies.[77–80]

Its molecular weight can reach 8 x 10^6 Da, 10^7 Da or 10^8 Da according to various authors, depending on the enzyme that catalyzes its synthesis.[81,82] Due to the high molecular weight and strong

intramolecular interactions, the aqueous solutions of HA are highly viscous and exhibit a typical shear thinning behavior. Under physiological conditions, all carboxylic groups of glucuronic acid are completely ionized, giving the hyaluronic acid molecule the ability to coordinate many water molecules, reaching a high degree of hydration. In the amorphous matrix of a connective tissue and in general in the extracellular matrix, hyaluronic acid deals with maintaining the degree of hydration, turgidity, plasticity and viscosity by retaining a significant number of water molecules. This polymer is also able to act as absorber for mechanical shocks as well as an efficient lubricant (for example in the synovial fluid) preventing damage to the tissue cell from physical stress. The high molecular weight of HA together with its high degree of hydration allows multiple chains to organize themselves to form a dynamic reticular structure. It has also been shown and confirmed that HA is involved in intracellular activities, which include regulatory processes, cell migration and adhesion.[79,83,84] The high molecular weight gives HA, among others, anti-angiogenic and anti-inflammatory properties, while low molecular weight HA fragments cause opposite biological activities, i.e. inflammation, immunostimulation and angiogenesis.[85] HA has specific binding sites on some receptors such as CD44, RHAMM and ICAM-1 all involved in cellular mechanisms such as cell repair, proliferation, motility and regulation of the inflammatory response.[86,87] Many authors have reported and reviewed the numerous functions of HA and its fragments

in wound healing processes, as well as in tumor growth and cancer proliferation, during which CD44 receptors are over-expressed.[88,89] The reactive groups -OH and -$NHCOCH_3$ determine the specific properties of hyaluronic acid. As a biomaterial for tissue engineering it is used for the regeneration of the dermis, epidermis and cartilage.

1.5.4.2 Chitosan

Chitosan is a copolymer consisting of residues of N-acetyl-2-D-glucosamine and 2-D-glucosamine, which derives from the partial deacetylation of chitin. Chitin is the most abundant biopolymer in nature after cellulose and is found mainly in the exoskeleton of arthropods and in the cell wall of fungi. Chitosan structure makes it structurally similar to GAGs (Figure 5).

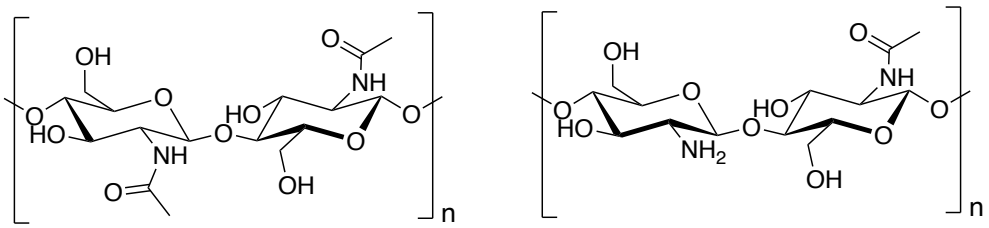

Chitin Chitosan

Figure 5: Chitosan-Chitin chemical structures

The microstructure of the chitosan influences the properties of the polymer itself and depends on the conditions in which the deacetylation

reaction is carried out: in heterogeneous conditions a chitosan insoluble in water but soluble at acidic pH is obtained, on the contrary the homogeneous deacetylation of the chitin produces a soluble chitosan in water. The physico-chemical properties of chitosan, such as water solubility, biodegradability and reactivity, depend on the percentage of free amino groups in the chain and therefore on the degree of acetylation of the polysaccharide.[90,91] Chitosan is available in a wide range of molecular weights and degrees of acetylation; moreover it can be chemically modified by intervening on the $–NH_2$ and –OH groups to generate derivatives useful for the development of new formulations. Chitosan is biocompatible, biodegradable, non-toxic and mucoadhesive, characteristics that make it interesting for applications in the medical and pharmaceutical fields.[90] It is broken down by lysozyme in serum and by lipase, an enzyme present in saliva and gastric and pancreatic fluids; the products of enzymatic degradation are not toxic.[90] Chitosan increases the permeability of cell membranes, acting as an absorption promoter because it prolongs the residence time of the delivery systems at the absorption site and is able to open the tight junctions of cell membranes. It also shows mild microbial antiadhesive properties and immunoadjuvant activity.[92,93]

1.6 Hydrogel

Even if classic biomaterials, such as metals, ceramics, and synthetic polymers, have been used to successfully replace the mechanical function of tissues (e.g., bone, teeth or knee joints), their use is limited to mimic hard tissue.[94] Therefore, the necessity of developing new biomaterials, composed of biologically derived building blocks, such as extracellular matrix (ECM) components (for example, collagen, elastin and hyaluronic acid), is increasing more and more. In fact, proteins, glycoproteins and proteoglycans, are important starting materials to design and develop heterogeneous micro-architectures that may facilitate ECM-cell interactions, providing chemico-physical structures and specific biochemical properties, in order to mimic native ECM environment. Regarding this, biomaterials formulated in form of hydrogels are taken in account.[95]

Hydrogels consist of a three-dimensional network of hydrophilic molecules, capable of swelling incorporating large quantities of water.[96] On the basis of the chemical structure and the swelling ability hydrogels can incorporate quantities of water equal to several times the initial weight of the material itself.[97] These materials can be chemically stable for a determined period of time, or degrade and eventually dissolve; in the first case they are defined as permanent or chemical hydrogels, characterized by a cross-linked network through covalent bonds, while in the second case the hydrogels are defined

reversible or physical, in which the network is held together by ionic interactions. The possibility of being made, theoretically, with any water-soluble polymers, allows obtaining a wide range of chemical compositions and physical properties. Furthermore, hydrogels can be synthesized in different forms, such as plates, microparticles, nanoparticles, coatings and films.[98] For this reason they are now commonly used in clinical practice, or in experimental medicine for various fields of application, such as regenerative medicine, diagnostic, pharmaceutical, cosmetic and nutraceutic.[99] When a hydrogel begins to absorb water, the first molecules enter the network hydrating the groups with greater affinity to water; this quantity is defined as "primary bound water".[96] After interacting with the polar groups, the network swells, thus exposing the hydrophobic groups that interact in turn with the water molecules. This quantity is referred to as “secondary bound water”.[96] After the interaction between the water and the hydrophilic and hydrophobic groups has taken place, the network continues to absorb water which tends to lead to an infinite dilution: the chemical or physical crosslinks present between the chains contrast water absorption. The result of these two opposing forces is the achievement of an equilibrium at a certain swelling value, a balance between the expansion forces of the solvent, which leads to lowering of the system enthalpy, and the forces elastic contraction of the network.[96,100] Although both the hydrophilic and hydrophobic groups are now saturated, there is an additional amount of water that is incorporated,

defined as free water or bulk water, which fills the free space between the chains.[100] The swelling capacity of hydrogels is mainly attributed to the presence of hydrophilic groups (-OH, -$CONH_2$, -COOH -SOH_3), and depends on factors such as the hydrogel structure and the degree of crosslinking. The swelling capacity is lower at higher crosslink ratio: the degree of crosslinking influences the area permitted for diffusion across the hydrogel network and, subsequently, the capacity for hydrogels to take up water. The chemical structure of the polymer determines the ratio between hydrophilic and hydrophobic species and the water absorption.[100]

The classification of hydrogels can be based on various criteria, such as morphology (particles, powders, spheres, membranes, fibers and emulsions), or the synthetic method (graft-polymerization, crosslinking), or also based on the response of the material from the application environment (smart hydrogels).[100] Most commonly they are classified based on the origin of the starting material (synthetic, natural and semi-synthetic).

1.6.1 Crosslinking Methods for Hydrogel Synthesis

Several crosslinking strategies are available for the control of homo- or heteropolymer based hydrogels. The final hydrogel properties, such as mechanical and biochemical ones, are strongly related to crosslinking methods employed in hydrogel formulation. For instance,

crosslinking nature, density or degree, determines various physical properties of hydrogels, including elasticity, water content, mesh size and degradation rate. The crosslinking methodology is therefore selected based on the final biomedical application. The features and the desired properties of injectable hydrogels for therapeutic use will be different if compared with hydrogels for tissue engineering and 3D *in vitro* culture models. Considering 3D bioprinting manufacturing processes, the opportunity to encapsulate cell populations during the printing processes, require a crosslinking methodology that does not interfere with cell viability and distribution.

A homogeneous crosslinking of polymers that constitute the final hydrogels is necessary to prevent uncontrolled release of macromolecular chains in cell media and the consequent loss of tissue construct morphology. Various crosslinking strategies were employed and validate for the formulation of hydrogels. Depending on the nature of the crosslinking we can discern the physical hydrogels, or the chemical hydrogels.

Particularly, chemical crosslinking methods covalently couple reactive functional groups using functional groups already available on polymer chain or by the introduction of new functional groups, while physical ones utilize non-covalent interactions between functional groups, such as ionic or electrostatic interactions, hydrogen bonds, hydrophobic/hydrophilic interactions or π- π stacking.

1.6.1.1 Physical Cross-Linking

Physical or reversible hydrogels have gained attention because of their relatively facile production. All of these interactions do not require starting materials modifications, are reversible, and can be disrupted by changes in physical conditions such as ionic strength, pH, temperature, application of stress, or addition of specific solutes that compete with the polymeric ligand for the affinity site on the protein:

• Hydrogen bonds: in this case the secondary intra and intermolecular forces are able to build network in environmental conditions.

• Amphiphilic grafting and block copolymers: Amphiphilic block copolymers consist of at least two parts with different solubility, causing their self-assembly into superstructures in the sub-micrometer range with cores consisting of their hydrophobic, surrounded by a corona of their hydrophilic parts,[101–103]

• Crosslink by ionic interactions: Ionic cross-linked polymers which are formed by the addition of di- or tri-valent counter ions are considered in this category. B-glycerolophosphate and sodium tripolyphosphate are the anionic molecules are commonly used for ionic crosslinking.[104–106]

Physical or reversible hydrogels have gained attention because of their relatively facile production. All of these interactions do not require starting materials modifications, are reversible, and can be disrupted

by changes in physical conditions such as ionic strength, pH, temperature, application of stress, or addition of specific solutes that compete with the polymeric ligand for the affinity site on the protein.

1.6.1.2 Chemical Crosslinking

Interest in chemically cross-linked hydrogels has grown, thanks to the advancement of the use of the 3D Bioprinting technique which requires hydrogels with superior physical properties.[107] Chemical crosslinking may be considered a suited technique to formulate hydrogels based on proteins and polysaccharides, since these biomaterials have numerous functional groups in their chains (primary amines, carboxylic acids, hydroxyl groups, etc.). To achieve an even more tailorable chemical crosslinking, synthetic and natural biopolymers can be previously functionalized with selected functional groups before obtaining hydrogel.

Chemical crosslinking:

• Crosslink by aldehydes: glutaraldehyde (GA) is inexpensive, highly reactive and is very soluble in an aqueous environment. These characteristics allow it to be used as a cross-linking agent for the synthesis of chemical hydrogels. Polymers containing amine and hydroxyl groups as gelatin, chitosan or polyvinyl alcohol may be crosslinked by GA. The reaction occurs through a Schiff's base

reaction between aldehyde groups of GA and amine and hydroxyl groups of the polymers. However, problems can arise with GA due to excessive cross-linking and potential cytotoxicity. GA is non-environmentally friendly and toxic even at low concentrations and may leach out into the body during hydrogel degradation, inhibiting cell growth.

• Crosslink by high energy irradiation and photocrosslinking: high energy electron beams (e-beams) and γ rays induce crosslinking and sterilization in a single step.[108–112] This method is advantageous as it is not necessary to use a cross-linking agent, nor a catalyst or an additive, which can vary the properties in terms of biocompatibility.[113,114] Another advantage is the possibility of controlling the degree of crosslinking and the size of the pores inside the hydrogel can be controlled by varying the duration of irradiation.[113] This method is commonly used for the synthesis of hydrogels based on PVA, PEG and acrylic acid.[114]

Radical polymerization is widely used for non-specific bioconjugation in biomaterials field and represents an excellent tool for several applications in tissue engineering. It involves the formation of free radicals via decomposition of an initiator by light, temperature, or redox reaction. The following reaction of multifunctional free radical building blocks leads to the development of a polymer network. This kind of mechanism offers some advantages, such as well-characterized reaction kinetics and facile *in situ* polymerization in presence of cells, with spatiotemporal control. However damage by

free radicals and exothermic reactions which may lead to a local increase in temperature, could cause the loss of cell viability and function. A widely used example is methacrylated gelatin (GelMA), which undergoes photoinitiated radical polymerization (i.e. under UV light exposure with the presence of a photoinitiator) to form covalently crosslinked hydrogels.[115]

• Enzymatic Crosslink: the use of enzymes in order to catalyze the polymer crosslinking is very interesting for the formation of injectable hydrogels, which are formed *in situ*, thanks to the enzymatic condition reactions witch are suitable for the physiological environment. Furthermore, this makes it feasible to inject through a syringe the formulation that contains the precursors, which will later gel inside the body, without the formation of toxic substances. Both physical and chemical hydrogels can be synthesized, depending on the activity of the enzyme itself. For example, the fibrin gel is formed by the enzymatic activity of thrombin, which converts fibrinogen into fibrin (monomer). The monomers polymerize by forming fibrin fibers, physically cross-linked.[116] The advantage of an enzymatic crosslink is the strongly covalent bonding as well as rapid gelation (always no more than 10 minutes) under physiological conditions.[117]

• “Click chemistry”: defined by Sharpless in 2001, Click reactions possess advantages such as high yields under mild conditions, no by-products, high specificity and selectivity.[118] This new way of looking at processes involves several mechanisms; among all, the most

employed for the synthesis of hydrogels are the Michael addition and the Diels-Adler cycloaddition.[119,120] Michael addition is a reaction of addition of a nucleophile which are defined as Michael donors, to a compound containing an unsaturated α-β carbonyl, which play the role of Michael acceptors.[121] Generally, nucleophiles capable of carrying out Michael-type addition include halide ions, cyanide ions, thiols, alcohols, and amines; however, only thiols, alcohols, and amines are suitable in cross-linking of biomaterial hydrogels, given the relative toxicity of halides and cyanides in the body.[122–127] On the other hand, Michael acceptors consist of maleimides, α,β-unsaturated ketones and methacrylates. Furthermore, the reactions are achievable in presence of water and salts, making easy their employment in biomaterial applications.[128] Several polymers and precursors are compatible with this reaction, with high conversion rates and process speed. It can be used for the synthesis of linear, branched, dendritic and network polymers.[121] The Diels–Alder (DA) reaction is a [4+2]-cycloaddition between a conjugated diene and a dienophile, to form a substituted cyclohexene derivative. The maleimide moiety is a dienophile widely used in Diels–Alder reactions. Interestingly, once the maleimide function is inserted in a biomaterial, it becomes suitable for both Michael and Diels–Alder ligations. As far as the diene moiety is concerned, furan, cyclopentadiene, and photogenerated orthoquinodimethanes (photoenols) have been used to functionalize the starting biopolymers for subsequent Diels–Alder conjugations with

maleimide. In recent years, methylfuran was used to replace furan, because it provided more electron-rich diene, thus, accelerating the DA reaction at pH 7.4.[129] Polymers were usually modified with furan or furan derivatives to react with poly(ethylene glycol) dimaleimide for hydrogel formation.[129,130]

1.7 3D Bioprinting

While 3D printing, which allows direct digital manufacture (DDM) of a large variety of polymers and metal items, is driving a manufacturing revolution, far more surprising is its application in the biological field. Indeed 3D Bioprinting represents one of the most recent and promising tissue engineering techniques.[131]

A definition of Bioprinting was given in 2009 at the International Conference on Bioprinting and Biofabrication, held in Bordeaux: *"Bioprinting can be defined as the use of computer-aided transfer processes for patterning and assembling living and non-living materials with a prescribed 2D or 3D organization in order to produce bio-engineered structures serving in regenerative medicine, pharmacokinetic and basic cell biology studies. In this context, additive manufacturing of 3D scaffolds able to instruct or induce the cells to develop into a tissue mimetic or tissue analog structure, for example, through distinctive cell interaction, hierarchical induction of differentiation, or functional evolution of the manufactured scaffolds falls within bioprinting ".*[132]

1.7.1 Fundamental Concepts for the Birth of 3D Bioprinting

As previously discussed, cell biology is of particular importance in the 3D Bioprinting technique.[133] It is essential to study and understand the mechanisms that regulate the formation of organs and tissues (morphogenesis) to develop a model that emulates the natural one and reproduces its morphology and functionality (Figure 6).[134]

Nature is therefore assumed as a model and attempts are made to replicate and exploit its dynamics for the creation of constructs that are as similar as possible to the originals, in order to regenerate or replace them without the appearance of undesirable effects that currently limit known techniques.[135]

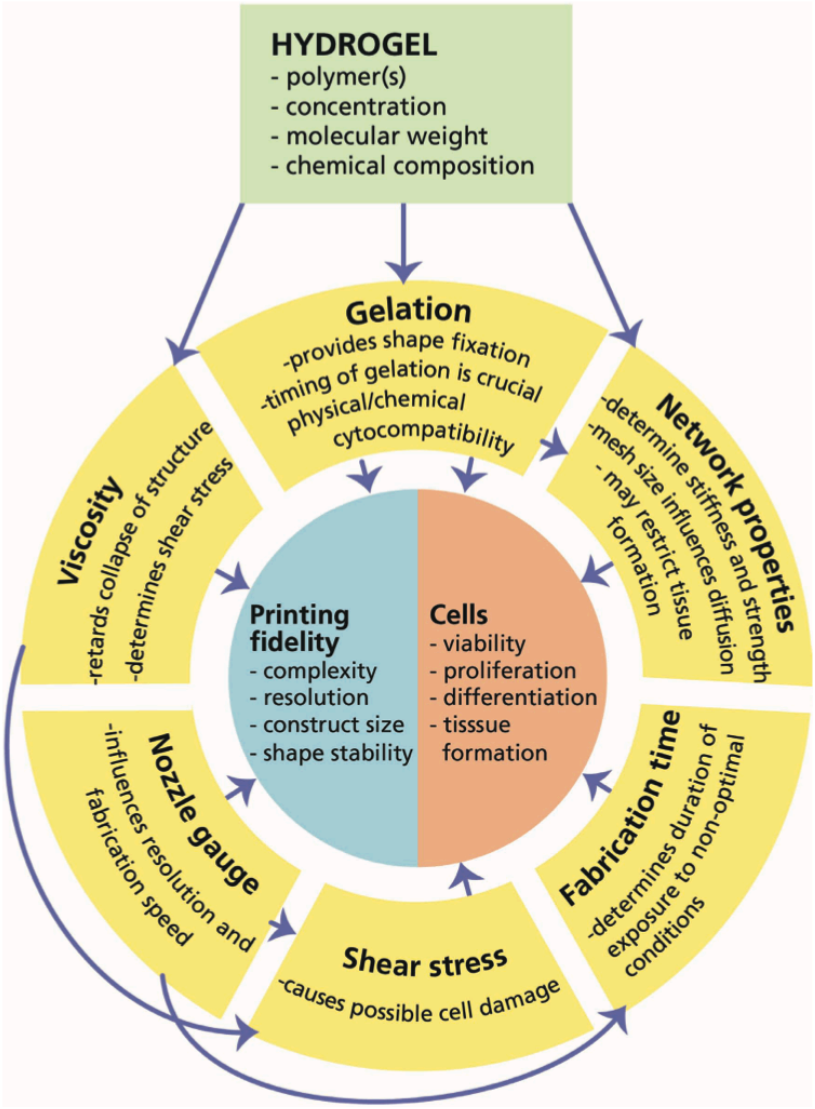

Figure 6: Concept map of variables and relations critical to biofabrication. The hydrogel (polymer type(s), concentration, molecular weight and chemical composition) directly determines the viscosity, gelation mechanism and speed, and mechanical properties of the final gel. This -in combination with processing parameters, such as nozzle gauge and fabrication time- influence the main outcomes Printing fidelity and Cell viability and function. Adapted from [135]

1.7.2 Stages of the Process

Scaffold-based regenerative medicine therapies require scaffold fabrication, the implantation of cells on the latter, and then the conditioning of the construct in a bioreactor in order to obtain adequate cell proliferation.

Traditionally, the fabrication of the scaffold and the implantation of cells are two separate and distinct phases of the process. The most recent 3D Bioprinting techniques combine the two steps in a single step, allowing the layer-by-layer writing of biomaterials, chemical molecules and living cells in order to form a heterogeneous 3D construct of the desired shape.

The fundamental skill in 3D Bioprinting consists in the ability to accurately control the amount of bioink ejected from the nozzle and deposited on the substrate, employing a cell-compatible protocol.

The 3D Bioprinting process begins with the definition of a digital model of the architecture to be fabricated that can be directly obtained from CT (Computed Tomography) and MRI (Magnetic Resonance Imaging) images of the patient who needs tissue transplantation.[136]

Through the automatic processing of CAD (Computer-Aided Design) images we then obtain a 3D model to be created. Software tools can also help in the construction of a complex system, finely controlling the location of different biomaterials, biological molecules and cells lines.

Through specific algorithms, the digital model is then converted into a series of instructions necessary to guide the hardware systems; the exact format of machine instructions, in this CAM (Computer-Aided Manufacturing) manufacturing process, depends on the printing technique and hardware configuration used.

Once the print signal is activated, the control system guides the hardware components for the physical realization of the desired construct. Complex engineered tissues will be formed by spatially modeled layers of cells, which aggregating together will form the specialized tissue.[137,138]

The entire procedure must take place in a sterile environment to limit contamination of both the raw materials and the final construct.

Since living cells are also involved in the manufacturing process, a critical aspect to consider is the time and the physical conditions (i.e. pressure, temperature) required to produce the construct: the amount of time available depends on the cell type used and, unless conditions are particularly favorable, it should not exceed one hour. Longer times will result in reduced cell viability and abnormally high cellular stress, which will lead to a degradation of functions.[139]

The 3D constructs developed should be characterized to confirm the functional and structural features of the obtained synthetic tissue and they can then be used for drug screening, as models for tumor studies or as implant materials.[137,140]

1.7.3 3D Bioprinting Techniques

1.7.3.1 Ink-Jet Based Bioprinting

Ink-jet 3D Bioprinting is a printing process that involves the precise deposition of drops of bioink, ranging in size from nanoliter to picoliter, on the biopaper according to a precise digital model. It is an adaptation of the traditional ink-jet printing process and in most cases is achieved by partially modifying commercially available desktop printers.[141]

The ink-jet printing methodologies are basically two:

- CIJ (Continuous Ink-Jet): a continuous stream of droplets is produced by forcing the ink through a microscopic nozzle under pressure and deflected onto the substrate by an electric field. Where, in the digital model, the deposition of bioink is not required, the droplets are guided into a sort of gutter and collected for reuse;
- DOD (Drop-on-Demand): ink droplets are emitted through the nozzle by means of an impulse pressure only when requested by the model. In 3D Bioprinting, the DOD approach is preferable due to its impulsive nature and the risk of contamination due to the recirculation of bioink in the CIJ technique (Figure 7).

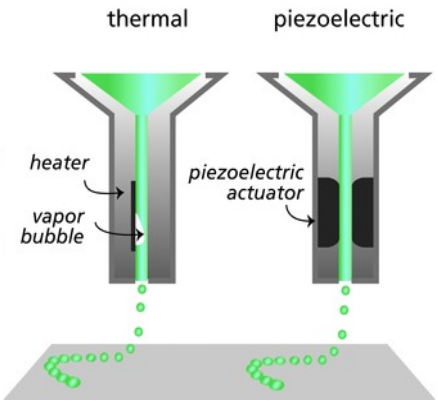

Figure 7: Schematic representation of Ink-Jet Based Bioprinting. Adapted from [135].

The size of the drops and the spatial resolution in ink printing are determined by various factors: the viscosity of the bioink, the size of the nozzles, the distance between them and pressure selected.

The ink-jet technique offers the possibility to print different cell species, biomaterials or their combinations through different print heads in a single manufacturing process, allowing the creation of complex multicellular constructs.[142]

1.7.3.2 Laser Assisted Bioprinting

Laser printing technology (LAB: Laser-Assisted Bioprinting) is a direct, non-contact writing process. LAB systems are characterized by three main components: an impulsive laser source, a donor “ribbon” containing cells suspended in a gel and a receiving substrate. They are analyzed individually in more detail below:

- Laser pulses lasting a nanosecond, with wavelengths near UV or UV, are used as an energy source;
- The "ribbon" consists of a glass or quartz plate, transparent to the wavelengths of laser radiation, with one side coated with thermosensitive bioink encapsulated within a thin layer of hydrogel.
- Depending on the optical characteristics of the bioink and the wavelength of the laser, the system may also contain a thin (~ 100 nm) laser absorption layer, consisting of metals (such as Au, Ti, Ag) or metal oxides (TiO2), to protect cells from direct exposure to the beam and to allow them to be kept alive during transfer;
- The receiving substrate is mounted on a base with triaxial drive, positioned under the belt at a distance between 700-2000 μm. This substrate is usually coated with a low viscosity biopolymer (such as hydrogel) carefully chosen to cushion the impact of the cells, favor their adhesion and maintain the structure of the construct. [143]

The laser pulse is focused through lenses on the donor slide, containing the cells suspended in the gel, creating a vapor bubble from which shock waves are generated that push the cells towards the receiving substrate (Figure 8).

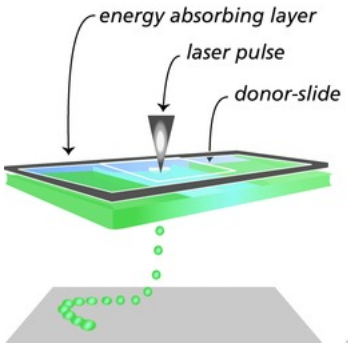

Figure 8: Schematic representation of laser- assisted bioprinting. Adapted from [135].

The growth and subsequent compression of the bubble depends on the following factors:

- intensity of laser energy (E);
- viscosity of the bioink (v);
- surface tension (v);
- thickness of the bioink film (ε);

In this case different cell types, Bioprinting is possible by selective propulsion of different cells from the donor slide to the recipient substrate. Laser printing technology, as well as inkjet technology, takes place simultaneously with the printing of the biopaper, allowing the creation of three-dimensional fabric constructs.

The latter are obtained through laser writing performed in conjunction with the photo-polymerization of the hydrogel: the cells are deposited according to a precise pattern on a receiving substrate by means of a laser beam, and this operation is followed by the hydrogel

printing on the top of the surface of each cell; the process is repeated for several cycles until a three-dimensional structure is obtained.[143]

In order to work with living cells and biomaterials, the radiation used must not induce alterations in the biological material due to the potential denaturation of DNA by UV radiation. The duration, intensity and frequency of the pulse must therefore be taken into account in order not to cause excessive cellular overheating, as well as the quality of the laser beam and focal lenses to contain their divergence.

1.7.3.3 Extrusion-Based Bioprinting

Also extrusion-based printing was introduced in the early 2000s and it is the most common and affordable bioprinting technique. This technique uses high pressure or mechanical force to extrude the bioink, overcoming the problem of droplets formation and drawing the bioink in the form of cylindrical filaments in both 2D and 3D patterns. According to its working mechanism, extrusion based bioprinting can be classified into: pneumatic micro extrusion, mechanical or solenoid (Figure 9).

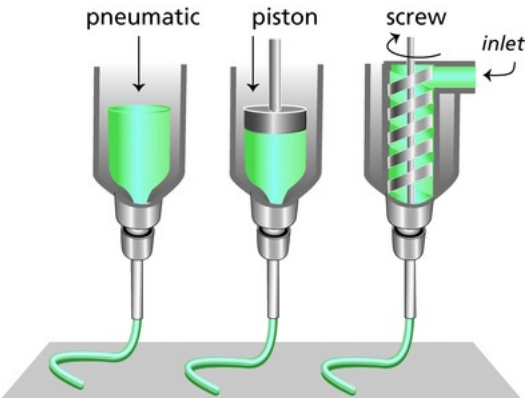

Figure 9: Schematic representation of Extrusion-based Bioprinting technique. Adapted from [135].

Some advantages of this method are:

- a wide material selectivity;
- ability to disperse highly viscous bio-inks with high cell densities, cell pellets, tissue spheroids and tissue strands;
- Possibility to use scalable production and synthetic polymers;

o high cell viability, typically above 90%.

However, extrusion-based printing has a downside, as it has a relatively low resolution (> 100 μm). Indeed, to obtain a construct with high cell viability it is necessary to decrease the printing pressure or increase the nozzle size. Nevertheless, using a nozzle with a bigger diameter, a corresponding lower resolution is obtained.[144]

1.7.3.4 Comparison of Bioprinting Techniques

Systems based on laser writing have a high resolution with an error that falls around 5.6 ± 2.5 μm compared to the digital model.

This resolution cannot be obtained with any other 3D Bioprinting technique, which makes laser printing excellent for micro cellular techniques of organs and tissues such as micro vascularization.[145,146] However, the laser shock linked to the thermal and mechanical deformations induced to the cells and the interactions of the cellular components with the radiations emitted represent risk factors for the viability of the printed construct. [147]

It is therefore necessary to optimize parameters such as:

- pulse duration;
- wavelength;
- pulse repetition speed;
- energy and focus diameter of the laser beam;
- rheological properties of the bioink (surface tension, viscosity);
- properties of the receiving substrate.

The inkjet and extrusion valve systems are versatile and low cost.[131,145,148] These techniques favor the encapsulation of the cells and , through the use of multiple print heads, allow a simpler realization of cellular constructs compared to laser writing. However, similar technologies face drawbacks such as sedimentation and cell aggregation in the orifice of the nozzle, with consequent clogging of the latter. Therefore, the construction process must be short-lived, since the material settles under static conditions. Furthermore, the diameter of the nozzle must be adequately designed in order not to damage the cell during deposition. In conclusion, the parameters to be optimized in

order to make this technique functional are the nozzle diameter, the viscosity of the biological material and the delivery time of the bioink.[147]

1.7.4 3D Bioprinting Prospective

The field of tissue engineering has grown significantly since its inception in the late 1980s. 3D bioprinting is assuming a key role in the fabrication of advanced 3D cellular constructs for tissue repair and regeneration. Among the wide range of biofabrication techniques currently available to generate cellular constructs for Tissue Engineering, 3D bioprinting is one of the most attractive owing its ability to print multiple biomaterials, cells and biochemicals (termed as "bioinks") in precise spatial locations with high resolution, accuracy and reproducibility. Bioprinting technologies enable the automated biofabrication of cell-laden constructs through the layer-by-layer deposition of bioinks in both *in vitro* and in vivo.[144,149]

There are many tissue engineered products now commercially available and generating revenue, or in clinical trials. However, the products that have reached commercialization are relatively simple in tissue structure. There is a significant need for improved ability to fabricate complex tissues that effectively mimic the native architecture of tissues found in the human body. Furthermore, there is a need for bioink materials to be accessible, easy to use and formatable for

various uses. Fulfillment of this need will push the field of tissue engineering from the research lab to the clinic.

1.8 Outline Thesis

The introduction of this thesis presents a general overview of the tissue engineering field and gives a more detailed literature overview including various aspects of 3D Bioprinting technique and applications. Discussed topics are the general requirements involved in scaffold design, well-known and frequently used biomaterials and commonly applied scaffold fabrication methods. Additionally, this section includes the specific biomaterials and fabrication method adopted in the following chapters of this thesis. Chapter 1A presents how Diels Alder reaction could be used to generate a novel Gelatin-Chitosan based bioink. Whereas Chapter 1A deals with formulation, characterization and application of this bioink, Chapter 1B describes how to tune the morphology of the novel scaffold by Ice Binding Protein inclusion.

The same cross-linking technique was employed in Chapter 2, where a multimodal Gelatin, Chitosan and Elastin based hydrogel has been formulated and characterized. The successful use of this technique applied on different biomaterials, together with the set up analysis platform to outline the physical-chemical properties of the obtained constructs, offers a wide range of applications in the field of tissue engineering. Finally, in Chapter 3, hyaluronic acid conjugated to small molecule inhibitors was tested on spheroid models of glioblastoma, to study the metalloproteinases expression inhibition for future applications in the clinical field.

CHAPTER 1A

GelChiDA: Chitosan-Gelatin Hybrid Hydrogel for 3D Bioprintable *in vitro* Models

Hydrogels are used as bioinks in cell-laden three dimensional (3D) bioprinting, since those structures mimic the physical features of native ECM.[150,151] The major challenges in bioinks development consist in encapsulation of cells, bioprintability and high post-printing morphological stability, allowing at the same time ECM remodelling.[152–154] The crosslinking process is pivotal for all these aspects, leading to the gelification of the molded structure essential to preserve the shape and ensure its stability.[155] It is therefore necessary to have an effective crosslinking process both from a mechanical and chemical point of view and, at the same time, it has to be compatible with encapsulated cells.

The aim of the work is to develop new hybrid bioinks that provides mammalian cells with the essential properties of their native environment, in order to obtain 3D structured tissue mimetics suitable for *in vitro* test clinical studies.

To better emulate the ECM network, we decided to represent both protein and polysaccharidic contributions. Gelatin was chosen to mimic collagen, the most abundant structural protein present in human ECM,

since it is the corresponding hydrolyzed form. Besides its low cost and easy supply, the use of gelatin has several advantages in biomedical field: it is a biocompatible polymer well-soluble in water at 37 °C, provides RGD recognition sequences and exhibits amphoteric behavior.[156,157] Therefore, gelatin has already been extensively employed as biomaterial for tissue engineering applications and 3D *in vitro* microfluidic systems.[158–160]

The ECM is also characterized by a large variety of GAGs and proteoglycans (PG). Considering the structural and biochemical role of polysaccharidic chains in the ECM, we introduced chitosan as polysaccharidic component. Over the past several decades, chitosan has emerged as a promising biomaterial for biomedical applications due to its natural origin and structural similarity to GAGs naturally presented in native tissues. Furthermore, its biocompatibility, biodegradability, and antimicrobial activity make chitosan an attractive biomaterial for the development of medical devices and tissue engineering strategies.[161]

For these reasons, the combination of gelatin and chitosan biopolymers has been already widely explored for disparate biomedical applications as drug delivery controlled system, implantable scaffolds or injectable hydrogels for wound healing or tissue engineering.[162–170] Multiple crosslinking strategies were investigated to obtain the ultimate construct. The most employed methods include chemical reaction of complementary groups (i.e. glutaraldehyde, b-glycerophosphate) or

photopolymerization (or photocrosslinking), in presence of UV light and a photoinitiator.[167,171–173]

These methods, despite giving advantages as stability and fast curing rate, could be hazardous since might affect cells viability, triggering DNA and membrane firmness. Chemoselective ligation strategies have been extensively studied, including thiol-ene, azide-alkyne cycloaddition and Michael addition. In our work, Diels-Alder reaction has been employed as alternative to conventional crosslink method, guaranteeing multiple advantages as click chemistry reaction: hydrogel formation occurs at physiological pH, does not need toxic solvents or catalysts, and do not produce harmful by-products, allowing cells encapsulation without polymerization reactions which could affect their growth.[174,175] Diels-Alder reaction has already been employed as cross linking strategy in single polymer hydrogel formulation.[129,176] In this work its use has been optimized on hybrid material composed of polymers with different reactivity. Gelatin (GE) and chitosan (CH) have been functionalized with methyl furan as diene. Starting biomaterials functionalization was achieved through reductive amination of free chitosan and gelatin primary ammino groups, to generate the methyl furan functionalized biopolymers. A dienophile, such as an alkene with an electron-withdrawing group, capable to readily react with the diene in DA cycloaddition, is needed. We selected commercial four arm Star-PEG decorated at the ends with maleimide groups, acting as crosslinker.

After a thorough study, the optimal formulation to obtain a stable and functional construct has been reached. Its potential has been studied with different formulations, such as bioink, for the application of 3D tissue bioprints and as a scaffold for the inclusion of spheroids for brain tumor *in vitro* models purpose. The new hybrid hydrogel has been validated both from a chemical and biological point of view, with tests of vitality, stability and chemical-physical properties (Figure 10).[177]

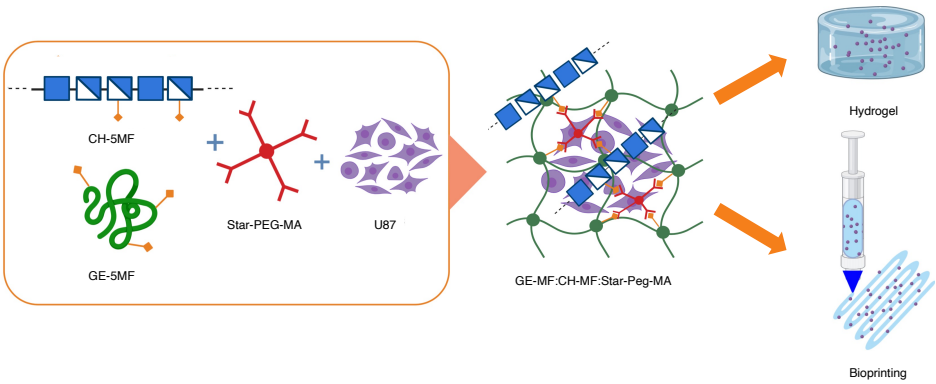

Figure 10: Graphical representation of hybrid formation, cell encapsulation, and formulation in a cell-laden hydrogel bioprinted construct.[177]

One of the limits of using natural biomaterials is their variability, which can occur between one batch and another, affecting the reproducibility of the formulations and thus applications.[174,177] Moreover, the characterization of complex structures can be challenging. Therefore, the development of such promising hybrid hydrogel requires a standardization of the process in order to guarantee reproducibility of batches, which is critical for frontier

research translation. Various analytical techniques have been used and optimized for a detailed report of both starting natural biopolymers and the final hybrid construct's physical and chemical properties.[178] Moreover, the crosslinking reaction has been followed and characterized. To this purpose, we exploited the combination of HP-SEC-TDA, UV, FT-IR, NMR, and TGA.[178]

1. RESULTS AND DISCUSSION

1.1 GelChiDA Formulaion

In order to formulate the hybrid hydrogel, starting materials amino free groups underwent derivatization reaction. As diene 5-methyl furfural was chosen as it allows faster reaction kinetics than furfural. After materials functionalization with orthogonal moieties that allow the Diels Alder reaction with the commercial 4arm-PEG10K-Maleimide (PEG-Star-MA), different formulations were tested (Scheme 1). The optimal formula was obtained after several tests with variation of protein and polysaccharide content, keeping unchanged the PEG-Star-MA quantities (Table 1).[177]

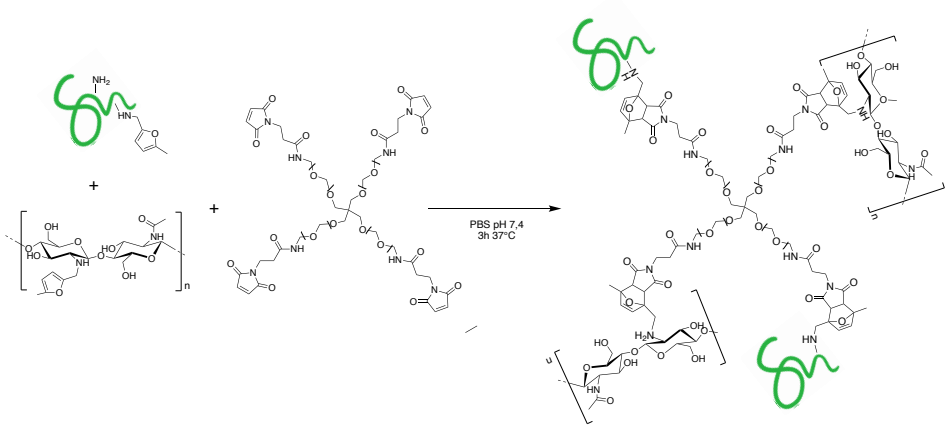

Scheme 1: GelChiDA reaction

Table 1: Tested different formulation

Entry	%W/V	Ratio	Gelification	Printability
Gel-MF:Chit-MF	**3%**	**1:1**	**X**	**X**
		1:3	**X**	**X**
		3:1	**X**	**X**
Gel-MF:Chit-MF	**5%**	**1:1**	✓	**X**
		1:3	✓	**X**
		3:1	**X**	**X**
Gel-MF:Chit-MF	**7,5%**	**1:1**	✓	**X**
		1:3	✓	**X**
		3:1	✓	**X**
Gel-MF:Chit-MF	**3%**	**2:1**	**X**	**X**
		1:2	**X**	**X**
Gel-MF:Chit-MF	**5%**	**2:1**	✓	✓
		1:2	✓	**X**
Gel-MF:Chit-MF	**7,5%**	**2:1**	✓	**X**
		1:2	✓	**X**

Given the higher presence of diene groups on the chitosan backbone, thanks to the higher availability of amino groups, as the polysaccaridic ratio was lowered, the softer the hydrogel became.

Below 5% biopolymers concentration there is no hydrogel formation while above that point the construct was lumpy, opaque and not bioprintable.

The GelChiDa hybrid hydrogel was selected with the final biopolymers concentration of 5% (50 mg/ml) with polymer ratio of

CH:GE:Peg-star=1:2:0.16. The hydrogel transition is completed after 3 hours at 37 °C.

1.2 Gelatin-MF Chemical Characterization

Gelatin has been functionalized with 5-methyl furfural and the obtained functionalized biomaterial studied with Nuclear magnetic resonance (NMR) characterization. The spectrum complexity is due to signals overlapping to which the various amino acid functional groups refer. The ^{1}H-NMR gelatin spectrum shows principal peaks at δ = 0.91 ppm (CH_3, Val), δ = 1.40 (CH_3, Ala), δ = 3.00 and 2.9 ppm (Lys), δ = 3.25 ppm (Arg) and 7.48 ppm (Tyr and Phe).[179] In methyl furan derivate, the lysine signal at 2.9 ppm decreases compared to the intensity of the same peak in the gelatin spectrum, pointing its involvement in functionalization (Figure 11). By comparison between the integral of the peaks of H-1 (6.5 ppm) and H-2 (6.1 ppm) in methylfuran and the peak of the reference, we calculated the amount of methylfuran. In particular, we estimated $6.29 \cdot 10^{-4}$ mmol of methylfuran per mg of Gelatin-MF. Considering the weighted average of aminoacids' molecular weight, we estimated the degree of functionalization as 12,7%. The signal of the methyl moiety at 2.3 ppm has not been considered since it is influenced by the underlying signals of aminoacidic chains in gelatin.

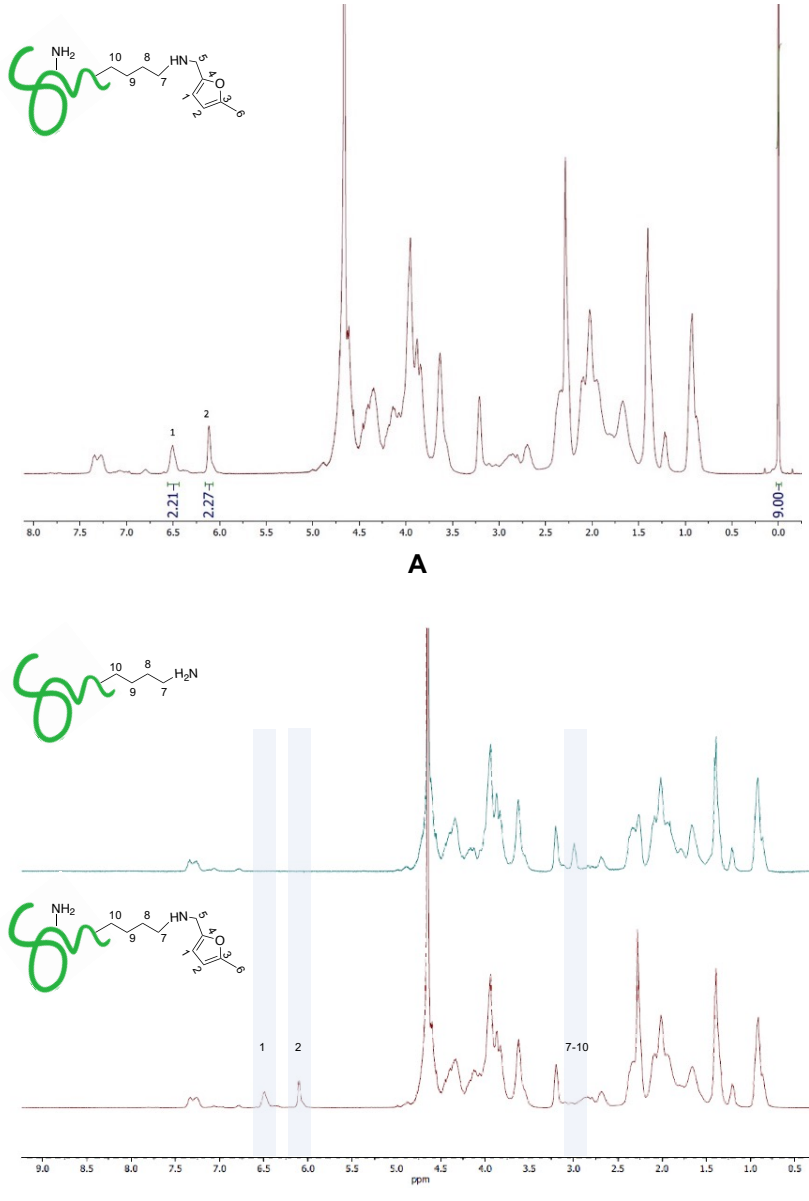

Figure 11: A) 1H NMR spectrum of gelatin-MF. B) comparison between ^{1}H NMR spectra of gelatin and gelatin-MF. ^{1}H NMR (deuterated PBS pH 7.4 with 0.05% wt 3-(trimethylsilyl)propionic-2,2,3,3-d4 acid sodium salt, 37°C, 400 MHz): δH 6.5 (s), 6.1 (s), 4.2 (s), 2.3 (s).

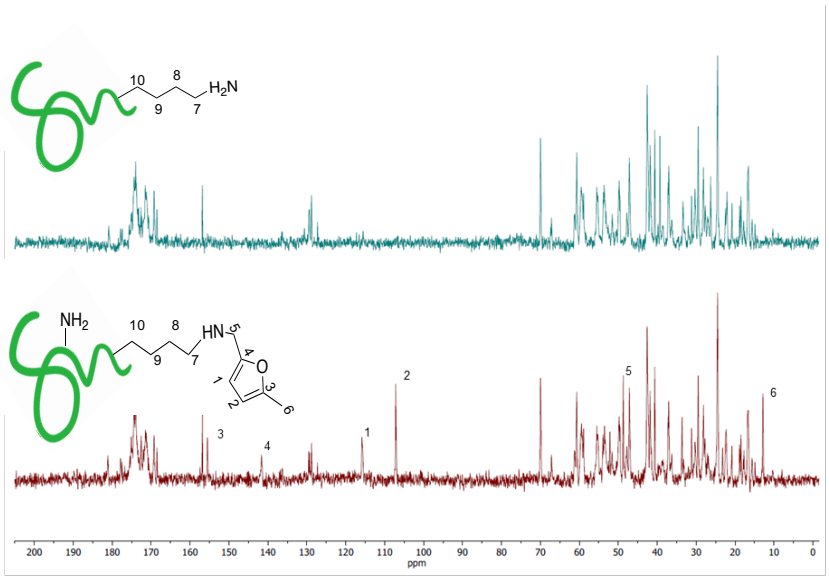

A

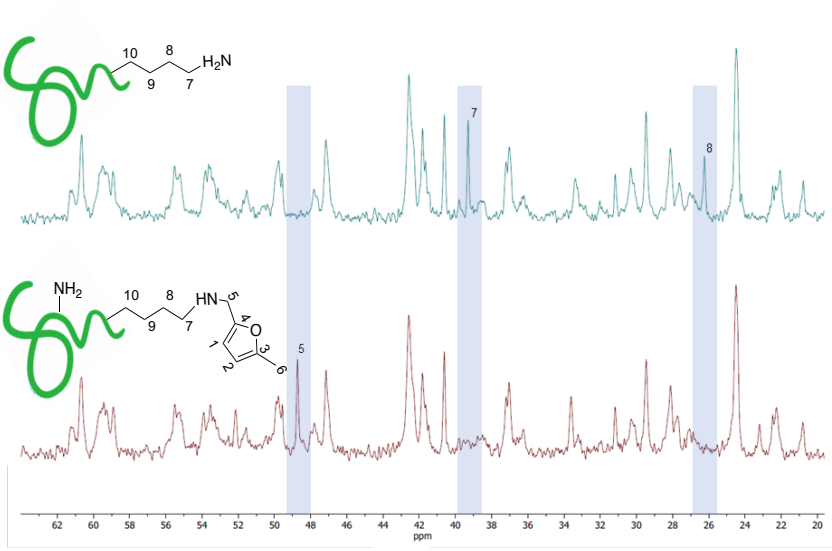

B

Figure 12: A) comparison between ^{13}C NMR spectra of gelatin and gelatin-MF. B) focus on the area between 62 and 20 ppm. ^{13}C NMR (deuterated water, 37°C, 400 MHz): δC 181-168, 156.8, 155.5, 141.5, 129.4-128.7, 115.7, 107.1, 70.0, 67.1-14.9, 12.9.

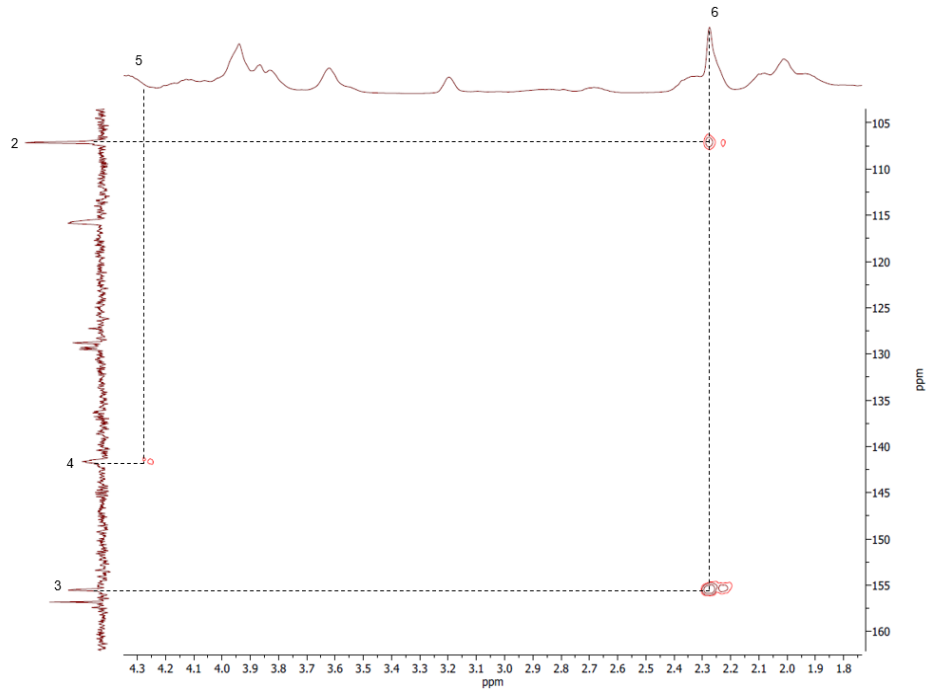

Figure 13: gHMBC spectrum of gelatin-MF.

Gelatin and Gelatin-MF were analyzed through ^{13}C NMR analysis (Figure 12). The chemical shifts of specific carbon atoms, and the evaluation of certain pairwise contribution parameters between the substituents, provide information on the structure of the considered proteins. In particular, gHMBC experiment was performed and permited to obtain a 2D heteronuclear chemical Shift correlation map between long-range coupled ^{1}H and ^{13}C: H-6 (2.3 ppm) correlates with C-2 (107.1 ppm) and C-3 (155.5 ppm), while H-5 (4.3 ppm) correlates with C-4 (141.5 ppm) (Figure 13).

As a further characterization of the successful functionalization, the Fourier-transform infrared spectroscopy (FT-IR) was performed. FT-IR spectrum of Gelatin-MF was compared with that of the untreated gelatin as control. The spectrum of starting material shows the

characteristic two peaks at 1635 and 1535 cm^{-1} (highlighted in green in Figure 14), corresponding to the C=O and -NH- of the amide II respectively. In the case of Gelatin-MF, in blue scale the signals of C=C, C-H and -C-O-C- of the furan rings respectively at 843, 786 and 1079 cm^{-1} can be observed.

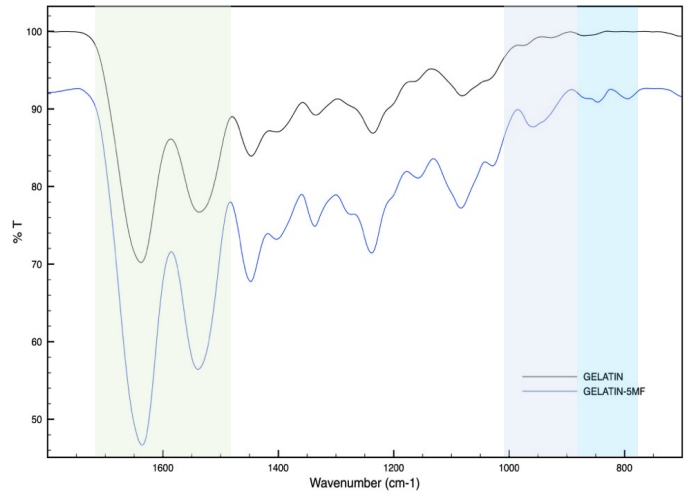

Figure 14: FTIR Gelatin and Gelatin-MF

To better define the features of the functionalized starting polymers, Molecular weight distribution by size exclusion chromatography with triple detector array (HP-SEC-TDA) analysis were employed to characterize gelatin-MF compared to the unfuctionalized protein. The solvent systems induce complete denaturation and loss of higher orders protein structure of gelatin. In this way, good separation is obtained and accurate molecular weight information can be acquired. Chromatographic profiles of gelatin and gelatin-MF have a large bell-shape chromatographic peaks, with a quite high polydispersion index value. The average molecular weight of gelatin has been calculate around 196 kDa (Figure 15).

The obtained results reveal no significant variations in molecular weight values and viscosity between the gelatin and gelatin-MF samples analyzed. As expected, the derivatization of amino groups of lysine to N-methyl-(5-methylfurfuyl), after reductive amination with 5-methylfurfural, does not significatively change the molecular weight values (Table 2).

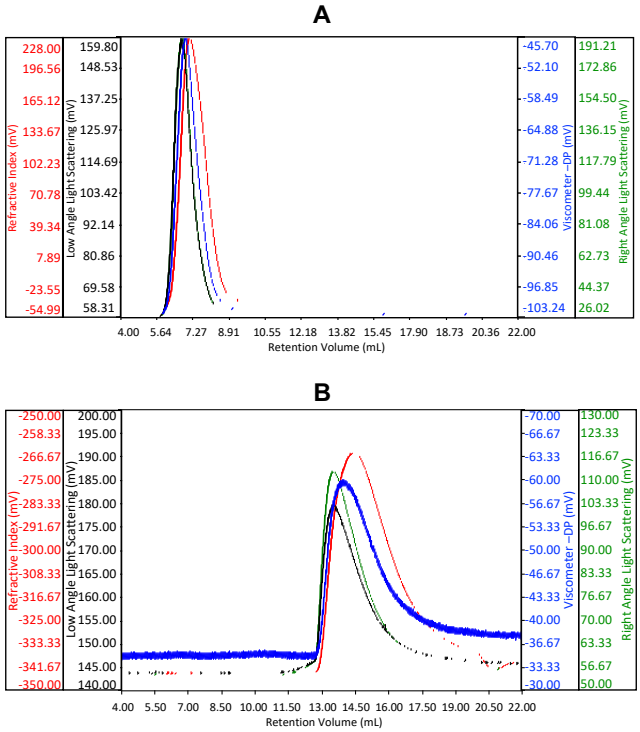

Figure 15: HP-SEC-TDA chromatogram of gelatin (a) and gelatin-MF (b)

Table 2: Main results of the HP-SEC-TDA analysis for the gelatin and gelatin-MF samples.

Sample	Mw kDa	Mn kDa	D (Mw/Mn)	[η] dl/g
Gelatin	210	115	1.9	0.51
Gelatin-MF	196	140	1.4	0.46

1.3 Chitosan-MF Chemical Characterization

Chitosan has been functionalized with 5-methyl furfural and the obtained functionalized biomaterial was characterized through NMR technique. ^{1}H-NMR spectra was acquired in D_2O at 37 °C. By comparison between the assigned integrals of the peaks of H-8 (2.2 ppm), H-10 (6.2 ppm) and H-11 (6.0 ppm) of methylfuran, H-2b (2.6 ppm) on the functionalized monomer of chitosan and H-2a (2.9 ppm) of the unreacted monomers, we estimated the degree of functionalization as 20% (Figure 16).

^{13}C NMR spectra of chitosan-MF compared with chitosan has been performed and gHMBC permitted the assignment of all proton and carbon chitosan chemical shift (Figure 17). In particular, H-8 (2.2 ppm) correlates with C-11 (106.0 ppm) and C-12 (152.7 ppm), while H-7 (2.0 ppm) correlates with C-14 (174.6 ppm) (Figure 18).

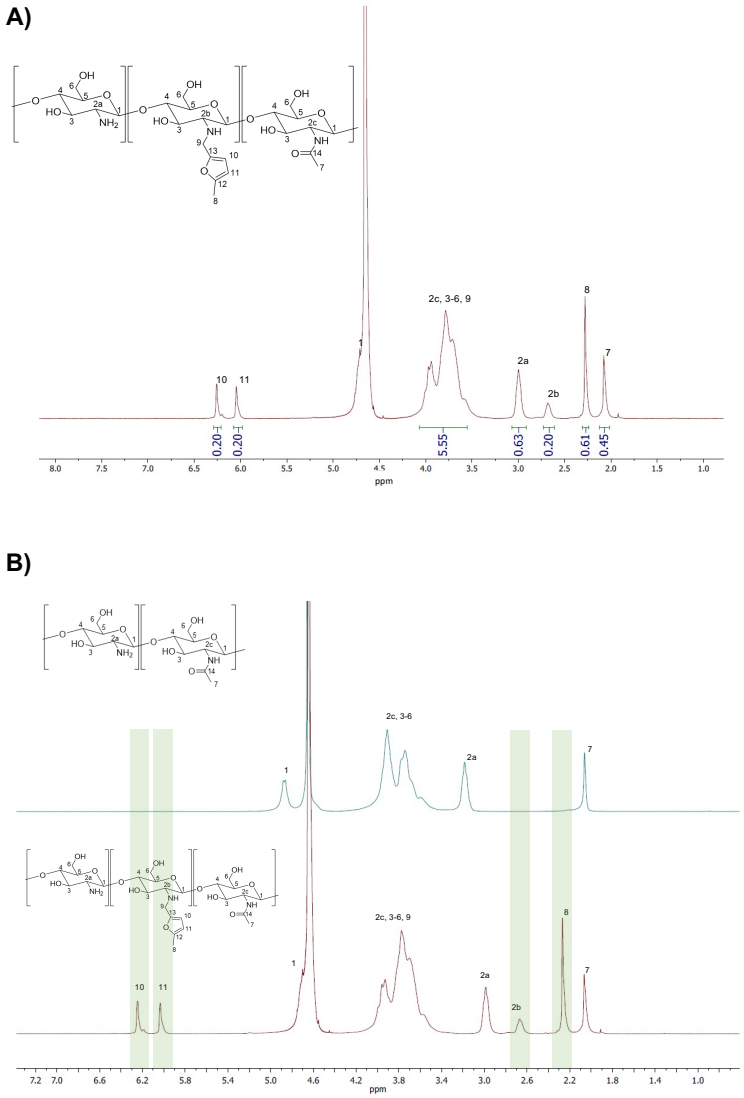

Figure 16: (A) ^{1}H NMR Chitosan. ^{1}H NMR (deuterated PBS pH 7.4 with 0.05% wt 3-(trimethylsilyl)propionic-2,2,3,3-d4 acid sodium salt, 37°C, 400 MHz): δH 6.2 (0.20 H, s), 6.0 (0.20 H, s), 4-3.6 (5.55 H,m), 2.9 (0.65 H, s), 2.6 (0.20 H, s), 2.2 (0.60 H, s), 2.0 (0.45 H, s) (B) Chitosan and chitosan-MF ^{1}H NMR spectra compared.

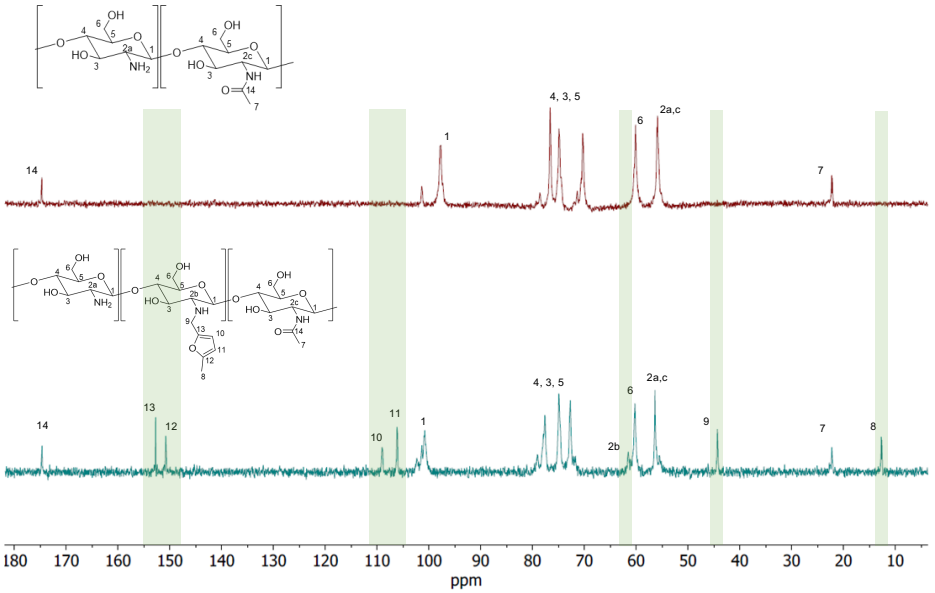

Figure 17: ^{13}C NMR spectra of chitosan-MF compared with chitosan. ^{13}C NMR (deuterated water, 37°C, 400 MHz): δC 174.6, 152.7, 150.8, 109.0, 106.0, 102.2-100.5 (m), 77.5-71.6, 61.4, 60.2, 56.2, 55.4, 44.3, 22.2, 12.7.

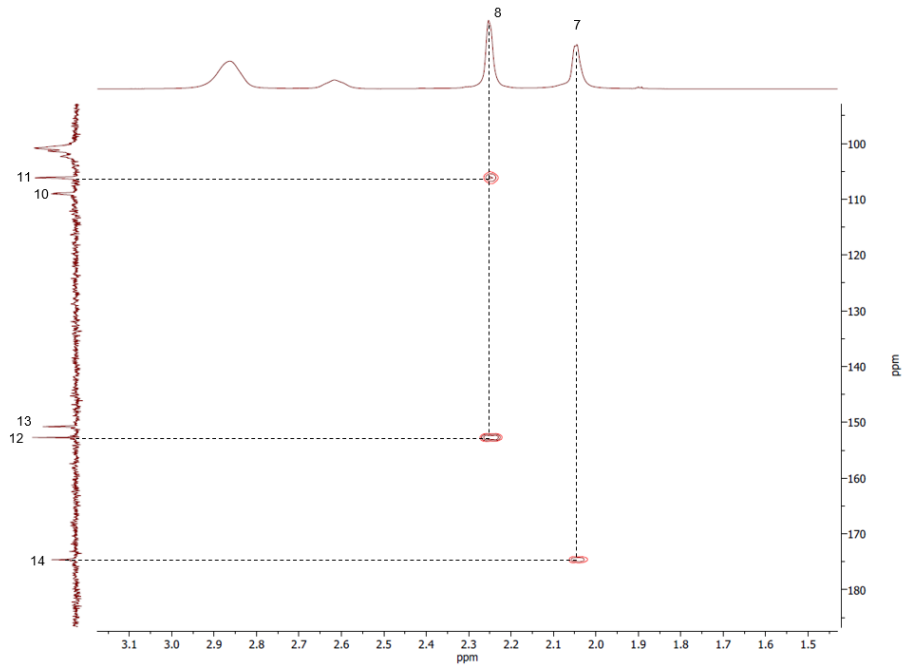

Figure 18: gHMBC spectrum of chitosan-MF.

Examining FT-IR spectrum, variations are detected at 1566 cm^{-1} and 790 cm^{-1} corresponding to C=C stretching and C-H bending of aromatic furan, respectively (Figure 19). Another modification at 1079 cm^{-1} highlighted by yellow band was detect and associated to the alkoxy C-O stretching.

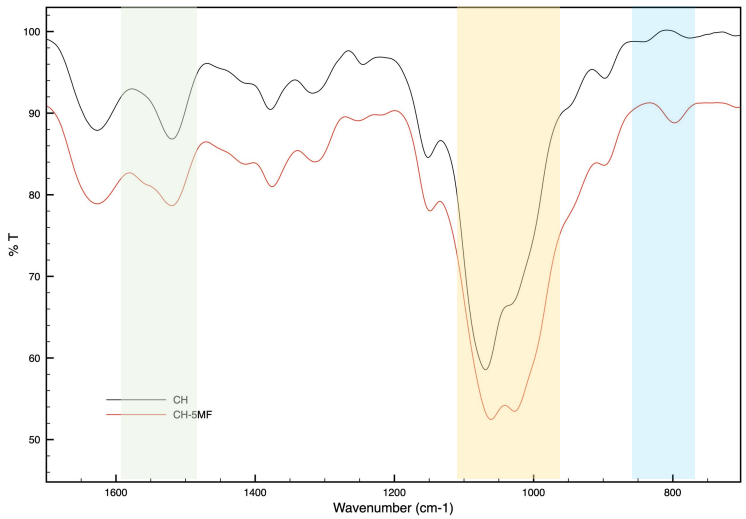

Figure 19: FTIR of chitosan and Chitosan-MF

Molecular weight distribution by size exclusion chromatography with triple detector array (HP-SEC-TDA) analysis were employed to characterize Chitosan-MF compared to the unfuctionalized polysaccharide. The chromatografic profile with a large asymmetric bell-shape chromatographic peak indicate a quite high polydispersion index value (Figure 20). As seen for gelatin, it has not been detected a high variation in chitosan chemical properties indicating that the polymer maintains its structure after the functionalization reaction with 5-methylfurfural with a slight increase in molecular weight (Table 3).

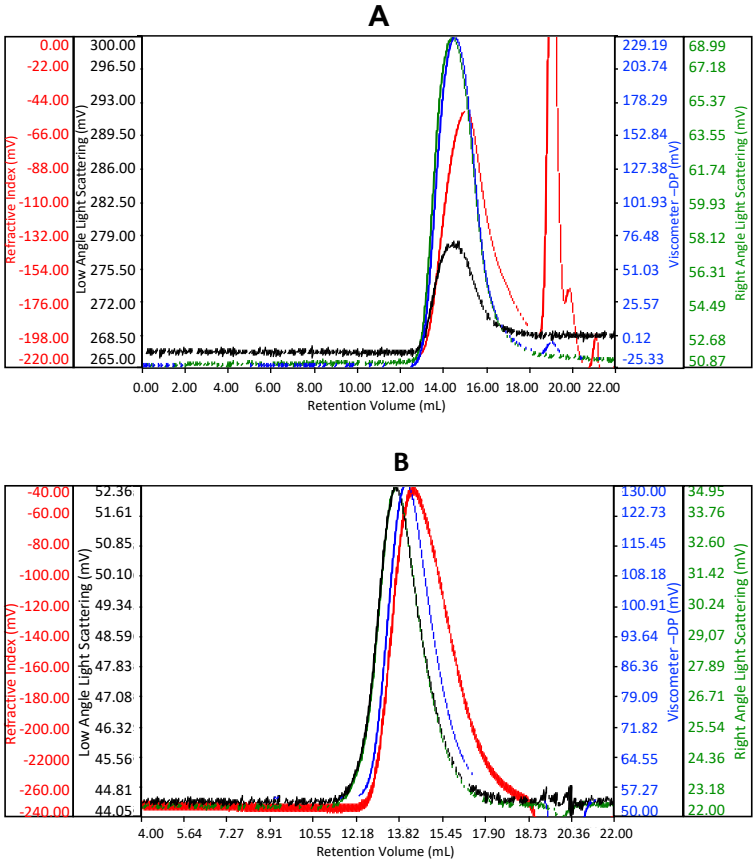

Figure 20: HP-SEC-TDA chromatogram chitosan (A) chitosan-MF (B) samples.

Table 3: Main results of the HP-SEC-TDA analysis for the Chitosan and Chitosan-MF salmples.

Sample	Mw kDa	Mn kDa	D (Mw/Mn)	[μ] dl/g
Chitosan	47.5	28.7	1.7	1.5
Chitosan-MF	57.0	30.0	1.9	1.7

1.4 GelChiDA Characterization

1.4.1 Inverting Tube Test

Together with the starting biomaterials polymers, the hydrogel has been studied and deeply characterized. The very first, rapid and straightforward test is the inverting tube. Thanks to its simplicity and high efficiency, this method is often used to determine the sol-to-gel transition.[180] In the case reported here, it was a valid technique to provide visual evidence of hydrogel formation and its compactness. Indeed, unlike control formulated without PEG-Star-MA addition, hydrogel remains well adhered to the walls of the bottom of the vial, demonstrating mechanical resistance to the gravity force. The test was led at 37 °C, to avoid spontaneous gelatin gelification at lower temperature independent from crosslinking process (Figure 21).

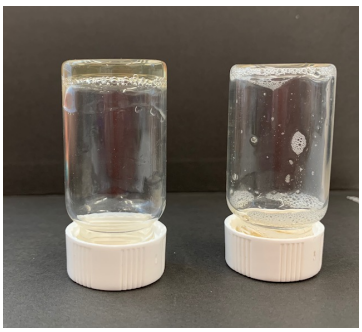

Figure 21: Test inverting tube of GelChiDA and control

1.4.2 Rheological Analysis

Rheological analyses were carried out since they are fundamental for identifying the intervals of strain and applied stress in which the sample respond. The rheological analysis was performed on homogenous GelChiDA hydrogel formulations prepared as previously described.

The rheological analysis was carried out on homogenous hydrogel solutions prepared as described in the Material and Methods section. The strain sweep test (Figure 22A) showed a linear viscoelasticity zone (LVE), where the intrinsic structural properties of the samples are independent of the applied stress and where the storage modulus (G′) is higher than the loss modulus (G′′). In the terminal LVE, the deformation is so large that a liquid-like behavior prevails; that is, the yield point is reached. The crossover points of the dynamic moduli were calculated. GE-CH hydrogel showed a linear strain region up to about 40% (Figure 22A). The 2% strain value was then selected for subsequent sweeps. The crossover point occurred at a very high value of strain. This value of LVE is typical of entanglement networks and strong gels (Ross-Murphy and Shatwell, 1993). Mechanical plots were obtained by means of frequency sweep tests performed at a strain value below the critical strain γc, in the LVE zone (2% for all samples). Measurements of the viscoelastic moduli G' and G" were registered with a range of oscillation frequencies at a constant oscillation amplitude. Figure 22B shows how the viscous (G") and the elastic (G') moduli vary with frequency. The storage modulus G' was higher than the loss modulus G". This reflects the existence of three- dimensional

networks similar to those of strong gels. Thus, in the LVE region, the sample shows solid-like properties. The mechanical plots are representative of hydrogel properties and classification. The hydrogels can be classified as “strong” hydrogels when G’ > G” showing linear viscoelasticity at high strains. “Weak” hydrogels exhibit G′ > G′′ linear viscoelasticity just at low strain values at all the detected frequencies (Lapasin and Pricl, 1995). Consequently, the GE-CH hydrogel under study can be considered as a strong gel because of the slight dependence of G’ and G” on the frequency. The data presented here are similar to those in a study by Martínez-Ruvalcaba et al. (2007) on chitosan/xanthan hydrogels. According to the theory of weak gels (Bohlin, 1980), the assessment of the viscoelastic behavior of hydrocolloid gel allows the quantification of the intensity of colloidal forces acting within the polymer network and the interactions among components that interact with each other to a certain extent, forming a single strand. Therefore, the relationship between the mesostructure of a hydrogel and its rheological behavior can be established. The Bohlin coordination number *z* quantifies the number of flow units interacting with one another to give the observed flow response of the material:

$$G'(\omega) \sim \omega 1z \quad (3)$$

By processing the G’ (w) data of the GE-CH hydrogel, the *z* value was equal to 25.6, confirming the status of the robust structured gel network. Traditional hydrogels are characterized by weak properties if subjected to a mechanical stimulus or stress. Compared to other hydrogels presented in the literature, the growth of the viscoelastic

behavior in response to deformation of the produced GE-CH hydrogel extends the plausible application of the hybrid polymer to different tissue engineering or biomedical applications. In particular, the self-healing properties of hydrogels have an increased value for both 3D bioprinting procedures and injectable systems (Taylor and in het Panhuis, 2016). Therefore, the self-healing properties of the hydrogel were investigated by the application of 800% oscillatory shear strain. After shear removal, the restoration of the dynamic moduli was followed in real time (g 2%, ω 1Hz). The healing efficiency (HE) was calculated according to Equation 3. A value of HE closer to one indicates the more desirable self-healing capability, whereas a value closer to zero indicates less efficient self-healing (the result is shown in Figure 22C). A completely destructured network and transformation into a liquid-like material (G”>G’) are the immediate results of high shear strain (g = 800% for 3 min, ω 1 Hz). Right after cessation of destructive strain, the sample exhibited solid gel responses, with values of instantly restored G′ of around 90% of the original value, with a calculated HE index equal to 0.89. The healed hydrogels were strong enough to sustain repeated stretching; indeed, upon repeating this change of amplitude force, the structure of the hydrogel did not change significantly from that after the first step, and the same healing efficiency (HE=0.88) was obtained. Generally, the self-healing ability of the hydrogel and the time required for the healing process increase with the growth of the viscoelastic behavior in response to deformation of the hydrogels. The observed self- healing properties of the hydrogel

may be related to the physical interactions between the amino groups of chitosan and the carboxylic groups of gelatin.

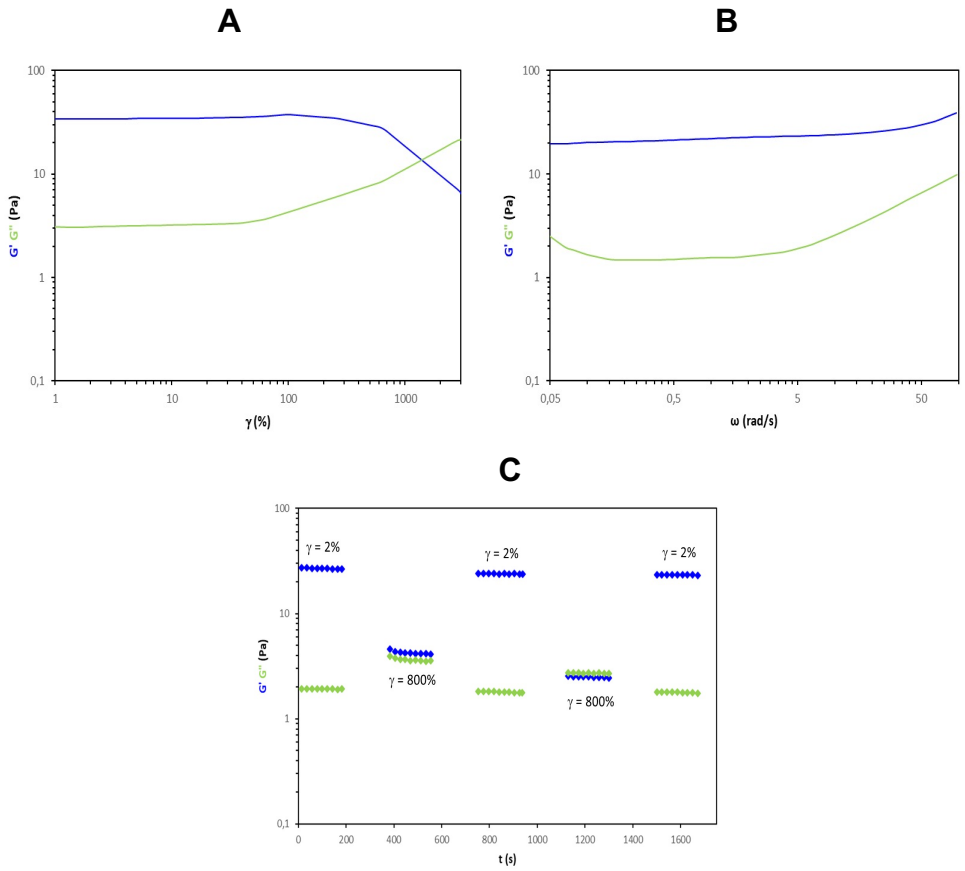

Figure 22: **A)** Storage (G , blue) and loss (G , green) moduli vs. oscillation strain (γ) for GE-CH. **(B)** Storage (G′, blue) and loss (G , green) moduli vs. angular frequency (ω) for GelChiDA hydrogel. **(C)** Structural recovery behavior of the GE-CH as a function of time, assessed by monitoring G′(t) (γ2%, ω1 rad/s) after destruction by applying an 800% oscillatory shear strain. Modulus G′ (blue) and G" (green).

1.4.3 Swelling Analysis

An important property of biomaterials is the ability to undergo volumetric changes, in response to increased water uptake in physiological wet tissues. Therefore, the swelling analysis was performed according to the literature.[181] To determine GelChiDA swelling properties, dried samples were immersed in PBS (pH 7.4) at 37 °C and the weight measured at intervals for days, until reaching a stationary condition. The following equation was employed to calculate the swelling ratio:

$$Swelling\% = \frac{\mathrm{Ws} - \mathrm{Wd}}{\mathrm{Wd}}\ x\ 100$$

[Wd = Weight of polymer; Ws = weight of swollen polymer]

The construct showed the highest swelling rate between 2 and 24 hours followed by an important decrease probably due to a free polymer chain organization during the water uptake. An equilibrium has been reached at 72 hours, and the structure has been maintained for 40 days (Figure 23).

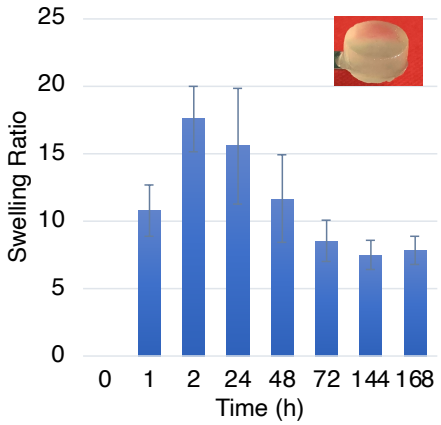

Figure 23: GelChiDA swelling in PBS pH7.4

1.4.4 Scanning Electron Microscope (SEM) Analysis

The dried samples obtained as previously described were analyzed under the scanning electron microscope (SEM). SEM images are collected at different magnifications and allow for greater resolving power compared to optical microscope images, given the shorter length wave of electrons with respect to photons. This type of microscope works with greater depth of field, going to capture good images to evaluate the porosity of the scaffold. GelChiDA SEM images has been compared with those of control, made up following the same protocol excepted for addition of PER-Star-MA crosslinker. The analysis shows that GelChiDA displays a more regular compact and porous structure with much smaller pore size compared to the control, probably due to the crosslinking reaction (Figure 24).

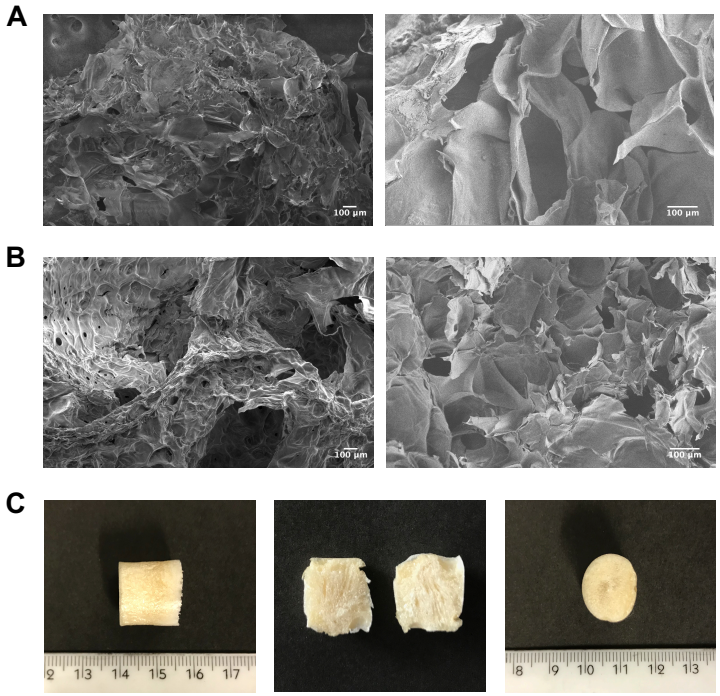

Figure 24: A) Control's SEM analysis, made by no-functionalized polymers B) GelChiDA SEM analysis C) GelChiDA dried sample.

1.4.5 UV and FT-IR Analysis Real Time

As the starting biomaterials, the hybrid obtained construct was characterized through FT-IR analysis. To follow the progress of the reaction, the sample was freeze-dried at different time in liquid nitrogen during the Diels Alder crosslinking reaction. Each sample was freeze-dried and reduced in powder before the FT-IR analysis. The obtained spectra show an intensity decrease of signal at 862 cm^{-1} over the time, attributed to C-H vibration of double bond in furan ring, meaning the ongoing Diels Alder reaction and and the consequent adduct formation (Figure 25).

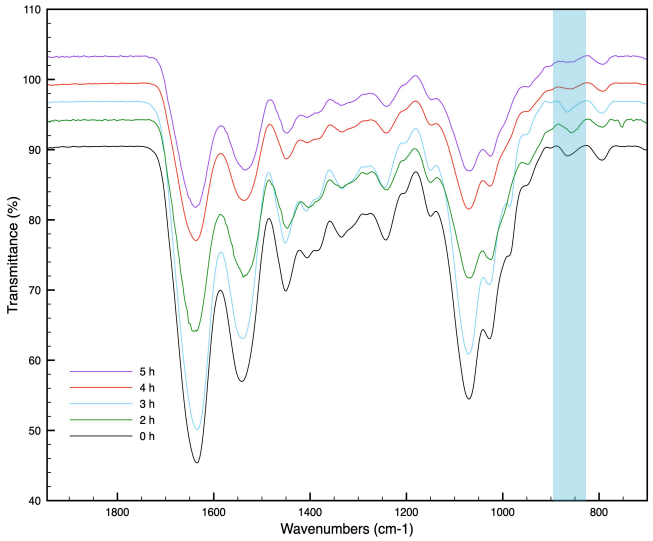

Figure 25: FT-IR spectra of GelChiDA Diels Alder Reaction

The kinetics of the Diel Alder reaction was studied with UV analysis by following the maleimide peak at 293 nm. The reaction between the furan ring and the maleimide, which bring to the adduct formation, was associated to the maleimide peak decrease as shown in Figure 26.[182] Scattering effect causes absorbance increment in all the samples.

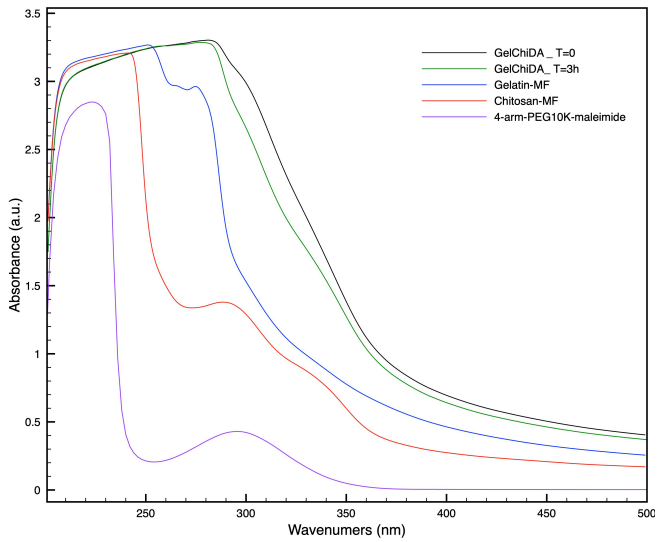

Figure 26: UV spectra of cross-linking reaction in real time

1.4.6 NMR Characterization

The NMR peaks identified in both starting polymers were employed to choose the right signals in order to follow the reaction kinetics. The analysis was carried out in deuterated PBS (dPBS) at pH 7.4 at 37 °C: 1ml of hydrogels was prepared as previously described and immediately inserted into a NMR tube after the addition of PEG-Star-MA to follow the cross-linking kinetics until completion. Spectral variations, such as reduction in peak intensities, line broadening, and chemical shift changes, are all aspects monitored to assess the degree of cross-linking reaction and to determinate the reaction kinetics.

In particular, the maleimide peak at 6.9 ppm, has been identified as overwhelming evidence of the reaction (Figure 27).

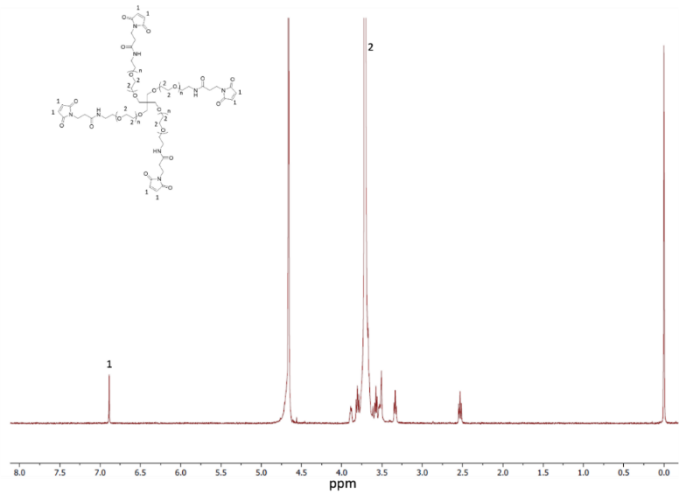

Figure 27: ^{1}H NMR spectrum of 4arm-PEG10K-Maleimide. ^{1}H NMR (deuterated PBS pH 7.4 with 0.05% wt 3-(trimethylsilyl)propionic-2,2,3,3-d_4 acid sodium salt, 37°C, 400 MHz): δ_H 6.90 ppm (8H, s), 3.71 ppm (PEG backbone, s)

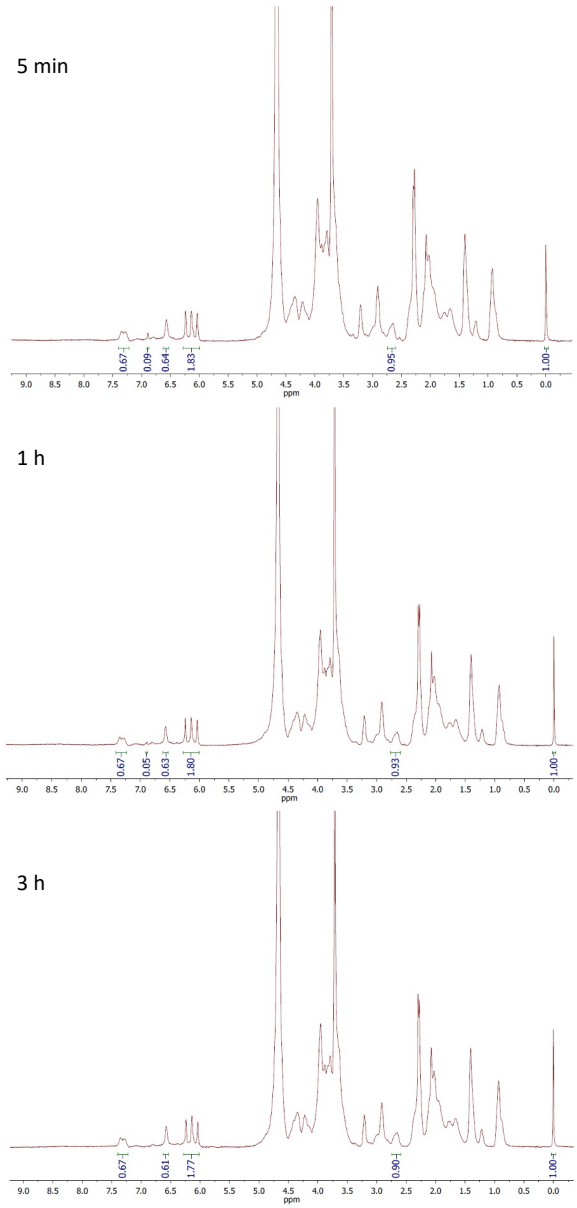

Figure 28: ^{1}H NMR spectrum of hydrogel at 5 minutes and 3 hours.

Figure 28 and Figure 29 show the spectra of the hydrogel formation in real time. Observing the comparison of timepoints of the kinetics, the signal at 6.9 ppm, assigned to maleimide moieties, a progressive lowering of the intensity of the peak is clear until disappears after 3 h.

Concurrently, a decrease attributed to furan ring peaks at 6.0 and 6.6 ppm were detected, indicating a partial MF conversion into the Diel Alder adduct (Figure 28). Moreover, the peak influenced by the signal of H-2 of chitosan-MF at 2.6 (CHN) shift by experiencing a change in the neighboring chemical environment, coherently with the reaction advance. A shift of the methyl motifs at 2.2 and 2.3 ppm is detectable as highlighted in Figure 29 B.

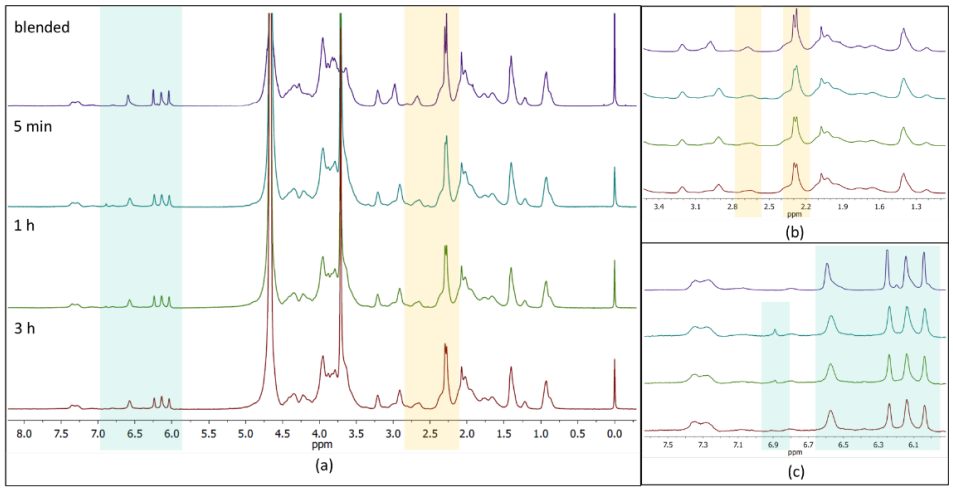

Figure 29: Comparison between ^{1}H NMR spectrum of blended polymers and real-time gel formation at 5 min, 1 h, and 3 h (a) with a focus on the area between 1–3.5 (b) and 6–7.5 ppm (c). at 5 min, 1 h, and 3 h (a) with a focus on the area between 1–3.5 (b) and 6–7.5 ppm (c).

A deeper characterization has been performed using DOSY-NMR spectroscopy, a technique based on the application of pulsed field-gradient (PFG), became the method of choice for determining and measuring the diffusion of molecules in solution. In principle, the diffusion coefficient of a molecular species, under certain conditions (e.g. specific concentration, solvent and temperature), depends on its actual molecular weight, size and shape. By measuring the diffusion

coefficient of a given molecular species, under controlled conditions, it is possible to obtain information on its actual size and molecular weight, and consequently also on its interactions with the surrounding environment and possibly other molecules. For this reason, DOSY-NMR analysis has been used to study and evaluate the effective interaction of the biopolymers in solution, resulting as a change in the molecular weight and thus the diffusion coefficient of the sample in solution. In Figure 30 the GelChiDa and blended spectra are compared and have two distinct diffusions, differing on average 1.10–1.11 m / s^2. Observing the graph of the hydrogel, the different signals appear on a straight line, with little difference from each other, indicating that all the polymers in solution are linked together to form a single construct. Conversely, gelatin and chitosan appear on two different levels in the blended sample, being unbound and having different molecular weights.

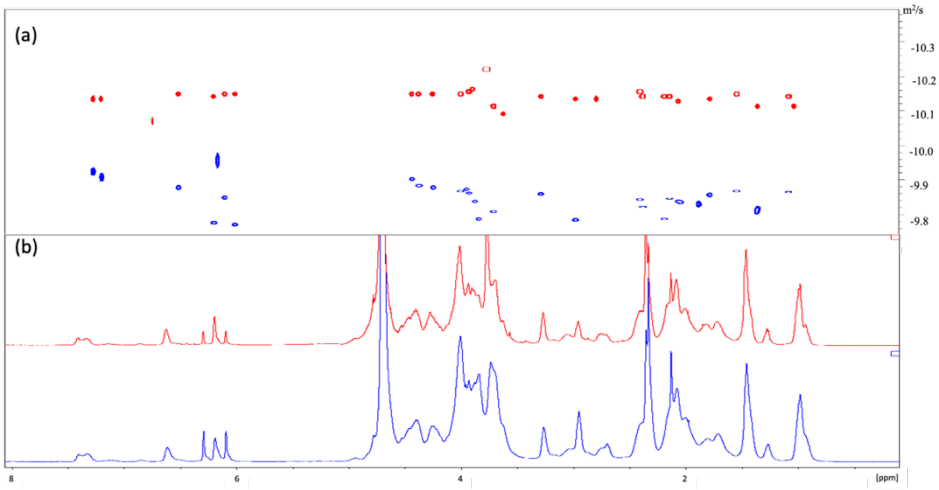

Figure 30: (a) Diffusion ordered spectroscopy NMR (DOSY) and (b) ^{1}H NMR spectra of blended (blue) and hydrogel (red) at the end of kinetics.

1.4.7 Thermogravimetric Analysis (TGA)

TGA is an analysis method in which the continuous recording of the mass variations of a sample in a controlled atmosphere as a function of temperature or time is carried out. The resulting diagram is called a thermogram or thermal decomposition curve. This technique has been selected to evaluate whether crosslinking has changed the material's thermal resistance properties. Samples TGA curve appears having a similar trend composed from two degradation steps. The first is probably due to the water content weight loss and occurs around 67-88 °C for all the materials. The second step takes place in a wider temperature range in view of biopolymers' collapse (Table 4). The TGA graphs show that the functionalization of biomaterials slightly increased the heat resistance capacity, compared to the starting materials (Figure 31). The GelChiDA hybrid hydrogel shows an average behavior between the two starting functionalized polymers at the corresponding stage, as it has a main degradation temperature higher than chitosan but lower than gelatin. Interestingly, GelChiDa has a lower % weight loss at high temperatures than all other materials, showing higher stability at high temperatures.

Table 4: TGA analysis results of GelChiDA compered to starting functionalized biopolymers

	Water desorption			Degradation		
	Peak (°C)	Range (°C)	Weight loss (%)	Peak (°C)	Range (°C)	Weight loss (%)
Gelatin	75	27-156	10.6	319	184-606	67.4
Gelatin-MF	67	27-148	8.6	324	170-604	68.1
Chitosan	88	27-155	12.9	226	180-361	44.7
Chitosan-MF	76	27-150	9.3	235	161-343	40
GelChiDa	75	27-156	8.2	309	167-650	55.3

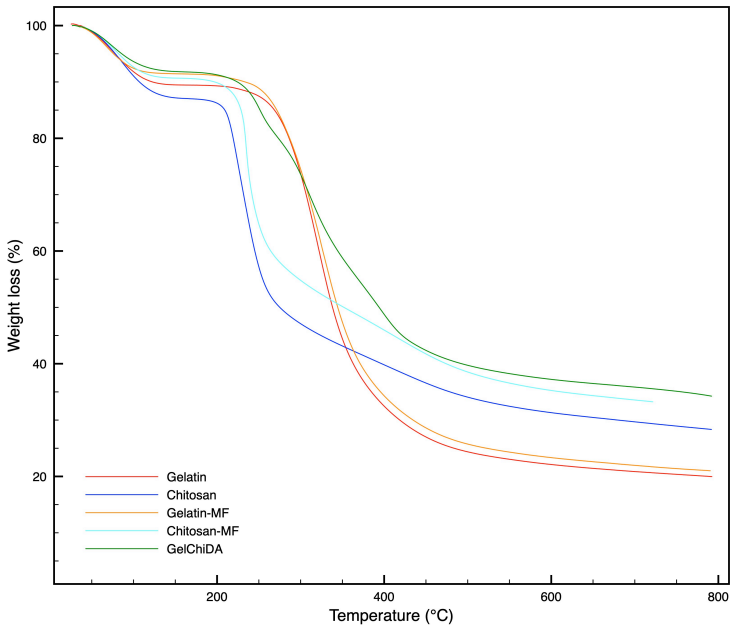

Figure 31: TGA curves of unfunctionalized and functionalized starting materials and GelChiDA.

1.5 Bioogical Evaluation

1.5.1 3D Bioprinting Model

The bioprinting protocol was assessed, adapting the printing condition of the hydrogel to cell culture. The formulation was printed after 2.5 hours, where the construct is in a jelly state, able to maintain the shape while the crosslinking reaction is still occurring. This strategy allows the hydrogel extrusion at low pressure, so that it does not affect cell viability. Furthermore, the semi-gel state allows to obtain a homogeneous bioink because it is possible to suspend the cells without concentration variability or cellular aggregates in the bioprinted constructs. To evaluate the compatibility of the novel hydrogel formulation with cell culture a viability test was conducted. The LIVE / DEAD® viability / cytotoxicity assay allows the detection of live cells and dead cells with two different fluorescent probes that recognize the intracellular esterase activity and the integrity of the plasma membrane. Live cells fulfill ubiquitous intracellular esterase activity, detected by the enzymatic conversion of calcein AM, a non-fluorescent cell permeant, into the deep green fluorescent polyanionic dye calcein (etc / em 495 nm / 515 nm). Cells with damage to the plasma membrane are instead permeable to ethidium homodimer-1 (EthD-1), which by binding to nucleic acids produces a red fluorescence, thus identifying dead cells (etc / em ~ 495 nm / ~ 635 nm). The LIVE / DEAD® test showed that the printing process does not significantly affect cell viability. As shown in Figure 32 which represents bioprinted GelChiDA, cell viability is guaranteed. Most of the cells within the

hydrogels are viable (green) at the different experimental times examined (day 1, day 3 and day 6).

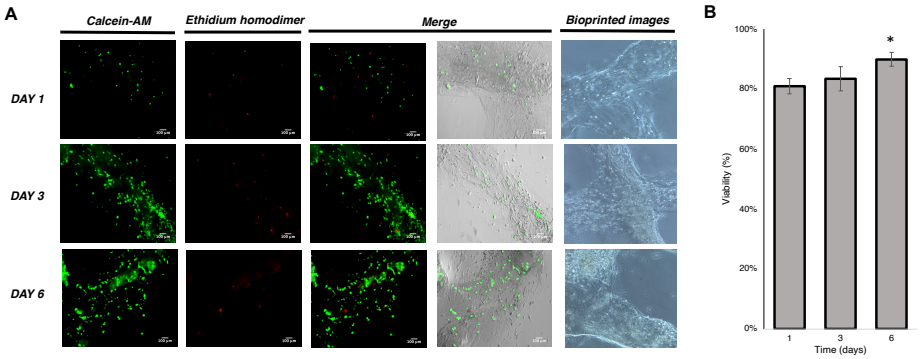

Figure 32: **A** LIVE/DEAD imaging of bioprinted U87 cells; **B** Resulting LIVE/DEAD histograms of viability's bioprinted cells. (Mean ± *SD* One-way ANOVA, $n = 3$: $*p < 0.005$).

1.5.2 3D Spheroid Cultures

To go further and to investigate the range of GelChiDA applications, 3D cell spheroid screening has been performed. Tumor microenvironments in vivo display multiple barriers to the penetration of antibodies, immunoconjugates or drugs and are therefore difficult to study *in vitro*. Cells cultured as monolayers show less resistance to therapy, requiring the development of more representative alternative models of the tumor as found in vivo. This difference in sensitivity can be explained as "multicellular resistance", a drug-resistance mechanism conferred by cell-cell contacts, cell-matrix network and the three-dimensional shape assumed by the tissue. Multicellular resistance acquired by tumor cells may contribute to the difficulty of translating promising results obtained with *in vitro* studies into therapy.

In vitro cultures of multicellular tumor spheroids have started to fill the gap between in vivo tumor complexity and monolayer cell cultures and have become valuable models for studying drug resistance. Therefore, several commercial materials are under investigation to better control the integrity of spheroid, to study the effect of the microenvironment, and to build up complex tissue-like studies. The viability of spheroids embedded in synthetic matrices or polymers has, in any cases, some limitations. Natural materials can induce undesirable phenomena, such as cell migration and differentiation, or, in certain cases, can be toxic or not appropriate for cell-adhesion purposes.[183]

The GelChiDA costruct was employed as a hydrogel to encapsulate and maintain U87 3D spheroids. U87 spheroids were cultured until obtaining spheroidal structures and a 500 μm diameter. GelChiDA hydrogel was employed to embed the 3D spheroids and to follow their integrity and viability over time. The preliminary results of spheroids hydrogel embedded are show in Figure 33.

By staining with H&E, cells in the external layer exhibit a polygonal morphology and tend to be tightly packed, while, in the center of the spheroid, U87 cells are fusiform and less densely packed. However, during all the monitored spheroid culture, cells appear viable and proliferative and do not show morphology suggesting sufferance or degeneration. An interesting observation for the produced hydrogel is related to its ability to maintain the spheroid dimensions and structure, maintaining viability over the culture time points, whereas many of the commercially available matrices result in increased cell migration.

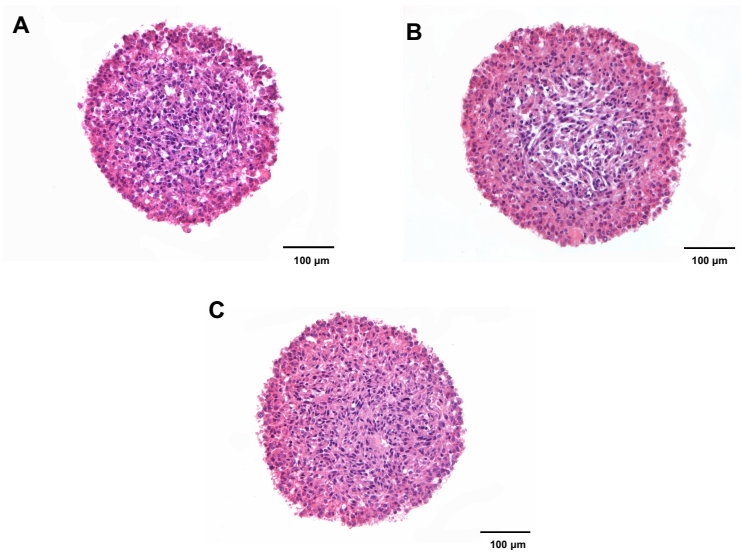

Figure 33: Histological images of spheroids embedded in hydrogel at days 1 **(A)**, 3 **(B)**, and 6 **(C)**.

2. MATERIALS AND METHODS

2.1. Materials

Water-soluble chitosan was purchased from Carbosynth Ltd, UK. A LIVE/DEAD Cell Viability Assay was purchased from ThermoFisher. All other chemicals were purchased from Merck KGa, unless differently stated, and used as received without further purifications. Deionized water (conductivity less than 0.1 S) was prepared with an inverse osmosis system (Culligan, Milan, Italy). PolyCAL TM Pullulan std-57k (Malvern Instruments LtD, Malvern, United Kingdom). The reagent grades were 98%.

2.2. Methyl-Furan Gelatin Functionalization (Gelatin-MF)

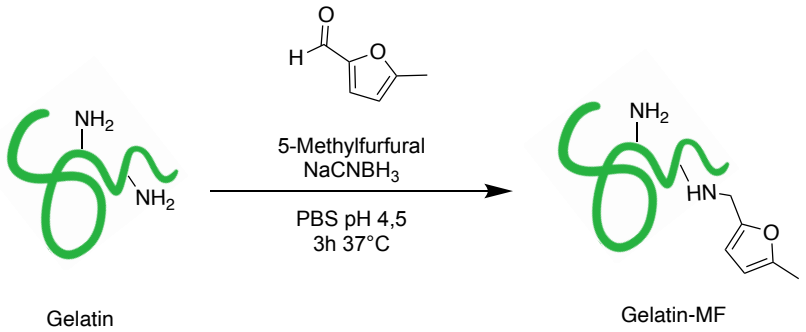

Scheme 2: Functionalization of Gelatin with Methyl-Furan through reductive amination.

Reagents	MW (g/mol)	Eq.	Mass (g)	Mol (mmol)	d (g/ml)	V (ml)
Gelatin-Lys (considering 5% of Lys)	146.19	1	2	0,684		
5-methylfurfural	110.1	100	7,52	68,37	1,107	6,8
$NaCNBH_3$	62,84	50	2,15	34,2		
PBS pH 4.5						30

To functionalize Gelatin, 30 ml of PBS at pH 4.5 were employed to completely dissolved Gelatin type A (2.00 g) powder at 37 °C under agitation. Once a homogeneous solution was obtained, 6.8 ml of 5-methyl furfural was added and left under gentle stirring at 37 °C. After 30 min, the amine first reacts with the carbonyl group to form

a hemiaminal species, which subsequently loses one molecule of water, to form imine. 2.15 g of $NaCNBH_3$ was added in order to reduce the intermediate in the final amine. The reaction occurs in 3 h at 37 °C. Dialysis has been use as purification method using a 14 kDa cellulase membrane at 40 °C. Dialyzation has been performed against a NaCl solution (0.1M) for 1 day, followed by mQ H_2O for 4 days. The obtained solution was filtered using 0.45 and 0.22 μm filters and then freeze-dried to give 1.73 g of a white spongy solid (Scheme 2).

2.3. Methyl-Furan Chitosan Functionalization (Chitosan-MF)

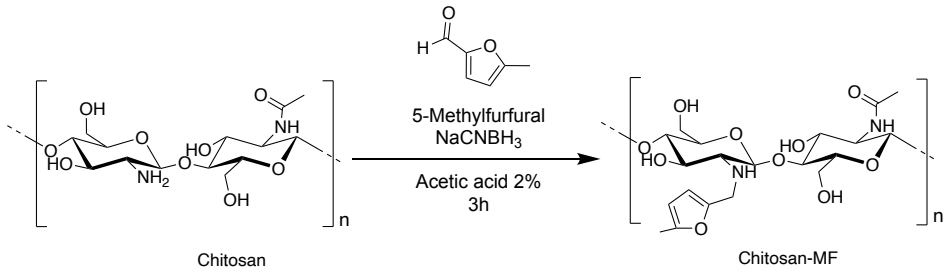

Scheme 3: Functionalization of Chitosan with Methyl-Furan through reductive amination.

Reagents	MW (g/mol)	Eq.	Mass (g)	Mol (mmol)	d (g/ml)	V (ml)
Chitosan	146.19	1	2	0,684		
5-methylfurfural	110.1	100	7,52	68,37	1,107	6,8
$NaCNBH_3$	62,84	50	2,15	34,2		
2% Acetic Acid						35

To functionalize Chitosan, 35 ml of 2% acetic acid solution were employed to completely dissolved Chitosan soluble powder (2.00 g). Sonication and vortex were used to speed up the dissolving process. 206 µl of 5-methyl furfural was added, and left under gentle stirring for 30 min. 65 mg of $NaCNBH_3$ were added, and the mixture was left to react under agitation for 3 h at room temperature. After that, the

reaction was dialyzed with 14 kDa cellulose membrane, against against a NaCl solution (0.1M) for 1 day, followed by mQ H_2O for 4 days at room temperature. The obtained solution was filtered using 0.45 and 0.22 μm filters and then freeze-dried to give 1.37 g of a white spongy solid (Scheme 3).

2.4. GelChiDA Hydrogel Formulation

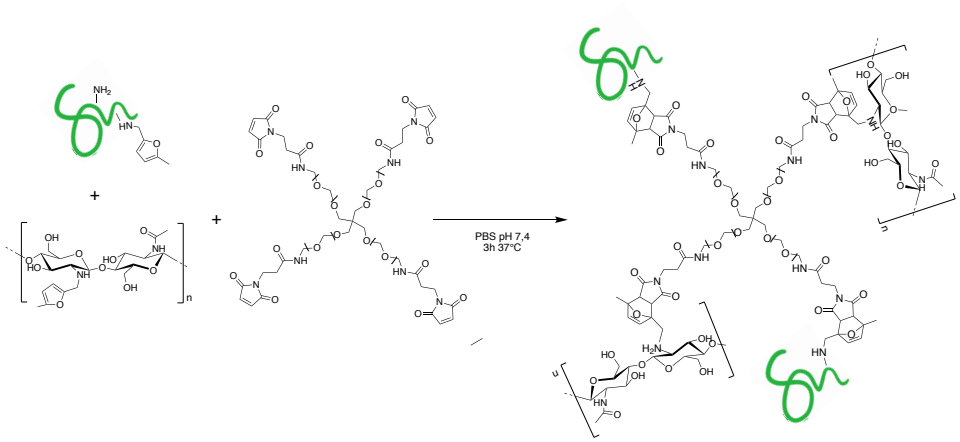

Scheme 4: Functionalization of Gelatin with Methyl-Furan through reductive amination.

Reagents	Eq.	Mass (g)	V (ml)
Chitosan-MF	1	16	
Gelatin-MF	2	33	
PEG-Star-MA	0.16	2.5	
PBS pH 7.4			1

In order to formulate the novel hybrid platform, to maintain the viability of embedded cells and to better control the reactivity, click chemistry has been chosen as crosslinking method. The hybrid hydrogel obtained through a Diel Alder (DA) reaction between methyl furfural and functionalized Chitosan (Chi) and Gelatin (Gel) has been called GelChiDA. As dienophile group a commercial maleimide functionalized PEG-star has been employed. Different amount of 4arm-PEG10K-Maleimide (PEG-Star-MA) and various two polymers ratio combinations were investigated in order to obtain the best kinetics hydrogel for the final construct. The hybrid hydrogel with % m/V ratio

of CH:GE:Peg-star= 1:2:0.16 of the final biopolymers concentration of 5% (50 mg/ ml) was selected. To formulate the bioink gelatin-MF (33 mg) and chitosan-MF (17 mg) were dissolved in 0.750 ml of PBS at 7.4 pH by vortexing at 37 °C until complete dissolution. PEG-Star-MA (2.5 mg) was dissolved in 0.250 ml at RT and added to the mixture. The reaction occurred in 3 hours at 37 °C (Scheme 4).

2.5. SEM Analysis

The gelatin-MF, chitosan-MF, and PEG-Star-MA solution formed as previously described was transferred into Teflon molds (15 mm diameter) and left for 3 h at 37 °C. Once the Diels-Alder reaction had occurred, the sample was transferred at –80 °C for 24 h and then freeze-dried for 48h to obtain cylindrical compact structure. SEM was employed to characterize the cross-section of the fibrous dried samples obtained. Samples from lyophilization were mounted onto SEM stubs with conductive adhesive carbon tape and silver paste, and sputter coated with 10nm chromium by means of high vacuum Quorum Q150T coating system. SEM-SE (Scanning Electron Microscopy - Secondary Electrons) micrographs were acquired by means of High Resolution Field-Emission Zeiss Gemini 500 SEM, operating with 5kV acceleration voltage.

2.6. Molecular Weight Distribution by Size Exclusion Chromatography with Triple Detector Array (HP-SEC-TDA) Analysis.

Evaluation of the molecular weight distribution of gelatin and gelatin-MF samples was performed by Size Exclusion Chromatography coupled with a multi-detector system (refractive index, right and low angle light scattering, viscometer, Viscotek mod. 305 Triple Detector Array, Malvern Instruments LtD, Malvern, Uk).[184] In particular, the analysis of gelatin was performed at 40 °C, using on TSKPWXL column (Tosoh Bioscience, 7.8 mm ID x 30 cm). A total of 0.01 M K buffer + 0.125 M $NaNO_3$, containing 0.05% NaN3, pre-filtered using 0.22 μm filter (Millipore), was used as mobile phase at a flow rate of 0.6 mL/min. 0.1 mL of sample were injected at about 1 mg/mL. Chromatographic conditions for gelatin-MF were set up using two TSKPWXL columns in series (Tosoh Bioscience, 7.8 mm ID x 30 cm, V_0 6 mL, Vt 11 mL each one) with an aqueous solution of 0.2 M $NaNO_3$ added with 0.05 % NaN_3 pre-filtered onto 0.22 μm filter (Millipore), used as mobile phase at a flow rate of 0.6 mL/min. 0.1 mL of each sample were injected at about 1 mg/mL. For both methods columns, injector and detectors were maintained at 40 °C. For chitosan and chitosan-MF samples, chromatographic conditions were set up using two gel columns TSKWXL mixed bed column (Tosoh Bioscience, 7.8 mm ID x 30 cm, V_0 6 mL, Vt 11 mL) with an aqueous solution of 0.3 M Sodium Acetate, 0.3 M Acetic Acid (pH 4) added with 0.05 % NaN_3 pre-filtered onto 0.22 μm filter (Millipore), used as mobile phase at a flow rate of 0.6 mL/min. 0.1 mL of each sample were injected at about 1 mg/mL.

Columns, injector and detectors were maintained at 40 °C. The detector was calibrated with the Pollulan narrow standard of known Mw, polydispersity, and intrinsic viscosity (Malvern Instruments LtD, Malvern, Uk). The chromatogram elaboration was performed using OmniSEC software version 4.6.2. For calculations, a differential refractive index increment (dn/dc) value of 0.180 for gelatin and its derivates and 0.167 chitosan and its derivates were used for converting RI voltages to solute concentration at each data slice across a chromatographic peak, as previously described.[184–186] The obtained Mw ad Mn values were rounded to the nearest 1000 Da.

2.7. FTIR-ATR

FT-IR was adopted to characterize the starting materials and to follow the Diel Alder reaction at different time point. The starting materials, after being freeze-dried, were placed on the steel instrument surface and measured at different regions. To record the GelChiDA reaction steps, the hydrogel was prepared as previously described, and freezed using Liquid Nitrogen to stop immediately the reaction. Once freeze-dried the samples were reduces in powder and analyzed. The absorption spectral range was collected between 4000 cm^{-1} and 650 cm^{-1} at a spectral resolution of 2 cm^{-1} and 40 scans and analysis were performed using PerkinElmer Spectrum 100 FTIR Spectrometer.

2.8. UV–Vis Measures

The UV-Vis absorption-solution was use to follow the rection kinetics from 0 to 3 hours. JASCO V-770 spectrophotometer was employed to record region between 200-500 nm. 1 mL of the hybrid GelChiDA starting solution was transferred into a quartz cuvette with a 0.1 mm optical path immediately after crosslinking addition. The sample has been maintained at 37 °C in between the measurements, to avoid gelatin gelification at RT.

2.9. Nuclear magnetic Resonance Spectroscopy Experiments

^{1}H-NMR and gHMBC spectra were acquired using a Varian 400 MHz Mercury instrument, operating at a proton frequency equal to 400 MHz at 37 °C. The preparation of the sample has been maintained as previously reported excepted for deuterated PBS pH 7.4 which was adopted as solvent. 0.05% wt of 3-(trimethylsilyl)propionic-2,2,3,3-d_4 acid sodium salt (0 ppm) was employed as internal standard. For all polymers analysis the pulse angle and the relaxion delay were set at 90° and 2 seconds respectively, while the number of scans varied between 160 and 240 depending on the signal-to-noise ratio. The hydrogel kinetics of GelChiDA was monitored by the acquisition of ^{1}H-NMR spectra over time, using 16 scans, with a pulse angle of 90° and 20 s of relaxation delay. Every 10 min, a spectrum was recorded for a total of 32 spectra. gHMBC spectra were obtained with 200 increments

of 512 transients each and relaxation delay of 2 s. The gHMBC experiment was optimized for long-range J-coupling ^{1}H-^{13}C of 8 Hz.

2.10. Diffusion Order Spectroscopy NMR (DOSY)

DOSY experiments were performed on GelChiDA hydrogel and on blended form. The latter was prepared with the hydrogel protocol and concertation except for the 4-arm-PEG10K-maleimide addition. The experiments were performed at 37 °C with Bruker ADVANCE NEO, 500 MHz spectrometer (Bruker, Karlsruhe, Germany) equipped TCI cryo-genic probe of 5mm and measured using the 2D stimulated echo sequence (STE experiment) using bipolar gradient pulse for diffusion. In ^{1}H dimension of the diffusion experiments a sweep width of 20 ppm was used. The diffusion time (Δ) and the gradient pulse (δ) were set to 300 ms and 5 ms respectively. The 2D DOSY experiments were acquired using the 2D-stimulated echo sequence with bi-polar gradient pulse for diffusion with gradients varied linearly from 5 to 95% in 32 steps with 16 scans per step. Spectra were processed by Top-Spin 4.0.6 software. A 1-Hz line broadening Lorenzian function was applied, and each row was phased and baseline corrected before Fourier transformation in the F2 dimension. The diffusion coefficients D for the 1H dimension in which molecules with different diffusion coefficients correlate to two distinct signals were calculated with Bruker Dynamic Center 2.5 (Bruker, Karlsruhe, Germany). The fitted function used is $I = I_0^{(-D\cdot x^2\cdot \gamma^2\cdot \delta^2)\cdot(\Delta-\frac{\delta}{3})}$ where I is the observed intensity, I_0 the reference intensity, x the gradient strength, D the diffusion coefficient, γ the

gyromagnetic ratio of the observed nucleus, δ the length of the gradient and Δ the diffusion time.

2.11. Rheological Analysis

The rheological properties of the hydrogel were studied using a CMT rheometer (DHR-2, TA Instruments, USA) equipped with a 40-mm-diameter plate–plate geometry. For all tests, the temperature and the gap between the plates were kept constant 37 °C and 1.0 mm, respectively, and a solvent trap was used to prevent loss of solvent. The viscoelastic behavior of the material at the mesoscale was investigated by means of dynamic measurements and quantified through the storage modulus [or elastic component of the complex modulus G∗(ω)] G'(ω), and the loss modulus [or viscous component of the complex modulus G∗(ω)] G"(ω) [Pa]. G'(ω) and G"(ω) characterize the solid-like and fluid-like contributions to the measured stress response that follows a sinusoidal deformation of the tested material, respectively. The range of linear viscoelastic response under oscillatory shear conditions was identified by means of a strain sweep test: the sample was subjected to an extended field of strains (0.01–100%) at a constant frequency of 1 Hz. The mechanical plots were then drawn by performing a frequency sweep test over the 0.01–100 rad/s frequencies at a constant strain (2%). Finally, a step strain sweep test was carried out to investigate the self-healing properties of the sample in response to applied shear forces. Viscoelastic properties were measured as a function of time in an oscillatory time sweep (3 min, 2% strain, 1 Hz frequency) before and after severe destruction of the gel

network (800% strain, 3 min, 1 Hz frequency). The extent of the self-healing behavior was calculated according to Zhao et al. (2014)[187] as the ratio of the storage moduli of the healed (G′h) and pristine gels (G′p). Data were analyzed with TRIOS 3.0.2 software.

2.12. Cell Culture

Human glioma U87-MG cells were maintained in adhesion condition in T75 tissue culture flasks. U87 cells were cultured in Dulbecco's modified Eagle's medium supplemented with 10% fetal bovine serum, 100 units/ml penicillin, and 100 mg/ml streptomycin at 37 °C under a humidified atmosphere with 5% CO_2.

2.13. Bioprinting Process

GelChiDA was formulated as previously reported, sterilized for 30min under UV-light and 2 h at 37 °C to obtain partial network formation of the hydrogel solution. U87 glioblastoma cells (7 × 105/ml) in complete medium were added to the GE-CH solution (5%, 2 ml) and after making the mixture homogeneous through a gentle pipette, the bioink was loaded into 5-ml bioprinter cartridge.[188] Each sample was bioprinted as a two layers grid on 35-mm Petri TC dishes using a 22G nozzle with a 0.41 mm diameter at 25– 35 KPa. After printing, cells were maintained at 37◦C with 5% CO_2. The culture media were refreshed every 2 days.

2.14. Spheroids Formation and Histological Analysis Procedure

Cell aggregation was induced by growing cell suspensions in 96-multiwell Ultra-low Attachment Surface as already described.[177] Briefly, once cell culture monolayers were detached via standard trypsinization, cells were counted and resuspend to reach the concentration of 5 x 10^4/ml. 100 µl of cells suspension (5 x 10^3) were pipetted into each well and allowed to grow for 5 days, until spheroids reach the diameter of ~500 µm. Spheroids were deposited in GelChiDA hydrogel using a 24-well plate.

In order to fix hydrogel-embedded spheroids and to obtain a compact hydrogel structure, 10% buffered formalin was added for 2 h at RT into the well. After fixation, hydrogel-embedded spheroids were washed in PBS and were moved into histological cassettes, adding filter paper pieces on top and bottom of the sample to avoid loss of material. Samples were paraffin-embedded with a tissue processor (ETP, Histo-Line Laboratories) using a standard protocol, cross-sectioned at 3-µm thickness by rotary microtome (Leica RM2265), mounted on glass slides, and stained with Haematoxylin and Eosin (H&E). Sample sections were observed under a light microscope (Olympus BX51). Representative images were captured with a digital camera (Evolution VF digital Camera) using Image-Pro Plus software.

2.15. LIVE/ DEAD Assay

To evaluate the viability of the cultured U87 bioprinted cells, the obtained 3D engineered tissues were stained by incubation in 1 mL of PBS containing 1 μM of calcein-AM for 20 min at 37 °C and then 1 ml containing 0.036 μM of ethidium homodimer (EthD-1) for an additional 10 minutes at 37 °C.[189] Reagents were provided by LIVE / DEAD Viability / Cytotoxicity assay kit (invitrogen). The test allows to evaluate the effect GelChiDA and bioprinting process on cell viability using two different probes: Calcein AM that stains the viable cells in green and the Ethidium homodimer that highlights dead cells in red. The stained bioprinted models were washed three times with PBS pH 7.4 prior to obtaining the images. Image analysis was performed with a CELENA digital imaging system with a PlanAchro 4X Ph TC objective. Cell viability was calculated as (number of green-stained cells / number of total cells) × 100 using Fiji software ImageJ.[190]

2.16. TGA Analysis

Mettler Toledo TGA/DSC1 Star-e System was employed to perform TGA analysis. Freeze dried samples of ~10 mg were subjected to temperatures ranging from 30 °C to 800 °C. The samples' weight changes were studied in function of temperature and time. Nitrogen was used as purge gas with a flow rate of 50 mL min^{-1}.

2.17. Statistical Analysis

Results are presented as mean ± *SD* and compared using one-way ANOVA. Statistical significance was set at $p < 0.05$.

CHAPTER 1B

TUNING GELATIN-CHITOSAN BASED SCAFFOLD POROUS STRUCTURE USING ICE BINDING PROTEIN (IBP)

The control of porous shape and dimensions to form mechanically stable 3D geometries with an adequate profile, is a critical aspect in fibrous scaffold formulations. Scaffolds must provide suitable mechanical properties as well as porous structure morphology and connectivity to enable cell growth.[191–193]

The pore connectivity, size, and shape are some of the major factors for appropriate cell ingrowth, with the optimal pore size differing according to the type of tissue e.g. 5 μm for neovascularization, 5-15 μm for fibroblast ingrowth, 20 μm for hepatocyte ingrowth or 20–125 μm for adult mammalian skin. [194–199] Therefore, the control of porosity and pore size is an important parameter. Among the most used methods to produce controlled porosity scaffolds, some are based on the leaching of soluble particles and gas-based techniques.[200,201]

In this study we decided to engage Ice Binding Protein (IBP) as alternative method to control hydrogel porosity.

IBPs comprise structurally different classes of proteins, which have the common ability to bind ice and inhibit its growth.[202] The antifreeze proteins activity on thermal hysteresis mainly consists of lowering of

freezing point. In contrast with the widely used antifreeze solutes, such as ethyl glycol or trehalose, IBPs do not lower the freeze point in proportion to concentration, acting in a non-colligative manner. As a result of their positive properties, IBPs are considered as thermo-resistance or thermo-tolerance strategies used by some organisms such as marine fish, insects, plants and bacteria for survive adverse environmental conditions.[203] The ability of IBPs to influence the growth of ice crystals and inhibit recrystallization allowed their application in a wide variety of industry sectors. They have been involved in food technologies, to improve the texture and properties of frozen foods during storage refrigerated, also reducing the loss of nutrients caused by products defrosting phase. A further use of these biological molecules concerns the improvement, through genetic engineering, of the frost tolerance in plants which in the natural environment they would be susceptible to.

In this study the possibility of exploiting the antifreeze properties of these peculiar proteins in the field of tissue engineering was investigated.

1. RESULTS AND DISCUSSION

1.1. Tuning Gelatin-Chitosan Based Scaffold Porous Structure Using Ice Binding Protein (IBP)

The idea is to include the protein in a scaffold before the freeze-dry process so that the porosity of the construct can be controlled. Adding an external element able to tune the morphological properties of a biomaterial can be exploit as a method of standardization of 3D constructs. For this aim *Efc*IBP supplied by Prof. Lotti was employed. *EfcIBP* is a bacterial IBP identified by metagenomic analysis of the *Antarctic ciliate Euplotes focardii* and the associated consortium of non-cultivable bacteria.[204,205]

First, the biocompatibility of the protein under study was tested on U87 bioprinted GelChiDA models. *EfcIBP* at different concentrations was added to the culture medium and an MTT test was performed of up to 48 hours. The protein was shown to have the best compatibility at 7.5×10^{-4} mM and therefore this concentration was chosen to test the effects of the protein on the effects of the biomaterial (Figure 34).

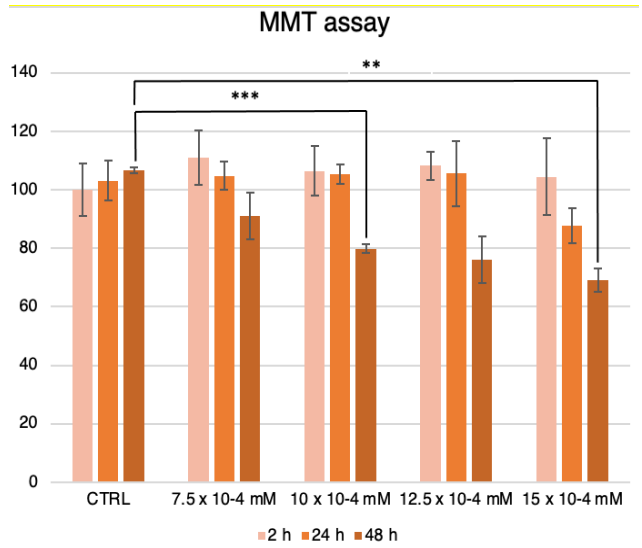

Figure 34: MTT assay on GelChiDA bioprinted with IBP in culture medium at different concentrations.

The effect of the protein on the material morphology was tested and already macroscopically the outcome was evident (Figure 35).

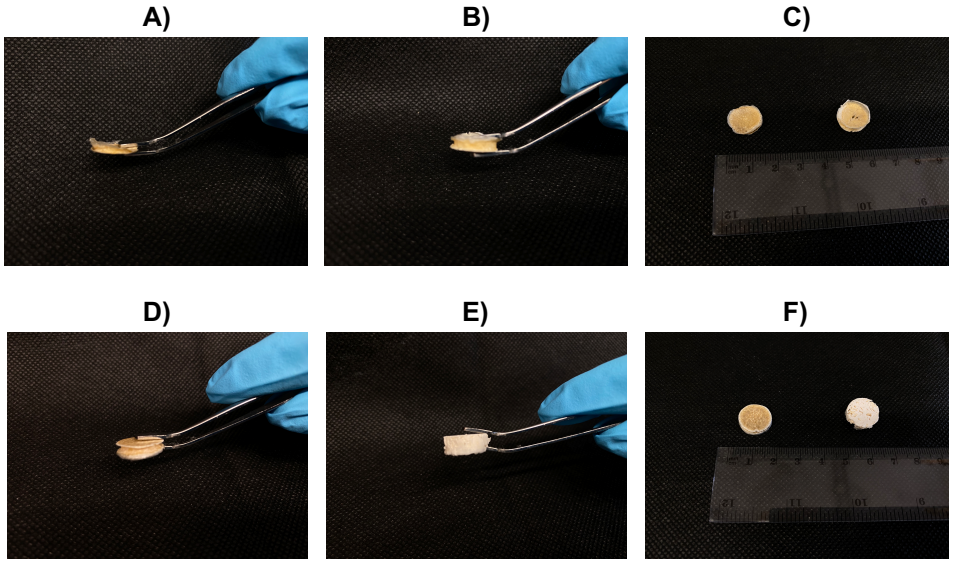

Figure 35: Images of **(A)** GelChiDA w/o IBP **(B)** GelChiDA with IBP freeze dried following freezing at -20°C **(C)**. Images of **(D)** GelChiDA w/o IBP **(E)** GelChiDA with IBP freeze dried following freezing at -80°C **(F)**.

The effects of freezing temperature on the porosity of materials have been reported in previous works. It is generally accepted that at a lower temperature, the number of crystal nuclei initially formed is greater than in samples frozen at a higher freezing temperature.[206] Consistent with these observations, differences in pore size are observed between the two control GelChiDA hydrogels prepared at different freezing temperatures without IBP, showing smaller pores in the higher temperature frozen sample (Figure 36). The situation is different and peculiar if we compare the samples in the presence of IBP. The biggest change can be seen when comparing the freeze-dried samples frozen at -20 °C with and without protein (Figure 36 A and 36 B), which appear to be the most different scaffolds from both macroscopic and microscopic points of view. The visual evaluation of SEM images reported in Figure 36 shows that GelChiDA sample with IBP display a significantly higher porosity than the same sample without IBP freezed at the same temperature. The porosity appears regular, and the material light, fibrous and foamy. Indeed, the freezing step takes place at a temperature close to the phase change, as the IBP is low melting protein. This change is not as pronounced in freeze-dried samples after freezing at -80 °C, which do not differ particularity, probably because the protein is not active under these conditions.

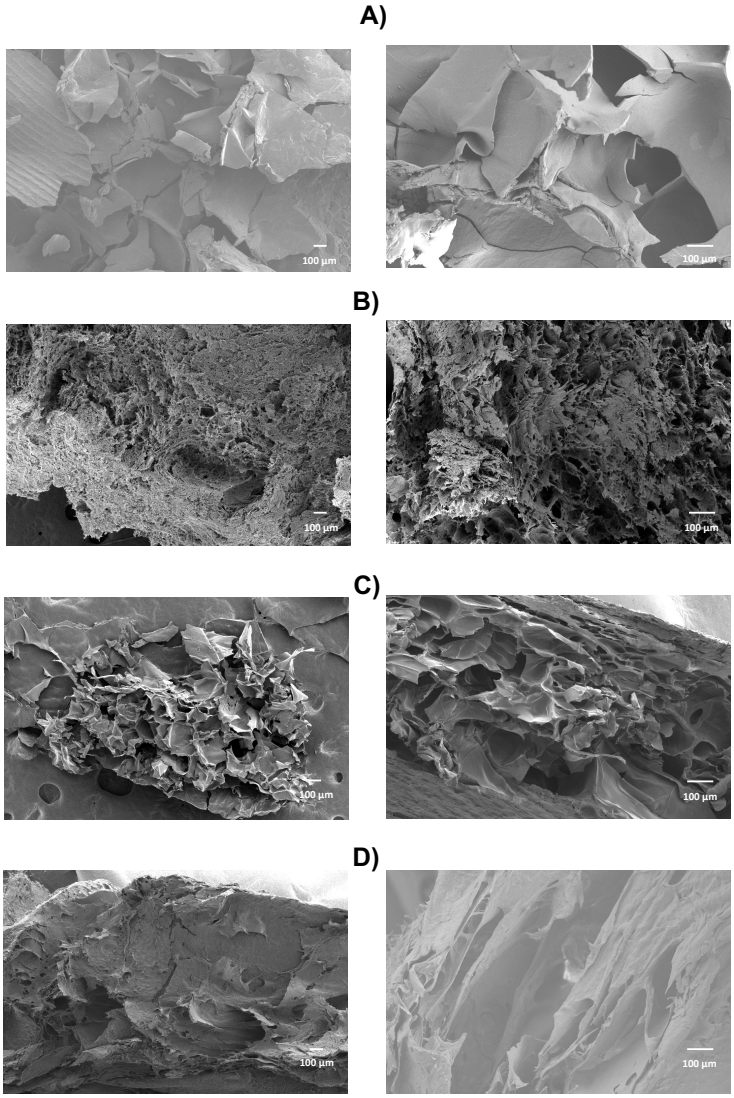

Figure 36: The inner structure of freeze-dried GelChiDa following freezing at -20 °C w /o(A) and in presence of IBP (B) and at -80 °C w/o (C) and with IBP (D)

2. MATERIALS AND METHODS

2.1 GelChiDA with IBP Addition Formulation

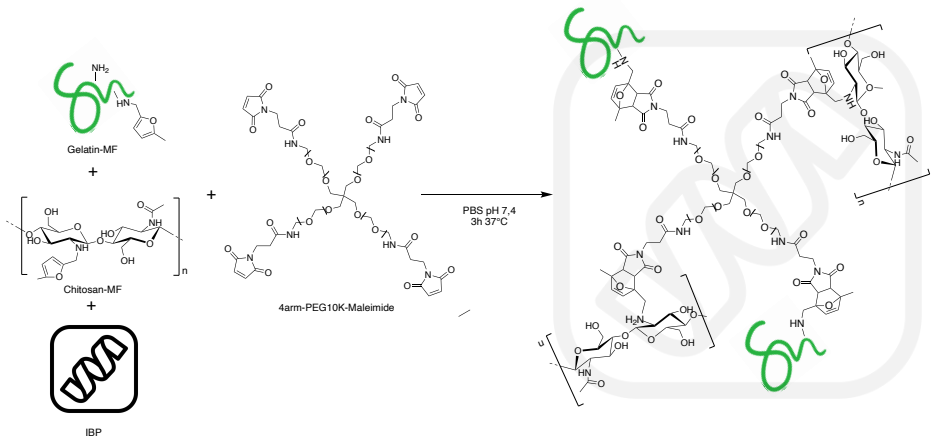

Scheme 5: Reaction GelChiDA scheme with IBP

Reagents	Eq.	Mass (mg)	V (ml)
Chitosan-MF	1	16	
Gelatin-MF	2	33	
PEG-Star-MA	0.16	2.5	
IBP	0.013	0.2	
PBS pH 7.4			1

To introduce IBP in the hydrogel network, 33 mg of Gelatin-MF and 16 mg of Chitosan-MF have been solubilized in 800 μl at 37 °C. Once the biomaterials were completely dissolved, 0.2 mg IBP in 100 μl of PBS 7.4 was added into the solution. 2.5 mg of PEG-Star-MA was solubilized in 100 μl at RT and then added to the reaction. After 3 hours at 37 °C, the hydrogel formation occurs (Scheme 5).

2.2 MTT Assay

U87 were bioprinted in 96-well plates at a density of $2x10^6$ cells/ml of GelChiDA, as previously reported in Chapter 1A paragraph 2.4. After 24 hours of incubation at 37 °C, the cells were treated with the different concentrations of IBP solubilized in the culture medium for 2, 24 and 48 hours. Two hours before the experimental time point, 10 µl of the MTT labeling reagent (final concentration 0.5 mg/ml) was added in each well. The plate was incubated at 37 °C and 5% CO_2. After two hours of incubation, the medium with excess MTT was removed and the cells were lysed wit isopropanol for 15 minutes. Finally, the absorbance was measured with a microplate reader (SPECTROstar nano microplate reader) at a wavelength of 570 nm.

2.3 SEM Analysis

SEM was employed to characterize the cross-section of the fibrous dried samples obtained. The gelatin-MF, chitosan-MF, and PEG-Star-MA solutions formed as previously described with and without IBP at different concentrations were transferred into Teflon molds (15 mm diameter) and left for 3 h at 37 °C. Once the Diels-Alder reaction had occurred, the samples were transferred at –80 °C and 20 °C for 24 h and then freeze-dried for 48h to obtain cylindrical compact structures. Samples from lyophilization were mounted onto SEM stubs with conductive adhesive carbon tape and silver paste, and sputter coated with 10nm chromium by means of high vacuum Quorum Q150T coating system. SEM-SE (Scanning Electron Microscopy - Secondary

Electrons) micrographs were acquired by means of High Resolution Field-Emission Zeiss Gemini 500 SEM, operating with 5kV acceleration voltage.

2.4 Statistical Analysis

Results are presented as mean ± *SD* and compared using one-way ANOVA. Statistical significance was set at $p < 0.05$.

3. Conclusion

In this work the functionalization of gelatin and chitosan with methylfuran was reported. The obtained polymers were used with a PEG-star-MA formulating GelChiDA as a new hybrid hydrogel platform. The novel hydrogel has the great advantage to combine polysaccharidic and proteic part representing the principal components of native ECM through click chemistry. The click chemistry-based hydrogel is formed spontaneously on mixing of reactive compounds, without further purifications or UV irradiation.

The starting materials and the resulting hybrid biomaterial were characterized in terms of physical-chemical properties: they were studied using HP-SEC-TDA, UV, FT-IR, NMR, a TGA. The proposed analytical strategy guarantees a comprehensive view of the critical properties of complex biomaterials and can, in principle, be applied to all constructs of this nature. GelChiDA showed interesting rheological properties, including self-healing characteristics and promising preliminary biocompatibility tests. The bioink formulation was optimized by modulating the concentrations of chitosan and gelatin and assessing the optimal timing to perform bioprinting process into grid-like structures. GelChiDa properties permits to extrude the biomaterial working at low pressure, without affect cells viability. Another application of GelChiDa was investigated as an *in vitro* tumor model using spheroids, proving to be a stable platform for future pharmacological tests as pathological models. A novel application of IBPs translated into the biological field has been proposed: the use of these proteins allows to tune the biomaterial according to the endmost

need without affecting cellular vitality. The possibility of using the GelChiDA hydrogel in 3D applications paves the way for more detailed studies in the field of tissue engineering and 3D culture for advanced biological studies.

CHAPTER 2

GELCHEL: Chitosan-Gelatin and Elastin as Multifunctional 3D Bioprintable Platform

Starting from GelChiDA construct, a novel hydrogel formulation has been developed. The crosslinking strategy through Diels Alder reaction was maintained but elastin was introduced into the network as new protein of ECM components. Elastin is a key ECM protein that provides support, elasticity and elastin fragments are involved in cell-signaling events such as proliferation and in inducing angiogenesis. All of these properties make elastin an attractive candidate for biomaterials scaffolds for medical applications, and for these reason it has been included as element in the new hydrogel propose.[207–210]

Elastin is a mammalian ECM protein consisting of cross-linked tropoelastin monomers, organized around a fibrillin-rich microfibrillar structure.[211] In vivo, elastin makes up part of the elastic fibers, endowing tissues with elastic properties and stiffness at low strain levels. Additionally, it allows tissues to get back into their original shape after stretching or compression. For these reasons, elastin can be found into wall vessels of arteries (32%), elastic ligaments (50%), lung (7%), tendons (4%) and skin (5%).[212,213] Fully polymerized mature elastin is basically insoluble, metabolically inert and extremely resistant to thermal and chemical insults.[214] Elastin has an uncommon amino acid composition, with about 75% hydrophobic residues (Gly, Val, Ala) and hydrophilic domains with many Lys residues which are important

in crosslinking reactions.[215] Structural stability, elastic resilience and bioactivity of tropoelastin, combined with its ability to self-assembly, make this protein a highly desirable candidate to design biomaterials. Such network would not only reflect ECM physical features, but would also have biological cues for target cell incorporation and signaling for ECM remodeling in tissue engineering applications.[216] Although elastin is a biopolymer with attractive properties, in vivo its crosslinking makes elastin fibers insoluble. Therefore, it is difficult to obtain pure elastin in large quantities. Elastin isolation can be achieved by a number of methods that lead to a wide range of final products, including insoluble elastin, decellularised tissue and purified elastin.[217,218] Insoluble elastin may be also hydrolyzed to obtain soluble elastin. Hence the need to develop elastin-like polypeptides (ELPs) which can be produced by synthetic or recombinant approaches.[216] ELPs can be employed instead of natural elastin and consist of the pentapeptide sequence VPGXG, where X represents a guest residue which can be any amino acid except proline.[219] An advantage in usage ELPs is the opportunity to incorporate specific sequences that have cell biological effects, such as Arg-Gly-Asp (RGD) motifs.[220] However, some limitations concern the limited quantities of ELP peptide obtainable by recombinant or synthetic methodologies, and furthermore it is important to study the in vivo reaction to the entire protein, which may give formulation advantages.

In this scenario, we present a simple approach to tame elastin properties and synthesizing elastin-based material.

The multicomponent GELCHEL (GELatin, CHitosan; ELastin) hydrogel conceived and studied in our work, combines in a single

construct the various advantages that each component provides and lends itself to future massive variety of biomedical applications. Chemical and mechanical characterization as FT-IR, ^{1}H NMR, ^{13}C-NMR, SEM, swelling test, AFM have been performed. GELCHEL hydrogel has been bioprinted with U87 cell line and cytotoxicity tests (live-dead, CCK-8 proliferation assay) highlight a great biocompatibility. Furthermore, cytoskeletal with nuclei staining showed a good cell distribution in the bioprinted constructs. As intrinsic additional feature of GELCHEL, the antibacterial property of chitosan in the construct has been evaluated.

1. RESULTS AND DISCUSSION

1.1 GELCHEL Hydrogel Formulation

After functionalization of Chitosan, Gelatin and Elastin with 5-methylfurfural, and subsequential chemical characterization, these three biopolymers have been employed to formulate a hybrid hydrogel by Diels-Alder reaction. The introduced dienes subsequently undergo cross-linking exploiting a Diels-Alder cycloaddition reaction using as dienophile a commercially available 4-arm-PEG10K-maleimide to obtain a heteropolymers based hydrogels (Scheme 6). As reported in a previous work, this cross-linking approach resulted in a highly reproducible, biocompatible, affordable product.[177] In fact, higher quantities of elastin give homogeneity problems to the hydrogel, with problems of solubilization, while increasing the quantity of peg gives problems of excessive crosslinking giving a lumpy and non-printable material. The optimal formula was obtained after several tests with variation of elastin and chitosan content, while keeping unchanged the Star-PEG-MA and elastin quantities (Table 5).[177] In fact, higher quantities of elastin give homogeneity problems to the hydrogel, with problems of solubilization, while increasing the quantity of peg gives problems of excessive crosslinking giving a lumpy and non-printable material.

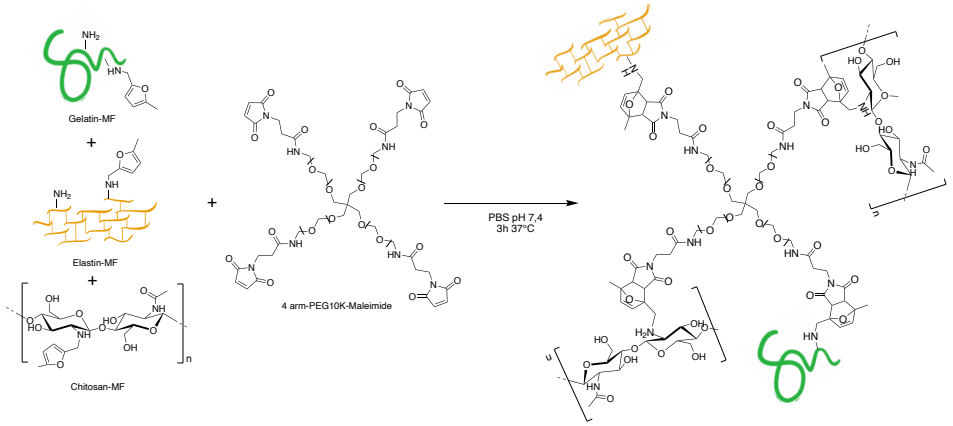

Scheme 6: GELCHEL formulation scheme.

Table 5: GELCHEL formulations tests

Entry	%W/V	Ratio	Gelification	Printability
Gel-MF:Chit-MF	3,5%	1.3:1	✓	✓
		1:1.3	✓	X
		1.5:1	✓	X
		1:1.5	✓	X
		1:2	✓	X
		2:1	X	X
Gel-MF:Chit-MF	5%	1.5:1	✓	X
		1:1.5	✓	X
Gel-MF:Chit-MF	6,5%	1.5:1	✓	X
		1:1.5	✓	X

The GELCHEL hybrid hydrogel formulation selected was obtained with the final biopolymers concentration of 3,5% (35 mg/ml) with

polymer ratio of CH:GE:EL:Peg-star=1:1.3:0.15:0.2. The hydrogel transition is completed after 3 hours at 37 °C.

1.2 Elastin-MF Chemical Characterization

As for the other polymers, Gelatin and Chitosan, that form the hybrid hydrogel, elastin has undergone functionalization and a deep chemical characterization. To maintain the efficiency of Diels Alder reaction, elastin was functionalized thought reductive amination with 5-methylfurfural.

The obtained functionalized biomaterial, Elastin-MF, was characterized through Nuclear magnetic resonance (NMR) technique. As we can see in elastin ^{1}H NMR spectrum, reported in Figure 36, the functionalization and the followed final product purification was successful. As in all complex protein, there is signals overlapping due to the presence of various aminoacidic. Generally being a hydrophobic protein, we decide to perform the elastin NMR spectra acquisitions analysis in DMSO, instead of D_2O as previously reported for the other polymers. In particular, considering the literature, ^{1}H-NMR spectrum shows principal peaks at δ 0.73 (CH_3 Val), δ 1.20 (CH_3 Ala), δ 1.90 (-CH_2-CH_2-Pro), δ 3.6-4.3 (overlapping of CH_2 and CH of amino acids).[221] Comparing with the unfunctionalized elastin two near peaks at δ = 5.96 and 6.19 ppm were observed, corresponding to the hydrogens of furan double bonds, and the peak at δ = 2.21 ppm that is associated to the methyl group of the furan. Furan peaks were characterized thought ^{13}C NMR analysis (Figure 37). This proved that

the reaction of functionalization occurred. Functionalization degree has been calculated using TMS as internal standard and considering the signals corresponding to the proton on the double bonds of methylfuran moieties. In particular, we estimated $9.46 \cdot 10^{-4}$ mmol of methylfuran per mg of elastin-MF. Considering the weighted average of aminoacids' molecular weight, with respect to the aminoacid composition of elastin, we estimated the degree of functionalization as 20% (Figure 38).[222]

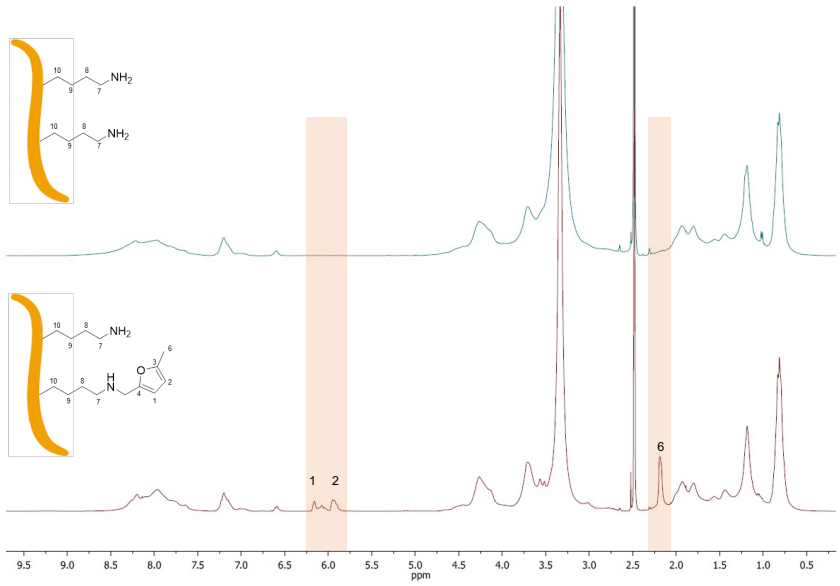

Figure 37: ^{1}H-NMR Elastin and elastin-MF spectra

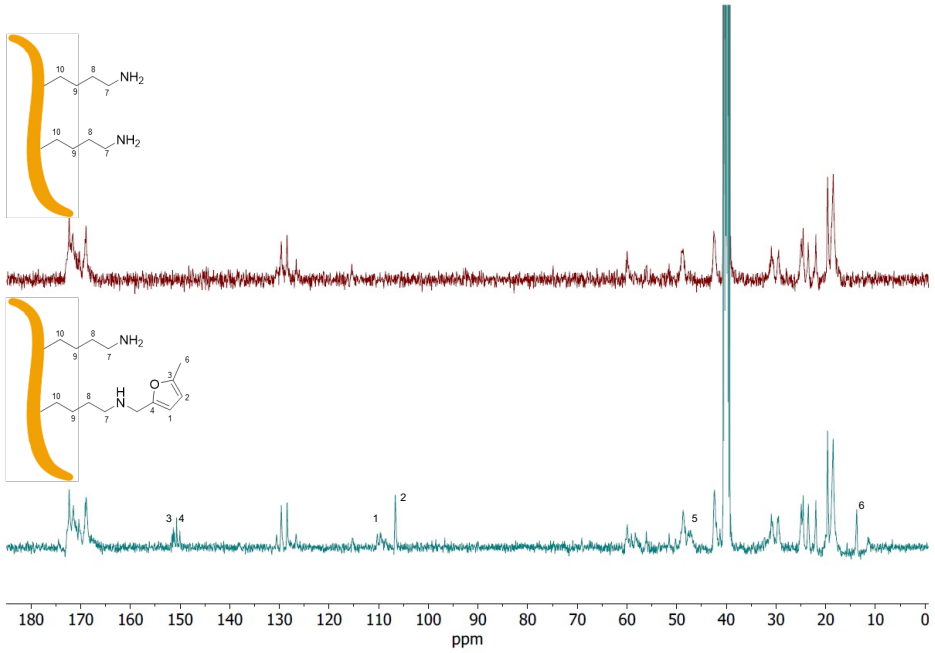

Figure 38: ^{13}C NMR Elastin and elastin-MF spectra

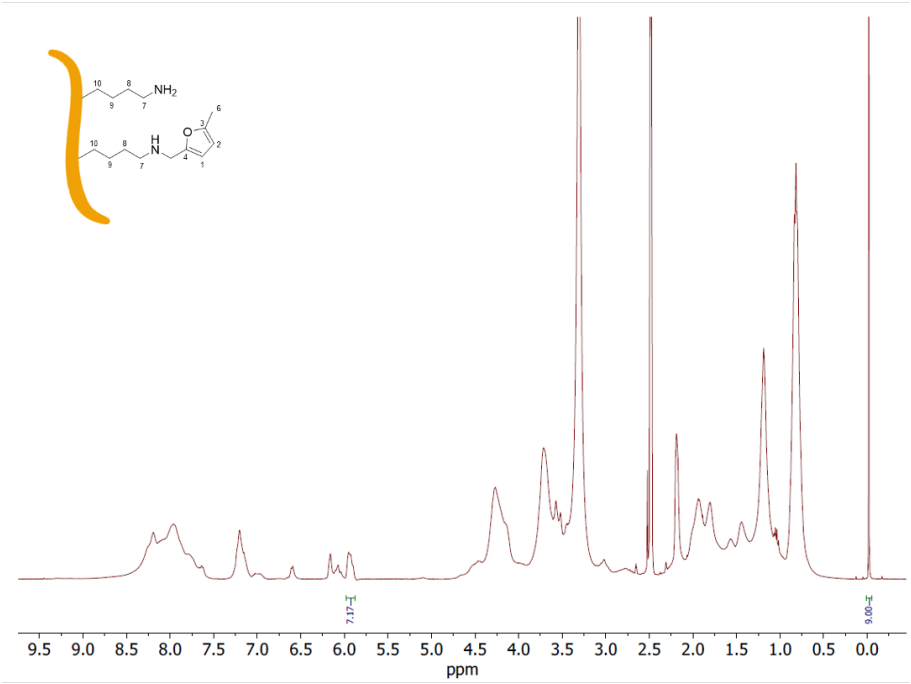

Figure 39: Elastin-MF quantification

FTIR spectroscopy is a powerful tool for the evaluation of the chemical composition of blend materials and, in the case of proteins, for investigation of their dynamics and conformation.[223]

The spectrum of untreated elastin shows the characteristic two peaks at 1635 and 1535 cm^{-1} corresponding to C=O and -NH- of the amide II, respectively, and at 1242 cm^{-1} for amide III, assigned to β-sheet conformation. By comparison with elastin-MF spectrum, the signals of C=C, C-H, and -C-O-C- of the furan are detectable between 800 and 1150 cm^{-1} (Figure 39).

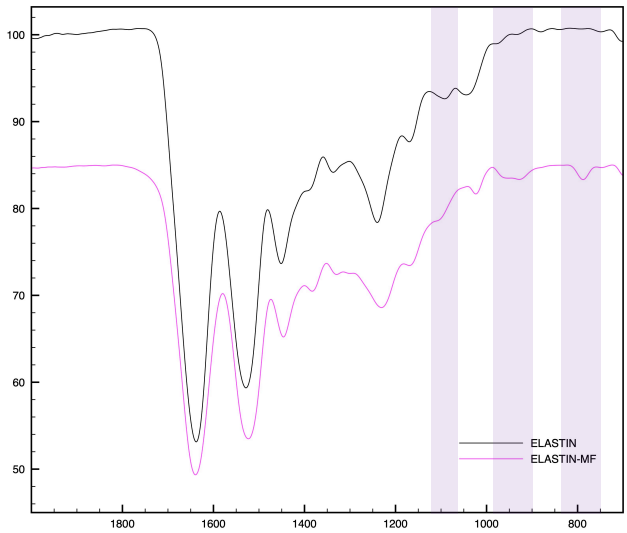

Figure 40: FT-IR elastin and elastin-MF spectra.

1.3 GELCHEL characterization

1.3.1 Inversion tube test

To confirm that hydrogel formation depends by the presence of 4arm-PEG10K-Maleimide as cross-linker agent, it has been performed the test inverting tube on GELCHEL hydrogel and on a blended control without the cross-linker. Both hydrogel and control have been prepared in the same way as reported in material and method paragraph and incubated at 37 °C to avoid spontaneous gelification of gelatin at room temperature. Figure 40 shows the GELCHEL hydrogel remains well adhered to the walls of the bottom of the Eppendorf, displaying mechanical resistance to the gravity force, unlike blended control.

Figure 41: Inverting tube test of GELCHEL (left) and Blended control (right)

1.3.2 FT-IR Analysis Real Time

To characterize the crosslinking reaction and the DA construct, real time FT-IR analysis was performed up to 3 hours. Once the crosslinking reaction was initiated after the addition of the crosslinker

PEG-Star-MA, several samples were frozen in liquid nitrogen at different times to stop immediately the reaction, then analyzed by FT-IR to follow the cross-linking. An increase of the DA cyclo-adduct peak was observed at 1180 cm^{-1} highlighting the cross-linking reaction success.[224] There are two broad absorption bands observed for proteins using FTIR, conventionally called amide I and amide II bands, at wavenumbers 1700–1600 cm^{-1} and 1600-1500 cm^{-1}, respectively. The Amide I band is more commonly used for characterizing the secondary structure, and it is primary governed by C=O stretching vibrations of peptide bonds, which are modulated by the secondary structure (α-helix, β-sheet, etc.), while amide II indicates the deformation along the C-N bonds. Figure 41 shows how the hydrogel crosslinking reaction does not affect amide bands, indicating the protein biomaterials conformations were well maintained throughout the reaction without any negative effects on structure and therefore functionality.

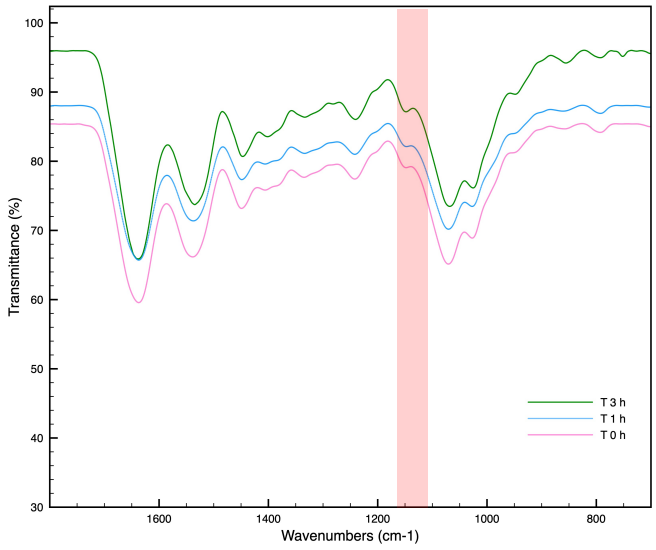

Figure 42: Stacked transmission FT-IR spectra of GELCHEL reaction

1.3.3 Swelling test

To evaluate behaviours of GELCHEL hydrogel in wet environment hydrogel swellability has been analysed incubating in PBS buffer at 37°C for 40 days. (Figure) That experiment has been carried out in triplicate and in PBS at different pH (pH 5.5, 7.4 and 8.5) in order to calculate the swelling ratio and evaluate the resistance at different pH.[225]

In the first part of the diagram there is a rapid growth of swelling ratio especially at pH 7.4. Comparing the three different pH it is possible to observe that at pH 7.4 the maximum value of swelling ratio, with an average value of 13, is achieved after 24h such as water content that reach the value of 34%. On the other hands swelling performed with PBS at pH 5.5 and pH 8.5 gain the maximum value of swelling ratio after 8 day with an average value of 16 and 14 respectively and a water content of 43% and 31% respectively (Figure 42). All the hydrogels show a good stability for 40 days, after that started degradation, due to polymer loss, resulting not possible performing further analysis.

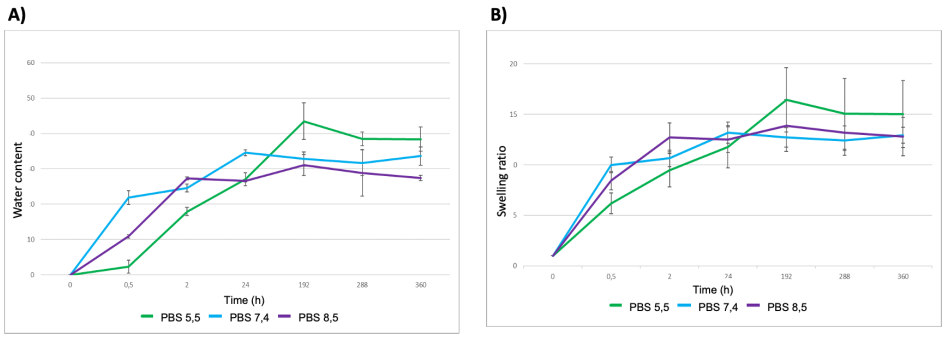

Figure 43: Graph swelling test with water content % (A) and swelling ratio (B).

Comparing these swelling data with the swelling results of the hydrogel proposed in Chapter 1, we observe that, unlike GelChiDA whose peak swelling ratio was reached in the first few hours, GELCHEL takes several days, probably due to presence of elastin hydrophobic domains. Furthermore, it can be observed how GELCHEL achieves and maintains higher Ratio Swelling levels over time: this may be due to the lower concentration of polymers used in the formulation (3.5% vs 5%) which enable to obtain a less compact material allowing a higher water uptake during swelling.

1.3.4 SEM (scanning electron microscopy) analysis

SEM is one of the most used techniques for characterization of materials, both from a morphological and chemical composition point of view. SEM was employed to visualize the detailed structural features of the hydrogel.[226,227] For blended control, the same GELCHEL's formulation protocol was followed without the addition of the crosslinker. Comparing the hydrogel with the control, which displays a flat laminar structure, a homogeneous morphology was observed with interconnected porous with an average diameters of 125 μm (Figure 43).

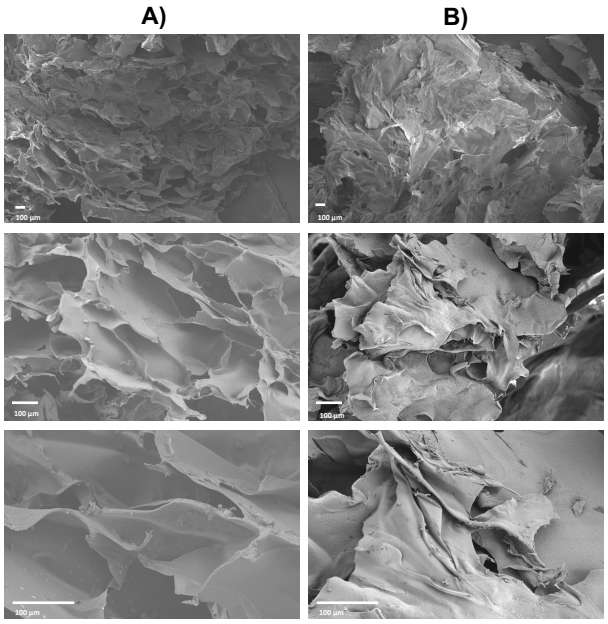

Figure 44: SEM images of hydrogel (A) and control (B) at different magnifications.

1.3.5 ^{1}H HR-MAS

The GELCHEL was analyzed by HR-MAS NMR. ^{1}H HR MAS spectra were obtained from all starting materials and then compared to the GELCHEL spectrum. In Figure 44 the spectra obtained from the analyzes have been reported stacked and a peak at 6.45 ppm has been identified, attributed to the adduct of the Diels Alder reaction.

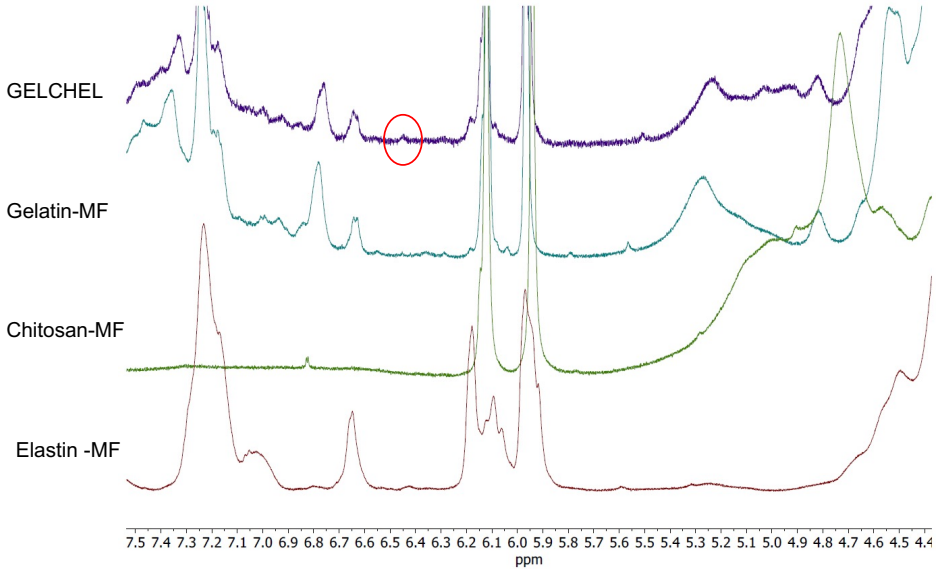

Figure 45: HR MAS NMR comparisons between GELCHEL and starting materials

1.3.6 Atomic Force Microscopy (AFM) Analisys

Stiffness is a prominent property for scaffolds study in tissue engineering applications. It is known that the rigidity of the scaffold can guide the differentiation of stem cells and affects cell migration, the latter important for cellular infiltration from tissues. Although biochemical stimuli are clearly very important in regulating cellular behavior, it has become clear that a scaffold with inappropriate stiffness can frustrate the tissue regeneration. Atomic force microscopy (AFM) has proven to be a valuable instrument to characterize quantitatively the mechanical and morphological properties of soft, medium and hard materials.[228]

In principle, the Young's modulus of a hydrogel can be measured by finding a relationship between a force applied to the hydrogel and the resultant deformation of the hydrogel. Young's modulus is usually

obtained by measuring the stress-strain curves of a hydrogel specimen through the compression or the tensile method and then finding the slope of the curve.[229]

AFM uses a small flexible cantilever to indent the sample and the mechanical stiffness can be assessed recording the sample deformation induced by the controlled force applied through a tip at the end of the cantilever. During this process, the AFM records the applied force as a function of the tip position (indentation) in the so-called force-distance curves. By fitting every force-distance curve to the Hertz-Sneddon model it possible to extract the apparent Young's modulus. This is proportional to the ratio between the applied force and the deformation and it is the evaluation of the sample stiffness.[230] The results pulled in the graph (Figure 45) show how GELCHEL falls into the range between 1.5 and 6 kPa, which mostly includes extracellular matrix of soft tissue with high complexity as brain and lungs.[231–233] Furthermore, the values follow in settle area demonstrating that the measured points and consequently the formulation of GELCHEL samples are reliable and reproducible.

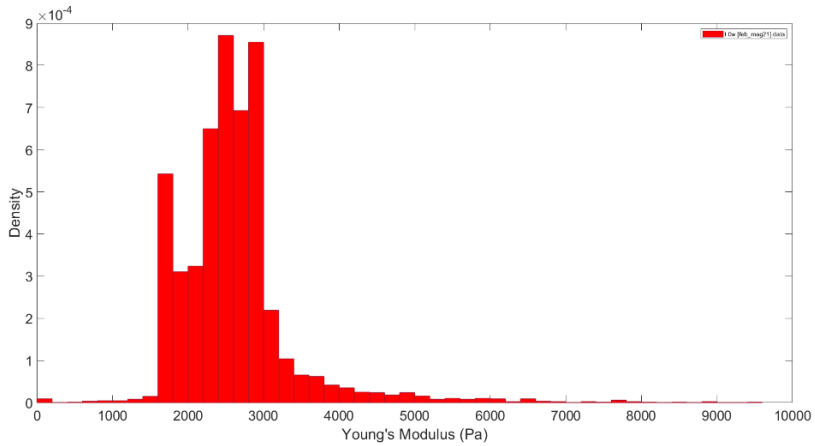

Figure 46: Young's modulus of GELCHEL scaffolds.

1.4 Biological Evaluation

1.4.1 3D Bioprinting Model

3D printing tests have been performed with the aim of creating defined shapes and verifying if hydrogel maintains its structure in presence of medium and cells. GELCHEL hydrogel has been prepared such as described paragraph 2.3 and a bioprinting protocols has been developed. After 2 h the hydrogel is in a semi-liquid state, as the DA reaction is not totally completed. This state permits to handle the biomaterial and enable the homogeneous cellular dispersion during the bioprinting process.

On bioprinted models, LIVE / DEAD assay has been performed to evaluate the biocompatibility of the novel hydrogel formulation with U87 cell culture. The LIVE / DEAD viability / cytotoxicity assay allows to discriminate viable cells from non-viable cells by using two fluorescent molecules: Acetoxy Methyl Calcein (Calcein-AM) and Ethidium Homodimer 1 (EthD-1). Calcein-AM is a hydrophobic, non-fluorescent substance capable of crossing the cell plasma membrane; once penetrated, the cytoplasmic esterases cause its transformation to Calcein, a fluorescent hydrophilic compound which is retained in the cytoplasm and which produces a green fluorescence (ex / em 495 nm / 515 nm). EthD-1, on the other hand, only penetrates cells that have damage to the cytoplasmic membrane and binds to nucleic acids, producing a red fluorescence (ex / em 495 nm / 635 nm). Therefore, viable cells, thanks to their intracellular esterase activity, will have cytoplasm colored green; the dead cells will instead have a red colored

nucleus. This technique is fast, sensitive and can be used to detect cytotoxic events.

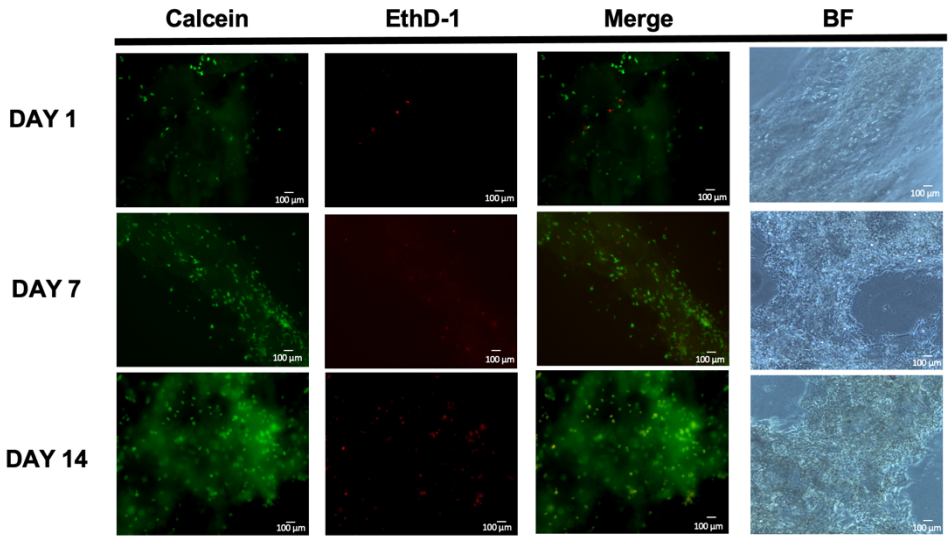

Figure 47: Live/dead assay on GELCHEL bioprinted with U87 cell line and microscope picture of the shape.

The assay was performed on bioprinted cells with a tissue pattern grid shape, and the analysis was carried out at 1, 7 and 14 days. The images reported in Figure 46, show that after 14 days the percentage of cells permeated by ethidium homodimer cells (red, dead cells) remains very low, with a vitality of 85%. In addition, brightfield images display that GELCHEL is able to maintain its structure for up to 14 days of cell culture.

The high biocompatibility of the new tissue model was then verified with a CCK-8 proliferation assay. In this case, since not going to evaluate the print stability of the biomaterial, the bioink was prepared following the same protocol and then bioprinted directly in a 96-multiwell plate. The needle size and pressure have been maintained. Cell viability was assessed by the WST-8 test (Cell counting kit-8). The highly water-soluble WST-8 (2- (2-methoxy-4-nitrophenyl)-3-(4-

nitrophenyl)-5-(2,4-disulfophenyl)-2H-tetrazolium, monosodium salt) tetrazolium salt is converted by mitochondrial dehydrogenases of live cells to formazan, a yellow-orange colored product. The optical absorbance of formazan can be measured spectrophotometrically at the wavelength of 450 nm and is directly proportional to the number of viable cells.

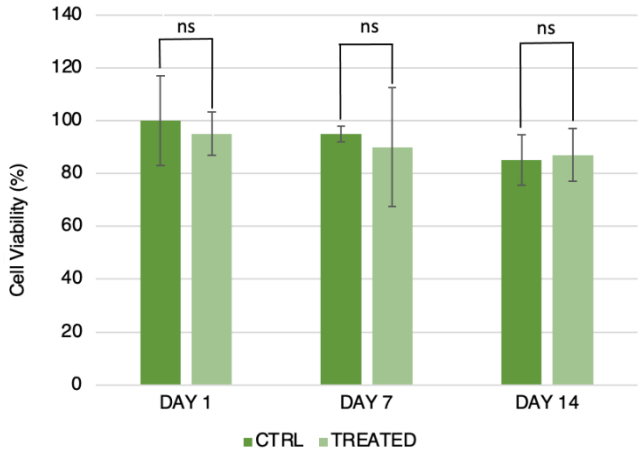

Figure 48: CCK-8 proliferation assays of bioprintend (Treated) compared to standard cells culture w/o biomaterials (control).

As shown in the graph reported in Figure 47, the presence of the biomaterial and the bioprinting technique, which involves mechanical stress, does not cause any toxicity for up to 14 days.

A fluorescence experiment with TRIC-conjugated phalloidin, a bright orange-fluorescent dye, and DAPI was carried out to underestimate the cellular behavior within the constructs. Phalloidin is a toxin from the Amanita Phalloides plant capable of binding at the interface of the F-actin filaments, preventing their depolarization. If conjugated to fluorophores it is visible under the fluorescence microscope. Using a High-Content Analysis System the samples were set up in 96-

multiweel. To qualitatively observe the shape and cell viability of the cultured cytoskeletal cells, the fluorescence images of DAPI (blue) / phalloidin (orange) were analyzed in Figure 48. The samples appear uniform, and the cell dispersion is homogenous. The cell population grows at different time points and, as expected, the aspect ratio (longest length / shortest length) of the cell cytoskeleton changes with increasing culture periods. Cells appear to get used to the presence of the material by interacting with it and forming cell-to-cell interactions.

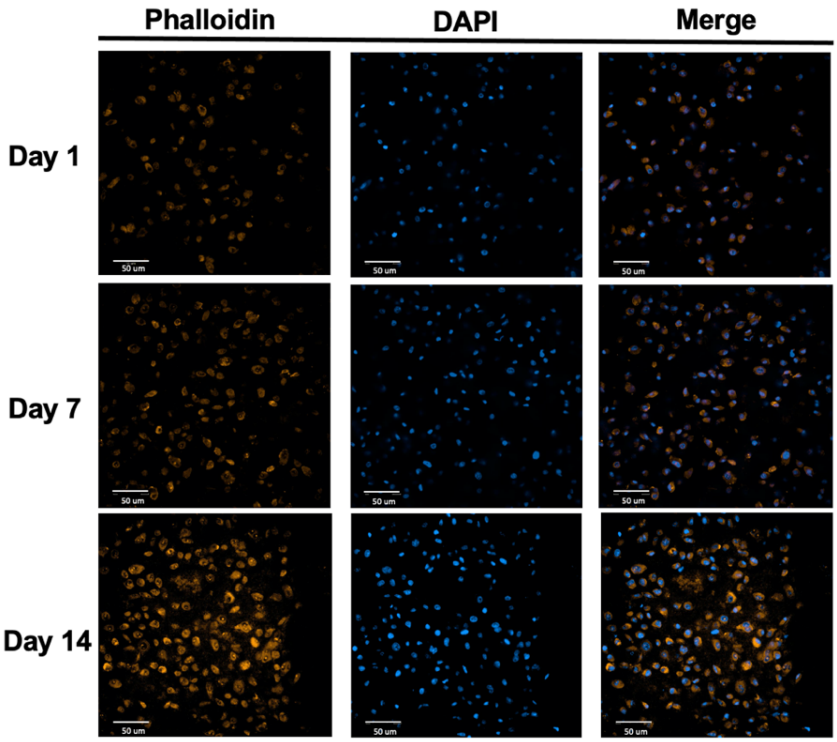

Figure 49: Phalloidin/DAPI staining on GELCHEL bioprinted models at 1, 7 and 14 days

Sem analysis was performed once again on bioprinted constructs.[234] The aim is to evaluate and confirm the cell morphology obtained with the previous fluorescience experiments. Micrographs obtained from

SEM showing the interaction of U87 by the cytoskeleton filaments with the surrounding cell-cell contacts.[235] Images in Figure 49 show how cells interact with the scaffold and with each others. Moreover, by comparison of bioprinted culture at different time the increase of the cell population is consistent.

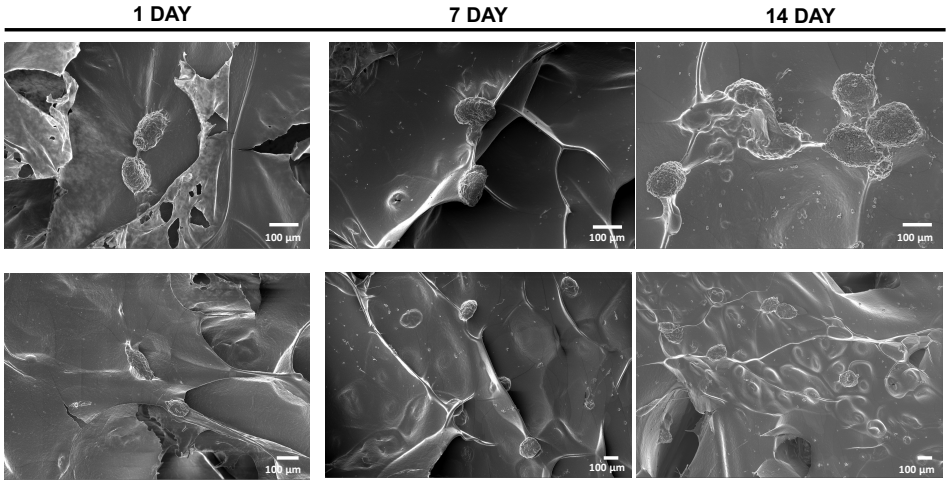

Figure 50: SEM images of U87 GELCHEL bioprinted scaffolds at day 1, 7 and 14 at different magnification

1.4.2 Bacterial-growth Inhibition Assay

Chitosan is a biomaterial known for its properties, including antiadhesive and antimicrobial activity. The introduction of antiadhesive properties represents an added value on biomaterials and cell constructs, considering the high contamination risks in both in vivo and *in vitro* applications. In order to investigate whether chitosan antibacterial activity is maintained in our construct, bacterial-growth inhibition assay was performed. Several controls were conducted with the different components of GELCHEL, maintaining the concentration

of the biopolymers constant: Gelatin, Chitosan, Gelatin + Chit (+), Gelatin + Chit (-) (for details see the caption), Gelatin + Elastin and PBS pH 7.4. The Figure 50 shows that the presence of chitosan inhibits bacterial growth even when engaged in the GELCHEL network. In fact, in all samples where chitosan is present there is an inhibitory halo of bacterial growth.

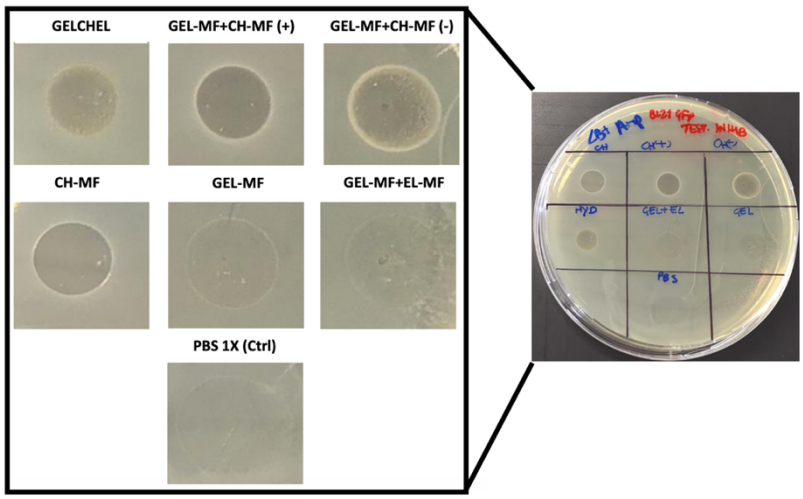

Figure 51: Bacterial-growth inhibition assay. 10 µl of different biomaterials: GELCHEL, Gelatin, Chitosan, Gelatin + Chit (+), Gelatin + Chit (-), Gelatin + Elastin and PBS pH 7.4 were dropped on an E.coli BL21 inoculated LB agar surface. The material tested were prepared maintaining GELCHEL biopolymers concentration. In Gelatin + Chit (+) the amount of chitosan has substituted the absent elastin contribution, while in Gelatin + Chit (-) the amount of elastin was covered from gelatin and the chitosan ratio is the same to the original hydrogel. Representative image of three independent experiments

2. Materials and Methods

2.1 Materials

Water-soluble chitosan was purchased from Carbosynth Ltd, UK. A LIVE/DEAD Cell Viability Assay was purchased from ThermoFisher. All other chemicals were purchased from Merck KGa, unless differently stated, and used as received without further purifications.

2.2 Elastin Functionalization (Elastin-MF)

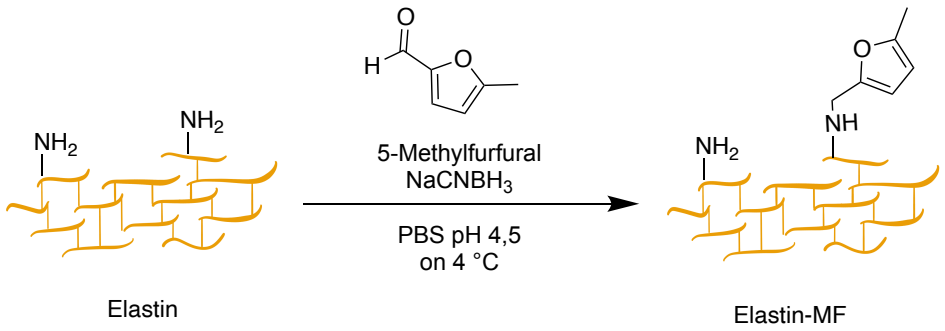

Scheme 7: Elastin functionalization with 5-methyl furfural reaction scheme

Reagents	MW (g/mol)	Eq.	Mass (g)	Mol (mmol)	d (g/ml)	V (ml)
Elastin	146.19	1	0,1	0,684		
5-methylfurfural	110.1	100	3,76	68,37	1,107	3,4
$NaCNBH_3$	62,84	50	1,08	17,1		
PBS pH 4.5						20

Elastin (soluble from bovine neck ligament salt-free, lyophilized powder) was dissolved in PBS buffer (20 mL, pH = 4.5) and placed

under agitation at 4 °C. Once a yellowish homogeneous solution was obtained, 3.4 ml of 5-methyl-furfural was added and the solution was kept at 4 °C under agitation. Lastly, 1.08 g of $NaCNBH_3$, was added and the reaction was stirred for 24 hours at 4 °C. A 0.22 µm bottle-top filter, kept in an ice bath, was used to filter and sterilize the elastin solution. Subsequently the product was freeze-dried to give 850 mg of a yellowish spongy solid and stored at -20 °C (Scheme 7).

2.3 GELCHEL Formulation

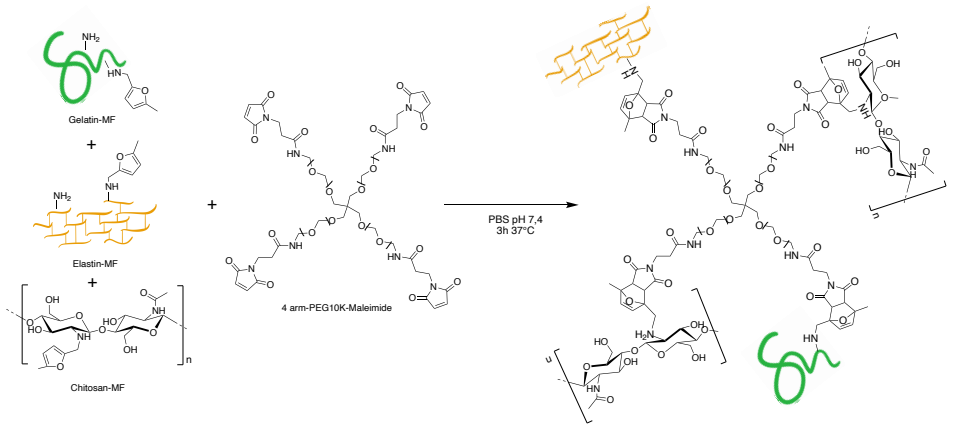

Scheme 8: GELCHEL reaction scheme

Reagents	Eq.	Mass (g)	V (ml)
Chitosan-MF	1	14	
Gelatin-MF	1,3	18	
Elastin-MF	0,15	2	
PEG-Star-MA	0,2	3	
PBS pH 7.4			1

To produce 1 ml of GELCHEL hydrogel 14 mg of chitosan-MF and 18 mg of gelatin-MF were dissolved in 800 µl PBS pH 7.4 at 37 °C to avoid solidification of gelatin and improve solubilization. Meanwhile 5 mg of elastin-5-methylfuran has been solubilized in 100 µl PBS pH 7.4 at 4 °C and 3 mg of PEG-Star-MA has been dissolved in 100 µl PBS pH 7.4 at room temperature. Solubilized Elastin-MF and PEG-Star-MA were added to the solution of chitosan-MF and gelatin-MF. The solution was vortex for few minutes and let to react at 37 °C. The hydrogel is completely formed in 3 hours (Scheme 8).

2.4 Swelling Test

The swelling test has been performed on 500µl of lyophilized hydrogel with 1 ml of PBS, the compound swollen at 37 °C. [181] To evaluate the behaviours of the hydrogel in acid, neutral and basic environments the assay has been performed at pH 5.5, pH 7.4 and pH 8.5.[181] The weight of the freeze-dried hydrogel was collected in order to calculate the weight's averages at different time points. Swelling ratio and water content has been calculate as indicated in the following formulas:

$$Swelling\ ratio = \frac{W\ swollen}{W\ dry}$$

$$Water\ content\ \% = \frac{W\ swollen - W\ dry}{W\ swollen} * 100$$

2.5 Cell Culture

Human glioma U87-MG cells were maintained in adhesion condition in T75 tissue culture flasks. U87 cells were cultured in Dulbecco's modified Eagle's medium supplemented with 10% fetal bovine serum, 100 units/ml penicillin, and 100 mg/ml streptomycin at 37 °C under a humidified atmosphere with 5% CO_2.

2.6 3D Bioprinting Protocol

Once 1 ml GELCHEL was formulated as previously reported, sterilized for 30 min under UV-light and an hour and half at 37 °C to obtain partial network formation of the hydrogel solution. $2x10^6$ cell/ml of U87 cells has been added to the hydrogel. After making the mixture homogeneous through a gentle pipette, the bioink was loaded into the bioprinter cartridge. Each sample was bioprinted as a two layers grid on 35 mm Petri TC dishes using a 21G nozzle with a 0.41 mm diameter at 50–60 KPa. After printing, cells were maintained at 37 °C with 5% CO_2. The culture media were refreshed every 2 days.

2.7 CCK-8 Assays

For label-free, non-invasive and long-term monitoring of cell viability, CCK-8 kit was chosen. In the extracellular microenvironment, WST-8 reacts with 1-Methoxy PMS reduced form to generate the WST-8 formazan (orange water-soluble product) and 1-Methoxy PMS. The WST-8 formazan is an orange-colored product and reflects the living

cell status. Hence, this system monitors the cell viability by the variation of orange intensity over time. The bioink was prepared following the same reported protocol and then bioprinted directly in a 96-multiwell plate. The needle size and pressure have been maintained. 100 µl of bioink was bioprited in 96-multiwel plate and 100 µl of culture media was added and refreshed every 2 days. The assay was performed on bioprinted costruct on day 1, 7 and 14, using as control cell culture in the absence of GELCHEL hydrogel. The control was seeded the day before at the concentration of $5x10^3$ per well. At the end of the treatment, each well was washed with PBS and cells were incubated with 100 µl of serum-free medium, supplemented with 10% of WST-8, for 2 hours at 37 °C in the dark. The formazan produced was then quantified using a microplate reader (SPECTROstar nano microplate reader) at 450 nm, subtracting a reference blank.

2.8 Morphological Analysis Protocol

100 µl of construct prepared as previously reported was bioprinted with pressure 50-60 KPa directly in 96-multiweel black for high content analysis. To perform the analysis, the samples were fixed with 10% formalin solution for 30 min at RT and then permeated with a 0.1% solution of Triton X diluted in PBS pH 7.4 for 15 min. After 3 washes of 10 min with PBS pH 7.4 the samples were stained with phalloidin-TRIC (phalloidin conjugated with Tetramethylrhodamine, a bright orange-fluorescent dye) 0.66ug / ml for 1 hour in the dark. After 3 washes of 5 min with PBS pH 7.4, the nuclei were labeled with 0.1 µg / ml DAPI dye solution for 8 min. After 3 washes of 5 min with PBS pH 7.4 the samples

were visualized with Operetta CLS High-Content Analysis System (PerkimElmer) the samples were analyzed at 1,7 and 14 days and of bioprint images at different layers were acquired, up to a thickness of 50 µm.

2.9 Antibacterial Activity Test Protocol

In this part of the investigation, bacteria-seeded agar was used. 1 ml of an *E. coli* BL21 ampicillin resistant cell culture (OD_{600} = 0.2) was spread on LB plate added by the antibiotic and dried under the flow bench for 30 min. Then, 10 µl of different biomaterials: GELCHEL, Gelatin, Chitosan, Gelatin + Chit (+), Gelatin + Chit (-), Gelatin + Elastin and PBS pH 7.4 (used as a control) were dropped on the inoculated agar surface, dried as described above and incubated for 16 h at 37°C. The material tested were prepared maintaining GELCHEL biopolymers concentration. In the case of gelatin and chitosan mixture, two condition were evaluated: in Gelatin + Chit (+) the amount of chitosan has substituted the absent elastin contribution, while in Gelatin + Chit (-) the amount of elastin was covered from gelatin and the chitosan ratio is the same to the original hydrogel. The amount of PEG-Star-MA has been maintained constant in each preparation.

2.10 AFM Analysis

AFM measurements were performed on GELCHEL hydrogel formulated as previously reported in PDMS cylindrical mold of 10 mm in diameter and 5 mm in height placed in a 36 mm petri dish and

covered with PBS 7.4. AFM measurements were performed using a Nanowizard II (JPK BioAFM, Bruker Nano GmbH, Berlin) equipped with a square-based pyramid probe (MLCT-BIO, cantilever E, 0.1 N/m nominal spring constant). Data were acquired force spectroscopy mode. Force-indentation curves were acquired with a maximum applied force of 1 nN, a 8 µm ramp length and a constant tip speed of 1 µm/s on several grids of 15x15 μm^2 with 16x16 points.

Data processing was performed using JPK data processing software (JPK BioAFM, Bruker Nano GmbH, Berlin) with the Hertz-Sneddon contact mechanics, taking account the shape of the tip.[236–238]

2.11 SEM Analysis

The GELCHEL hydrogel formed as previously described was transferred into Teflon molds (15 mm diameter) and left for 3 h at 37°C. Once the Diels-Alder reaction had occurred, the sample was transferred at –80 °C for 24 h and then freeze-dried for 48h to obtain cylindrical compact structure. Scanning Electron Microscopy (SEM) was employed to characterize the cross-section of the fibrous dried samples obtained. Same protocol has been followed for Gelatin-MF, Chitosan-MF and Elastin-MF without Star-PEG as blended control. SEM analysis was performed on U87 bioprinted constructs: once followed the bioprinting protocol, each grid was fixed with PFA for 2 hours at RT at 1, 7 and 14 days. After 3 washes of 10 minutes with millqH2O, samples were transferred at –80 °C for 24 h and then freeze-dried for 48h. Samples from lyophilization were mounted onto SEM

stubs with conductive adhesive carbon tape and silver paste, and sputter coated with 10nm chromium by means of high vacuum Quorum Q150T coating system. SEM-SE (Scanning Electron Microscopy - Secondary Electrons) micrographs were acquired by means of High Resolution Field-Emission Zeiss Gemini 500 SEM, operating with 5kV acceleration voltage

2.12 FTIR-ATR

FT-IR was adopted to characterize the starting materials and to follow the Diel Alder reaction at different time point. PerkinElmer Spectrum 100 FTIR Spectrometer was used to record the spectra. The starting materials, after being freeze dried, were placed on the steel instrument surface and measured at different regions. To record the GelChiDA reaction steps, the hydrogel was prepared as previously described, and frozen using Liquid Nitrogen to stop immediately the reaction. Once Freeze dried the samples were reduces in powder and analyzed. The absorption spectral range was collected between 4000 cm^{-1} and 650 cm^{-1} at a spectral resolution of 2 cm^{-1} and 40 scans.

2.13 NMR Spectroscopy Experiments

^{1}H-NMR spectra were acquired using a Varian 400 MHz Mercury instrument, operating at a proton frequency equal to 400 MHz at 37°C. The preparation of the sample has been maintained as previously reported excepted for deuterated PBS pH 7.4 was adopted as solvent. 0.05% wt of 3-(trimethylsilyl)propionic-2,2,3,3-d_4 acid sodium salt (0 ppm) was employed as internal standard. For all analysis the pulse

angle and the relaxion delay were set at 90° and 2 seconds respectively, while the number of scans varied between 160 and 240 depending on the signal-to-noise ratio. The HR-MAS NMR analysis were performed with a Bruker BioSpin FT-NMR Avance™ 500 (^{1}H frequency = 500 MHz) equipped with a superconducting ultrashield magnet of 11.7 Tesla, with the HRMAS probe (with pulse field gradient module on Z axis). The probes have been designed to perform solution type experiments, while spinning the sample at the magic angle. The probe is doubly tuned (^{1}H and ^{13}C), in addition to a 2H lock channel. The probe allows to perform high resolution MAS experiments at spinning rates of up to 15 kHz, for 4 mm Zirconia rotors, for liquid or liquid-like samples; in our work the spinning rates were optimized to 5KHz speed value, to rich a compromise between the needing to have the spinning side bands out of the 1H spectrum, the best resolution behavior and the minimum presence of rotational artifacts.

2.14 Statistical Analysis

Results are presented as mean ± *SD* and compared using two-way ANOVA. Statistical significance was set at $p < 0.05$.

3. Conclusion

Elastin-based materials are an emerging and promising topic in the field of biomaterials and the new proposed GELECHEL is a valid alternative to synthetic elastin-like polypeptides and can have great potential in the regeneration of soft tissues.[211] In this work, we demonstrate, for the first time, the use of elastin combined with gelatin and chitosan as an elastic bioink for 3D bioprinting. The synergistic association of the three biopolymers allowed a high-resolution printing with great cell viability. Since the importance role of elastin in brain blood vessels and angiogenesis, U87 Glioblastoma cell line were bioprinted and characterized. GELCHEL stability and bioprintable properties were showed highlighting a great biocompatibility; furthermore, cytoskeletal with nuclei staining showed a good cell distribution in the bioprinted constructs. GELCHEL showed antibacterial property due to presence of chitosan. Taken together, our results demonstrate the potential of GELCHEL as bioink for 3D bioprinting of functional tissue which could be employed for tissue engineering applications and studies.

CHAPTER 3

HA-MMPI for Biomedical Application

Glioma refers to a type of primary brain tumor originating from the glia cells, which represent the support and nourishment tissue for neuronal cells.[239] Glioblastoma multiforme (GBM), besides being the most prevalent among brain tumors (> 50% among central nervous system tumors), is the most common glial malignancy.[240,241] GBM is made up of highly atypical and irregular cells that multiply very rapidly.[242] This neoplastic form has hemorrhagic components and is histologically characterized by the proliferation of the vascular endothelium (neoangiogenesis) and by large areas of necrosis with consequent alteration of the blood brain barrier.[243] This tumor is characterized by a highly invasive behavior which contributes to the failure of currently available therapies and depends on specific enzimes.[244,245] Matrix metalloproteases (MMPs) constitute a family of structurally correlated zinc-dependent endopeptidases with the ability to degrade various protein components of the ECM and basement membrane.[246] These enzymes are synthesized at the level of tumor cells or normal stromal cells (fibroblasts, endothelial and inflammation cells) and their expression is regulated by numerous autocrine, paracrine and / or endocrine factors present in the cellular microenvironment.[247] In GBM, an increase in levels of MMP-2 (gelatinase A) and MMP-9 (gelatinase B) was observed compared to normal brain tissues or other brain tumors, indicating their active role in the highly invasive behavior that characterizes this type of

tumor.[248,249] The implication of MMP-9 seems to be mainly linked to the stimulation of angiogenesis, since these endopeptidases are present in abundance in the proliferating blood vessels.[250,251] Here they act as promoters of the vascular endothelial growth factor (VEGF) release, which mediates the activation of angiogenesis by interacting with the receptors present on endothelial cells,.[252] Furthermore, there appears to be a correlation between the levels of VEGF and MMP-9 and therefore the degree of progression of glioblastoma.[253,254] Differently, the activity of MMP-2 is associated with the degree of malignancy of GBM, as it is related to the metastatic invasiveness of the tumor.[255] Studies focused on the role of Membrane-type matrix metalloproteinases (MT-MMPs) in the carcinogenic process have highlighted the increase of MT1-MMP in some brain tumors, and in particular in gliomas. The elevated expression of MT1-MMP mRNA in gliomas was associated with the level of disease progression, having observed in these endopeptidases both a role in the degradation of ECM proteins and in the activation of pro-gelatinase A, MMP-2, which was the main cause of malignant progression of the tumor.[256,257] Therefore, in GBM, the increase in the levels of specific metalloproteases, first of all MMP-2, is associated with the degree of tumor progression and metastatic invasiveness, which make this type of tumor highly aggressive and difficult to treat.[246] This evidence can provide an initial basis for the development of innovative specific therapies against GBM, using specific MMPs as a selective target.[258] Given the importance that metalloproteases cover in tumor growth and invasiveness processes, and given the need for selective inhibitors, to minimize adverse effects, in the last years, MMP inhibitors (MMPI) with

high affinity towards these metalloenzymes have been synthesized and tested.[259–263]

In this context a new biopolymer was investigated in collaboration with University of Florence and University of Siena.

This work aims to characterize the suitability of hyaluronic acid (HA) based polymer conjugated with MMP-2 inhibitor (MMPI, structure not reported for IP reasons). In principle, grafting MMPI along the sodium hyaluronate backbone joined the HA outstanding viscoelastic and lubricating actions, with the inhibition of MMP-2 that is directly involved in disease progression. Moreover, this type of functionalization permits to slow down the HA degradation, reducing the low molecular weight HA fragments generated during physiological degradation, which are known to be responsible of inflammatory effects.[85,264]

The development of MMP-2 inhibitors based on biomaterial systems capable of acting directly at the tumor site could open new frontiers for the treatment of tumors with poor prognosis. These hydrogel materials with inhibitory activity used in the surgical environment after the removal of the tumor mass could be effective for the treatment of relapses, an important recurring problem in these diseases. We have been provided with HA-MMPI conjugated biomaterial and our role was to develop a fluorescent protocol on tumor 3D model in order to confirm the MMP-2 inhibition, seen *in vitro*.

1. RESULTS AN DISCUSSION

1.1 Immunofluorescence MMP-2 and MMP-9 Experiment

Once the new synthesis compound MMP-2 inhibitor grafted to hyaluronic acid was provided, the potential and applicability of this construct were validated in 3D. Spheroid models of U87-GM were used for the experiments. After hydrating the crosslinked material with the inhibitor, U87 spheroids were included and cultured for one day. HA without crosslinker at high concentration (4%) was used as control and the brightfield image shows the invasiveness of the tumor model leading to material degradation and cell migration. This degradation did not allow the fixation of the construct and subsequent histological analyzes. Differently, however, for the HA-MMI samples: after 24 hours the structure of the spheroids has been kept intact as can be observed from the images in Figure 51.

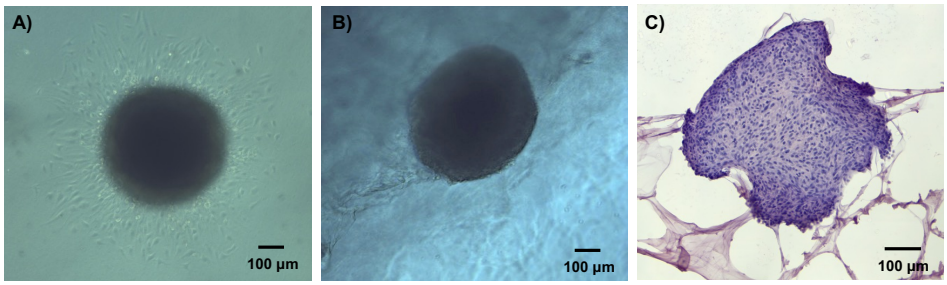

Figure 52: Images of U87 spheroid embedded in no crosslinked HA as control (A) and in functionalized HA-MMPI. Histological images of HA-MMPI embedded spheroid (C)

Therefore, the present study compared the expression profiles of MMP-2 and MMP-9, overexpressed in GBM. As a control, cultured spheroids in absence of the biomaterial were used. Strong

immunoreactivity was found for each of the proteins studied. The experiments were conducted in triplicate and a specific immunofluorescence protocol was developed. Each image obtained was loaded and reprocessed with MatLAB in order to conduct statistical studies. For each sample, images were taken on different regions, and therefore a normalization for the number of cells involved was necessary. The samples were normalized for the DAPI nuclear dye fluorescence intensity correlated with the amount of cells on each slide (Figure 52). From the data the presence of the hyaluronic material with the inhibitor functionalized reduces the expression of MMP-2. In fact, reporting the normalized data, the fluorescience value for MMP-2 appears higher in the control compared to the treated one. On the other hand, the data shows an increase in MMP-9 in the presence of HA-MMPI, with the control resulting to have a lower expression. This data confirm the expettations; it is known that the presence of hyaluronic acid increases the expression of MMP-2 and MMP-9.[264,265] The increase in expression is found only in MMP-9 and not in MMP-2, validating the immunohistochemistry method and the specific inhibitory capacity of the MMPI synthesis molecule linked to hyaluronic acid.

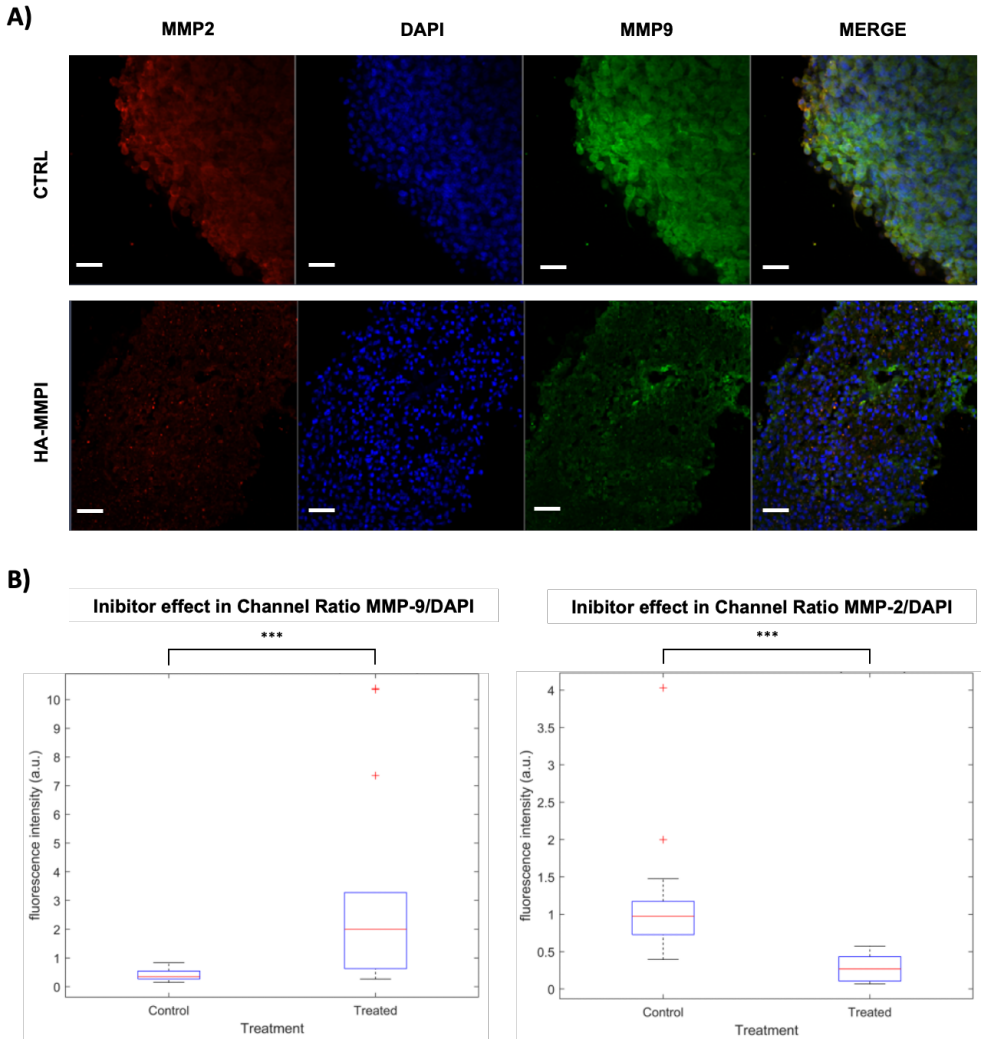

Figure 53: (A) Immunofluorescent images of HA-MMPI and Control spheroids.(B) Box-plots of inhibitor effect in channel ratio MMP9/DAPI and MMP2/DAPI. Lines represent median values. Plus signs denote outliers. *P < 0.05, ***P < 0.001 using Student's t tests.

2. MATERIALS AND METHODS

2.1 Materials

Buffer solution pH 6.0, Citric acid / sodium hydroxide solution was purchased from Honeywell Fluka. All other reagents were purchased from Merck KGa, unless differently stated, and used as received without further purifications.

2.2 Cell Culture

Human glioblastoma cell culture. The U-87 human glioblastoma cell line was obtained from Sigma-Aldrich (Milan, Italy). U-87 MG were grown in Minimum Essential Medium (MEM) supplemented with 2 mM L-glutamine, 1.0 mM sodium pyruvate, 10% fetal bovine serum, 100 units/ml penicillin, and 100 mg/ml streptomycin. Cell culture was maintained in 2D monolayers at 37 °C under a humidified atmosphere with 5% CO_2.

2.3 3D Spheroids Formation

Cell aggregation was induced by growing cell suspensions in 96-multiwell Ultra-low Attachment Surface as already described.[177] Briefly, once cell culture monolayers were detached via standard trypsinization, cells were counted and resuspend to reach the concentration of 5 x 10^4/ml. 100 µl of cells suspension (5 x 10^3) were

pipetted into each well and allowed to grow for 5 days, until spheroids reach the diameter of ~500 µm.

2.4 HA-MMPI Embedding

15 mg of HA-MMPI has been hydrated with 1 ml of PBS at pH 7.4. Once the buffer has been completely absorbed, the sample was splitted in 3 and inserted into a 96 well plate. In the meantime, after 5 days of growth, 10 resulting spheroids (diameter ~500 µm) were moved by 50 µl gentle pipetting fresh culture medium into PBS hydrated HA-MMPI coated well plate and cultured for 1 day.

2.5 Immunofluorescence and Histological Analysis

Embedded spheroids were fixed with 10% neutral buffered formalin for 1 h at RT, washed with phosphate-buffered saline (PBS), placed on filter paper and moved into histological cassettes. Using a standard protocol, samples were paraffin-embedded with a tissue processor (ETP, Histo-Line Laboratories) and cross-sectioned by rotatory microtome (Leica RM2265). Sections at 3 µm thickness were obtained, mounted on glass slides and stained with Haematoxylin and Eosin (H&E). Representative images were captured with a digital camera (Evolution VF digital Camera) using Image-Pro Plus software. Embedded spheroids were employed for immunofluorescence assays for MMP-2 and MMP-9 detection. Samples were deparaffinized with

xylene and rehydrated through a 100%, 95%, 70%, 50% ethanol series and lastly washed in water. Antigen retrival treatment using buffer solution pH 6 was performed at 90 °C for 10 min. After colling 20 min at RT, slices were incubated in permeabilization/blocking solution (5% goat serum, 1% Triton X-100 in PBS) at room temperature for 30 min. Sample were incubated overnight at 4 °C with a primary antibody against anti-MMP-9 (anti-MMP-9 produced in mouse, SAB1402274) and MMP-2 (anti-MMP-2 produced in rabbit, SAB2108458) diluted in PBS 1% goat serum 1:100. After incubation, slices were washed 3 times for 5 min with 1:5 diluted permeabilization/blocking solution. The secondary antibodies used were CF 488-conjugated goat anti-mouse IgG (SAB46000234) and CF 568-conjugated goat anti-rabbit IgG (SAB4600082) 1:200 diluted in PBS for 1 h. After 3 PBS washes, 5 min each, coverslips were mounted with a drop ofFluoroshield™ Mounting Medium with DAPI to visualize the nuclei and image by confocal fluorescence microscopy. As control, the same staining protocol has been followed on spheroids without the HA-MMPI biomaterial.

2.6 Confocal Analysis

A spinning disk confocal microscope (Zeiss Cell Obesrver SD) equipped with a high speed sCMOS Camera (Hamamatsu Orca flash 2.0) provide the fluorescence image acquisition of the labelled spheroids slices. A full three-dimensional image was acquired for each sample with a planar resolution of 600x600 nm^2 for a total area of 160X160 μm^2 and a z stack of five images spaced apart of 1μm. The objective used was a plan 20X with 0.4 of NA. Each plane consists of

a multichannel image with a time-separated acquisition using 405, 488 and 561 nm solid-state lasers for excitation and a three-band pass filter to acquire of the fluorescence signal in the 425-455, 500-535, 590-700 nm windows.

The signal quantification was executed following the subsequent procedure:

- Each channel is considered independently.
- A bi-dimensional Maximum Projection Image is obtained by the full three-dimensional image.
- An adaptive intensity threshold calculated as a fixed percentile (5%) of the intensity histogram is used to generate a binary mask to distinguish the signal (above the threshold) from what considered as noise (below threshold).
- The sum of the total intensity of the pixel inside the mask divided the area of the mask is computed as signal magnitude of this specific channel
- The Dapi signal that quantifies the nuclei presence is used as a further normalization of the fluorescence signal.

2.7 Statistical Analysis

Statistical analysis was determined with Student's t test for comparison between two experimental groups. $p<0.05$ was considered statistically significant.

3. Conclusion

The intrinsic biocompatibility and biodegradability together with the susceptibility to chemical modifications make HA attractive for the development of biomaterials with promising and wide clinical potential. The particular role of natural lubricant and the excellent properties of retaining water make HA a compound with great potential in the biomedical field. The novelty reported concerns a new hyaluronic acid derivative, which maintains the chemical-physical characteristics of natural hyaluronic acid displaying additional anti-inflammatory properties and greater resistance to enzymatic degradation. The property investigated in this work is the inhibitory capacity of MMP2, the metalloproteinase responsible for glioblastoma infection. To evaluate it, a 3D experiment with embedded spheroids was set up and the metalloproteinase expression quantified with immunofluorescence.

ACRONYMS

3D	Three Dimensional
CAD	Computer-Aided Design
CH	Chitosan
DA	Diels–Alder
ECM	Extracellular Matrix
EL	Elastin
FN	Fribronectin
FT-IR	Fourier-Transform Infrared Spectroscopy
GAGs	Glycosaminoglycans
GE	Gelatin
GELCHEL	Gelatin-Chitosan-Elastin Based Hydrogel
GelCHiDA	Gelatin-Chitosan Based Hydrogel
GelMA	Methacrylated Gelatin
HA	Hyaluronic Acid
MF	Methyl Furfural
NMR	Nuclear Magnetic Resonance
PCL	Polycaprolactone
PEG-Star-MA	4arm-PEG10K-Maleimide
PG	Proteoglycans
PGA	Polyglycol Acid
PLA	Polyacidic Acid
SEM	Scanning Electron Microscope
TE	Tissue Engineering
TGA	Thermogravimetric Analysis

List of Figures

List of Tables

List of Scheme

Published Papers and Book Chapters

1. **Magli, S.,** Rossi, G., Risi, G., Bertini, S., Cosentino, C., Crippa, L., et al. (2020). Design and Synthesis of Chitosan—Gelatin Hybrid Hydrogels for 3D Printable *in vitro* Models. FRONTIERS IN CHEMISTRY, 8.

2. Nicolas, J., **Magli, S.,** Rabbachin, L., Sampaolesi, S., Nicotra, F., & Russo, L. (2020). 3D Extracellular. Matrix Mimics: Fundamental Concepts and Role of Materials Chemistry toInfluence Stem Cell Fate. BIOMACROMOLECULES, 21(6), 1968-1994.

3. Pignatelli, C, Cadamuro, F, **Magli, S**, Rossi, L, Russo, L, Nicotra, F (2021). Glycans and hybrid glyco-materials for artificial cell microenvironment fabrication. In: (a cura di): Amélia Pilar Rauter;Thisbe K Lindhorst;Yves Queneau, Carbohydrate Chemistry : Chemical and Biological Approaches. CARBOHYDRATE CHEMISTRY, vol. 44, p. 250-276, Royal Society of Chemistry, ISBN: 9781788013680, ISSN: 2041-353X, doi: 10.1039/9781788013864-00250

4. **S. Magli,** L. Rossi, C. Consentino, S. Bertini, F. Nicotra, L. Russo, Combined Analytical Approaches to Standardize and Characterize Biomaterials Formulations: Application to Chitosan-Gelatin Cross-Linked Hydrogels, Biomol. 2021, Vol. 11, Page 683. 11 (2021) 683.

Conference Presentations

ORAL COMMUNICATIONS

1. ADVANCED SCHOOL ON CARBOHYDRATE CHEMISTRY (XVII CSCC-2020) - Certosa di Pontignano (SI), 21-24 June 2021 “Bioprinting of injectable hydrogels combining glyco and protein-based biomaterials for tissue engineering”

2. Workshop Ricerca e Nanomedicina 2021 - CHT - Centro Interdipartimentale di Tecnologie per la Salute l Università di Pavia, DDS - Department of Drug Sciences – Webinar – 15 June 2021 “Multifunctional hybrid hydrogels: potential as 3D bioprintable platforms in tissue engineering and preclinical investigation”

3. SCI - ViSYOChem 2020 - 1st Virtual Symposium for Young Organic Chemists - 3-6 November 2020- Sofia Magli - “Design, synthesis and applications of chitosan-gelatin based hydrogel for 3D cell culture systems”

4. 8th-12th September 2019. XXXIX Convegno Nazionale della Divisione di Chimica Organica della Società Chimica Italiana. Sofi a Magli - Multimodal Functionalization of Nanoparticles for β-cells Imaging: new diagnostic tools for pancreatic regenerative therapies

5. 8th June 2019. Ricerca e Nanomedicina. Department of Chemistry, University of Pavia. Sofia Magli. “New Smart Hybrid Hydrogels for 3D Printable Extracellular Matrix Biomimetics “ 6. 18th - 19th February 2019, 18th Symposium "Scientific days of the Consortium CINMPIS”, Sofia Magli - “Design and synthesis of natural biopolymers for 3d-materials and tissue engineering

POSTERS

1. 15th December 2020 - Btbsday 2021 – Universiity of Milan - Webinar “Engineered hybrid hydrogels as 3D bioprintable platform for pre- clinical investigations “ - **WINNER BEST POSTER PRESENTATION**

2. 11-14th Dicember 2019 NANODAY IV Magli S., Rossi G.B., Barbugian F., Renis D., Risi G., Bertini S., Cosentino C., Nicotra F., Russo L.Magli Sofia (University of Milano-Bicocca). Bioprintable hybrid ECM for cell modelling and bioengineering applications.

3. 2nd-3rd May 2019, Nanomedicine 2019. S. Magli, G. Frigerio, D. Renis, S. Bertini, C. Cosentino, I. Lampedecchia, L. Rabbachin, G. Risi, S. Sampaolesi, F. Nicotra, L. Russo. New printable hybrid hydrogels for 3D-materials and tissue engineering purpose

4.. 2nd-3rd May 2019, Nanomedicine 2019. S. Sampaolesi, S. Facchetti, A. Grittini, I. Lampedecchia, S. Magli, G. Risi, C. Cosentino, S. Bertini, F. Nicotra, L. Russo. Printable multicomponent hydrogels for 3D cell model and tissue engineering applications

5.. 11th-13th March 2019 Milan Polymer Days. S. Magli, J. Andrieu, S. Bertini, C. Cosentino, I. Lampedecchia, L. Rabbachin G. Risi, S. Sampaolesi, G. Stucchi, F. Nicotra, L. Russo. Functionalized biopolymers for 3D cell models and tissue engineering applications

6. 11th-13th March 2019 Milan Polymer Days. S. Sampaolesi, S. Bertini, C. Cosentino, I. Lampedecchia, S. Magli, G. Risi, F. Nicotra, L. Russo. Elastin-based hybrid hydrogels as ECM mimics in 3D cell culture and tissue engineering applications

7. 22th November 2018, BtbsDay. S. Magli, J. Andrieu, S. Bertini, C. Cosentino, I. Lampedecchia, L. Rabbachin G. Risi, S. Sampaolesi, G. Stucchi, F. Nicotra, L. Russo. New 3D printable Extracellular Matrix Mimetics as new bioink for cell microenvironment studies

8. 22th November 2018, BtbaDay. S. Sampaolesi, S. Facchetti, I. Lampedecchia, S. Magli, F. Nicotra, L. Russo. Bioprintable elastin based hybrid hydrogels for 3D cell model and tissue engineering applications

Bibliography

(1) Langer, R. Editorial: Tissue Engineering: Perspectives, Challenges, and Future Directions. *https://home.liebertpub.com/ten* **2007**, *13* (1), 1–2. https://doi.org/10.1089/TEN.2006.0219.

(2) Griffith, L. G.; Naughton, G. Tissue Engineering - Current Challenges and Expanding Opportunities. *Science (80-.).* **2002**, *295* (5557). https://doi.org/10.1126/SCIENCE.1069210.

(3) Hench, L. L.; Jones, J. R. *Biomaterials, Artificial Organs and Tissue Engineering*; 2005. https://doi.org/10.1533/9781845690861.

(4) Fioretta, E. S.; Motta, S. E.; Lintas, V.; Loerakker, S.; Parker, K. K.; Baaijens, F. P. T.; Falk, V.; Hoerstrup, S. P.; Emmert, M. Y. Next-Generation Tissue-Engineered Heart Valves with Repair, Remodelling and Regeneration Capacity. *Nature Reviews Cardiology*. Nature Publishing Group September 9, 2021, pp 92–116. https://doi.org/10.1038/s41569-020-0422-8.

(5) Nowik, K.; Langwińska-Wośko, E.; Skopiński, P.; Nowik, K. E.; Szaflik, J. P. Bionic Eye Review – An Update. *Journal of Clinical Neuroscience*. Churchill Livingstone August 1, 2020, pp 8–19. https://doi.org/10.1016/j.jocn.2020.05.041.

(6) Stavdahl, Ø.; Fougner, A. L.; Kölle, K.; Christiansen, S. C.; Ellingsen, R.; Carlsen, S. M. The Artificial Pancreas: A Dynamic Challenge. In *IFAC-PapersOnLine*; Elsevier, 2016; Vol. 49, pp 765–772. https://doi.org/10.1016/j.ifacol.2016.07.280.

(7) Stone, H. L. Implant Able Pressure Transducers - Future Needs and Applications of Totally Implantable Units. In *Indwelling and Implantable Pressure Transducers*; Academic Press, 2018; pp 11–19. https://doi.org/10.1201/9781351073516.

(8) Khademhosseini, A.; Langer, R. A Decade of Progress in Tissue Engineering. *Nat. Protoc. 2016 1110* **2016**, *11* (10), 1775–1781. https://doi.org/10.1038/nprot.2016.123.

(9) Wu, R. X.; Xu, X. Y.; Wang, J.; He, X. T.; Sun, H. H.; Chen, F. M. Biomaterials for Endogenous Regenerative Medicine: Coaxing Stem Cell Homing and Beyond. *Appl. Mater. Today* **2018**, *11*, 144–165. https://doi.org/10.1016/J.APMT.2018.02.004.

(10) Vacanti, J. P.; Langer, R. Tissue Engineering: The Design and Fabrication of Living Replacement Devices for Surgical Reconstruction and Transplantation. *Lancet* **1999**, *354* (SUPPL.1), 32–34. https://doi.org/10.1016/s0140-6736(99)90247-7.

(11) Hussey, G. S.; Dziki, J. L.; Badylak, S. F. Extracellular Matrix-Based Materials for Regenerative Medicine. *Nat. Rev. Mater.* **2018**, *3* (7), 159–173. https://doi.org/10.1038/s41578-018-0023-x.

(12) Ramos, T.; Moroni, L. Tissue Engineering and Regenerative Medicine 2019: The Role of Biofabrication - A Year in Review. *Tissue Engineering - Part C: Methods*. Mary Ann Liebert Inc. February 1, 2020, pp 91–106. https://doi.org/10.1089/ten.tec.2019.0344.

(13) R, L.; JP, V. Tissue Engineering. *Science* **1993**, *260* (5110), 920–926. https://doi.org/10.1126/SCIENCE.8493529.

(14) Frantz, C.; Stewart, K. M.; Weaver, V. M. The Extracellular Matrix at a Glance. *J. Cell Sci.* **2010**, *123* (24), 4195–4200. https://doi.org/10.1242/jcs.023820.

(15) Rouwkema, J.; Gibbs, S.; Lutolf, M.; Martin, I.; Vunjak-Novakovic, G.; Malda, J. In Vitro Platforms for Tissue Engineering: Implications to Basic Research and Clinical Translation. *J. Tissue Eng. Regen. Med.* **2011**, *5* (8), e164. https://doi.org/10.1002/TERM.414.

(16) Sengupta, D.; Waldman, S. D.; Li, S. From in Vitro to in Situ Tissue Engineering. *Ann. Biomed. Eng.* **2014**, *42* (7), 1537–1545. https://doi.org/10.1007/s10439-014-1022-8.

(17) Laurell, L.; Gottlow, J. Guided Tissue Regeneration Update. *Int. Dent. J.* **1998**, *48* (4), 386–398. https://doi.org/10.1111/J.1875-595X.1998.TB00701.X.

(18) Gaharwar, A. K.; Singh, I.; Khademhosseini, A. Engineered Biomaterials for in Situ Tissue Regeneration. *Nature Reviews Materials*. 2020, pp 686–705. https://doi.org/10.1038/s41578-020-0209-x.

(19) Ruan, M. Z. C.; Erez, A.; Guse, K.; Dawson, B.; Bertin, T.; Chen, Y.; Jiang, M. M.; Yustein, J.; Gannon, F.; Lee, B. H. L. Proteoglycan 4 Expression Protects against the Development of Osteoarthritis. *Sci. Transl. Med.* **2013**, *5* (176). https://doi.org/10.1126/scitranslmed.3005409.

(20) Huang, Q.; Goh, J. C. H.; Hutmacher, D. W.; Lee, E. H. In Vivo Mesenchymal Cell Recruitment by a Scaffold Loaded with Transforming Growth Factor B1 and the Potential for in Situ Chondrogenesis. *Tissue Eng.* **2002**, *8* (3), 469–482. https://doi.org/10.1089/107632702760184727.

(21) Li, S.; Sengupta, D.; Chien, S. Vascular Tissue Engineering: From in Vitro to in Situ. *Wiley Interdisciplinary Reviews: Systems Biology and Medicine*. John Wiley & Sons, Ltd January 1, 2014, pp 61–76. https://doi.org/10.1002/wsbm.1246.

(22) Haycock, J. W. 3D Cell Culture: A Review of Current Approaches and Techniques. *Methods Mol. Biol.* **2011**, *695*, 1–15. https://doi.org/10.1007/978-1-60761-984-0_1.

(23) Martin, I.; Wendt, D.; Heberer, M. The Role of Bioreactors in Tissue Engineering. *Trends Biotechnol.* **2004**, *22* (2), 80–86. https://doi.org/10.1016/J.TIBTECH.2003.12.001.

(24) Rosellini, E.; Zhang, Y. S.; Migliori, B.; Barbani, N.; Lazzeri, L.; Shin, S. R.; Dokmeci, M. R.; Cascone, M. G. Protein/Polysaccharide-Based Scaffolds Mimicking Native Extracellular Matrix for Cardiac Tissue Engineering Applications. *J. Biomed. Mater. Res. - Part A* **2018**, *106* (3), 769–781. https://doi.org/10.1002/jbm.a.36272.

(25) Hinderer, S.; Layland, S. L.; Schenke-Layland, K. ECM and ECM-like Materials - Biomaterials for Applications in Regenerative Medicine and Cancer Therapy. *Adv. Drug Deliv. Rev.* **2016**, *97*, 260–269.

(26) Kyburz, K. A.; Anseth, K. S. Synthetic Mimics of the Extracellular Matrix: How Simple Is Complex Enough? *Ann. Biomed. Eng.* **2015**, *43* (3), 489–500. https://doi.org/10.1007/s10439-015-1297-4.

(27) Gattazzo, F.; Urciuolo, A.; Bonaldo, P. Extracellular Matrix: A Dynamic Microenvironment for Stem Cell Niche. *Biochim. Biophys. Acta* **2014**, *1840* (8), 2506–2519. https://doi.org/10.1016/j.bbagen.2014.01.010.

(28) Naba, A.; Clauser, K. R.; Ding, H.; Whittaker, C. A.; Carr, S. A.; Hynes, R. O. The Extracellular Matrix: Tools and Insights for the “Omics” Era. *Matrix Biol.* **2016**, *49*, 10–24. https://doi.org/10.1016/j.matbio.2015.06.003.

(29) Alberts, B.; Johnson, A.; Lewis, J.; Raff, M.; Roberts, K.; Walter, P. The Extracellular Matrix of Animals. **2002**.

(30) Schlie-Wolter, S.; Ngezahayo, A.; Chichkov, B. N. The Selective Role of ECM Components on Cell Adhesion, Morphology, Proliferation and Communication in Vitro. *Exp. Cell Res.* **2013**, *319* (10), 1553–1561. https://doi.org/10.1016/j.yexcr.2013.03.016.

(31) Hynes, R. O. The Extracellular Matrix: Not Just Pretty Fibrils. *Science (80-.).* **2009**. https://doi.org/10.1126/science.1176009.

(32) G, H.; F, L.; X, Z.; Y, M.; Y, L.; M, L.; G, J.; TJ, L.; GM, G.; F, X. Functional and Biomimetic Materials for Engineering of the Three-Dimensional Cell Microenvironment. *Chem. Rev.* **2017**, *117* (20), 12764–12850. https://doi.org/10.1021/ACS.CHEMREV.7B00094.

(33) Ricard-Blum, S. The Collagen Family. *Cold Spring Harb. Perspect. Biol.* **2011**, *3* (1), a004978. https://doi.org/10.1101/cshperspect.a004978.

(34) Hynes, R. O. The Extracellular Matrix: Not Just Pretty Fibrils. *Science (80-.).* **2009**, *326* (5957), 1216–1219. https://doi.org/10.1126/science.1176009.

(35) Mithieux, S. M.; Weiss, A. S. Elastin. *Adv. Protein Chem.* **2005**. https://doi.org/10.1016/S0065-3233(05)70013-9.

(36) Sarrazin, S.; Lamanna, W. C.; Esko, J. D. Heparan Sulfate Proteoglycans. *Cold Spring Harb. Perspect. Biol.* **2011**, *3* (7), a004952. https://doi.org/10.1101/CSHPERSPECT.A004952.

(37) Walimbe, T.; Panitch, A. Proteoglycans in Biomedicine: Resurgence of an Underexploited Class of ECM Molecules. *Front. Pharmacol.* **2020**, *10*, 1661. https://doi.org/10.3389/fphar.2019.01661.

(38) Bosman, F. T.; Stamenkovic, I. Functional Structure and Composition of the Extracellular Matrix. *J. Pathol.* **2003**, *200* (4), 423–428. https://doi.org/10.1002/PATH.1437.

(39) Mao, Y.; Schwarzbauer, J. E. Fibronectin Fibrillogenesis, a Cell-Mediated Matrix Assembly Process. *Matrix Biol.* **2005**, *24* (6), 389–399. https://doi.org/10.1016/J.MATBIO.2005.06.008.

(40) Potts, J. R.; Campbell, I. D. Structure and Function of Fibronectin Modules. *Matrix Biol.* **1996**, *15* (5), 313–320. https://doi.org/10.1016/S0945-053X(96)90133-X.

(41) Proctor, R. A. Fibronectin: A Brief Overview of Its Structure, Function, and Physiology. *Rev. Infect. Dis.* **1987**, *9* (Supplement_4), S317–S321. https://doi.org/10.1093/CLINIDS/9.SUPPLEMENT_4.S317.

(42) Ruoslahti, E. RGD and Other Recognition Sequences for Integrins. *Annu. Rev. Cell Dev. Biol.* **1996**, *12*, 697–715. https://doi.org/10.1146/annurev.cellbio.12.1.697.

(43) Guldager Kring Rasmussen, D.; Karsdal, M. A. Laminins. In *Biochemistry of Collagens, Laminins and Elastin: Structure, Function and Biomarkers*; Nordic Bioscience: Herlev, 2016; pp 163–196. https://doi.org/10.1016/B978-0-12-809847-9.00029-5.

(44) Aumailley, M. The Laminin Family. *Cell Adhesion and Migration*. 2013, pp 48–55. https://doi.org/10.4161/cam.22826.

(45) Li, S.; Edgar, D.; Fässler, R.; Wadsworth, W.; Yurchenco, P. D. The Role of Laminin

in Embryonic Cell Polarization and Tissue Organization. *Dev. Cell* **2003**, *4* (5), 613–624. https://doi.org/10.1016/S1534-5807(03)00128-X.

(46) Markert, C. D.; Guo, X.; Skardal, A.; Wang, Z.; Bharadwaj, S.; Zhang, Y.; Bonin, K.; Guthold, M. Characterizing the Micro-Scale Elastic Modulus of Hydrogels for Use in Regenerative Medicine. *J. Mech. Behav. Biomed. Mater.* **2013**, *27*, 115–127. https://doi.org/10.1016/j.jmbbm.2013.07.008.

(47) Ramsey, W. S.; Hertl, W.; Nowlan, E. D.; Binkowski, N. J. Surface Treatments and Cell Attachment. *Vitr. 1984 2010* **1984**, *20* (10), 802–808. https://doi.org/10.1007/BF02618296.

(48) Edmondson, R.; Broglie, J. J.; Adcock, A. F.; Yang, L. Three-Dimensional Cell Culture Systems and Their Applications in Drug Discovery and Cell-Based Biosensors. *Assay Drug Dev. Technol.* **2014**, *12* (4), 207–218. https://doi.org/10.1089/adt.2014.573.

(49) BM, B.; CS, C. Deconstructing the Third Dimension: How 3D Culture Microenvironments Alter Cellular Cues. *J. Cell Sci.* **2012**, *125* (Pt 13), 3015–3024. https://doi.org/10.1242/JCS.079509.

(50) Hofer, M.; Lutolf, M. P. Engineering Organoids. *Nature Reviews Materials*. 2021, pp 402–420. https://doi.org/10.1038/s41578-021-00279-y.

(51) Ovsianikov, A.; Khademhosseini, A.; Mironov, V. The Synergy of Scaffold-Based and Scaffold-Free Tissue Engineering Strategies. *Trends Biotechnol.* **2018**, *36* (4), 348–357. https://doi.org/10.1016/j.tibtech.2018.01.005.

(52) Mathew, A. P.; Augustine, R.; Kalarikkal, N.; Thomas, S. Tissue Engineering: Principles, Recent Trends and the Future. In *Nanomedicine and Tissue Engineering: State of the Art and Recent Trends*; 2016; pp 31–82. https://doi.org/10.1201/b19867-3.

(53) Kay C. Dee, David A. Puleo, R. B. *An Introduction to Tissue-Biomaterial Interactions*; New Jersey, 2002.

(54) Advances in Nanopathology: From Vaccines to Food - Antonietta Morena Gatti, Stefano Montanari - Google Books https://books.google.it/books?id=VIkmEAAAQBAJ&pg=PT16&lpg=PT16&dq=%22Any+substance+or+combination+of+substances,+other+than+a+drug,+of+synthetic+or+natural+origin,+that+can+be+used+for+any+period+of+time,+alone+or+as+part+of+a+system+that+treats,+augments+or+replaces+any&source=bl&ots=jbAqr8a3D1&sig=ACfU3U0J6_Kq7Kc-c9hNtxQHiS_u3Jv3lg&hl=en&sa=X&ved=2ahUKEwi-

0M2b6ajzAhV8hf0HHXQwDbQQ6AF6BAgOEAM#v=onepage&q=%22Any substance or combination of substances%2C other than a drug%2C of synthetic or natural origin%2C that can be used for any period of time%2C alone or as part of a system that treats%2C augments or replaces any&f=false (accessed Oct 1, 2021).

(55) Gatti, A. M.; Montanari, S. Advances in Nanopathology From Vaccines to Food. *Adv. Nanopathology From Vaccines to Food* **2021**. https://doi.org/10.1201/9781003056225/ADVANCES-NANOPATHOLOGY-VACCINES-FOOD-ANTONIETTA-MORENA-GATTI-STEFANO-MONTANARI.

(56) Williams, D. F. On the Nature of Biomaterials. *Biomaterials* **2009**, *30* (30), 5897–5909. https://doi.org/10.1016/J.BIOMATERIALS.2009.07.027.

(57) Groll, J.; Burdick, J. A.; Cho, D. W.; Derby, B.; Gelinsky, M.; Heilshorn, S. C.; Jüngst, T.; Malda, J.; Mironov, V. A.; Nakayama, K.; Ovsianikov, A.; Sun, W.; Takeuchi, S.; Yoo, J. J.; Woodfield, T. B. F. A Definition of Bioinks and Their Distinction from Biomaterial Inks. *Biofabrication*. 2019. https://doi.org/10.1088/1758-5090/aaec52.

(58) Park, J.; Lakes, R. *Biomaterials: An Introduction*; 2007.

(59) Peppas, N.; Science, R. L.-; 1994, undefined. New Challenges in Biomaterials. *science.sciencemag.org*.

(60) S. Place, E.; H. George, J.; K. Williams, C.; M. Stevens, M. Synthetic Polymer Scaffolds for Tissue Engineering. *Chem. Soc. Rev.* **2009**, *38* (4), 1139–1151. https://doi.org/10.1039/B811392K.

(61) Cortiella, J.; Nichols, J. E.; Kojima, K.; Bonassar, L. J.; Dargon, P.; Roy, A. K.; Vacant, M. P.; Niles, J. A.; Vacanti, C. A. Tissue-Engineered Lung: An in Vivo and in Vitro Comparison of Polyglycolic Acid and Pluronic F-127 Hydrogel/Somatic Lung Progenitor Cell Constructs to Support Tissue Growth. *Tissue Eng.* **2006**. https://doi.org/10.1089/ten.2006.12.1213.

(62) Banoriya, D.; Purohit, R.; Dwivedi, R. K. Advanced Application of Polymer Based Biomaterials. *Mater. Today Proc.* **2017**, *4* (2), 3534–3541. https://doi.org/10.1016/J.MATPR.2017.02.244.

(63) Benatti, A. C. B.; Pattaro, A. F.; Rodrigues, A. A.; Xavier, M. V.; Kaasi, A.; Barbosa, M. I. R.; Jardini, A. L.; Filho, R. M.; Kharmandayan, P. Bioreabsorbable Polymers for Tissue Engineering: PLA, PGA, and Their Copolymers. *Mater. Biomed. Eng.* **2019**, 83–116. https://doi.org/10.1016/B978-0-12-816901-8.00004-3.

(64) Ma, P. X.; Langer, R. Degradation, Structure and Properties of Fibrous Nonwoven

Poly(Glycolic Acid) Scaffolds for Tissue Engineering. *MRS Online Proc. Libr.* **1995**, *394*, 99–104. https://doi.org/10.1557/PROC-394-99.

(65) Athanasiou, K. A.; Agrawal, C. M.; Barber, F. A.; Burkhart, S. S. Orthopaedic Applications for PLA-PGA Biodegradable Polymers. *Arthrosc. J. Arthrosc. Relat. Surg.* **1998**, *14* (7), 726–737. https://doi.org/10.1016/S0749-8063(98)70099-4.

(66) Duling, R. R.; Dupaix, R. B.; Katsube, N.; Lannutti, J. Mechanical Characterization of Electrospun Polycaprolactone (PCL): A Potential Scaffold for Tissue Engineering. *J. Biomech. Eng.* **2008**, *130* (1). https://doi.org/10.1115/1.2838033.

(67) Moussa, D. G.; Aparicio, C. Present and Future of Tissue Engineering Scaffolds for Dentin-Pulp Complex Regeneration. *J. Tissue Eng. Regen. Med.* **2019**, *13* (1), 58–75. https://doi.org/10.1002/TERM.2769.

(68) Nelso, D. L.; Cox, M. M. *Lehninger Principles of Biochemistry*, 7th ed.; Freeman, W. H., Ed.; New York, 2017.

(69) Vroman, I.; Tighzert, L. Biodegradable Polymers. *Mater. 2009, Vol. 2, Pages 307-344* **2009**, *2* (2), 307–344. https://doi.org/10.3390/MA2020307.

(70) Davidenko, N.; Schuster, C. F.; Bax, D. V; Farndale, R. W.; Hamaia, S.; Best, S. M.; Cameron, R. E. Evaluation of Cell Binding to Collagen and Gelatin: A Study of the Effect of 2D and 3D Architecture and Surface Chemistry. *J. Mater. Sci. Mater. Med.* **2016**, *27* (10), 148. https://doi.org/10.1007/s10856-016-5763-9.

(71) Rosenbloom, J.; Abrams, W. R.; Mecham, R. Extracellular Matrix 4: The Elastic Fiber. *FASEB J.* **1993**, *7* (13), 1208–1218. https://doi.org/10.1096/FASEBJ.7.13.8405806.

(72) Ayad, S.; Boot-Handford, R.; Humphries, M. The Extracellular Matrix Factsbook. **1998**, 313.

(73) Chrzanowski, P.; Keller, S.; Cerreta, J.; Mandl, I.; Turino, G. M. Elastin Content of Normal and Emphysematous Lung Parenchyma. *Am. J. Med.* **1980**, *69* (3), 351–359. https://doi.org/10.1016/0002-9343(80)90004-2.

(74) Debelle, L.; cell, A. T.-T. international journal of biochemistry &; 1999, undefined. Elastin: Molecular Description and Function. *Elsevier*.

(75) Sandberg, L.; Soskel, N.; of, J. L.-N. E. J.; 1981, undefined. Elastin Structure, Biosynthesis, and Relation to Disease States. *Mass Med. Soc*.

(76) Lee, H.; Lee, K.; Kim, I. K.; Park, T. G. Synthesis, Characterization, and in Vivo Diagnostic Applications of Hyaluronic Acid Immobilized Gold Nanoprobes.

Biomaterials **2008**, *29* (35), 4709–4718. https://doi.org/10.1016/j.biomaterials.2008.08.038.

(77) Day, A. J.; Sheehan, J. K. Hyaluronan: Polysaccharide Chaos to Protein Organisation. *Curr. Opin. Struct. Biol.* **2001**, *11* (5), 617–622. https://doi.org/10.1016/S0959-440X(00)00256-6.

(78) Fouissac, E.; Milas, M.; Rinaudo, M.; Borsali, R. Influence of the Ionic Strength on the Dimensions of Sodium Hyaluronate. *Macromolecules* **1992**, *25*, 5613.

(79) Laurent, T. C.; Fraser, J. R. E. Hyaluronan. *FASEB J.* **1992**, *6* (7), 2397–2404. https://doi.org/10.1096/fasebj.6.7.1563592.

(80) Aquino, R. S.; Park, P. W. Glycosaminoglycans and Infection. *Front. Biosci. - Landmark* **2016**, *21* (6), 1260–1277. https://doi.org/10.2741/4455.

(81) Kogan, G.; Šoltés, L.; Stern, R.; Gemeiner, P. Hyaluronic Acid: A Natural Biopolymer with a Broad Range of Biomedical and Industrial Applications. *Biotechnol. Lett. 2006 291* **2006**, *29* (1), 17–25. https://doi.org/10.1007/S10529-006-9219-Z.

(82) Girish, K. S.; Kemparaju, K. The Magic Glue Hyaluronan and Its Eraser Hyaluronidase: A Biological Overview. *Life Sci.* **2007**, *80* (21), 1921–1943. https://doi.org/10.1016/J.LFS.2007.02.037.

(83) TC, L.; UB, L.; JR, F. Functions of Hyaluronan. *Ann. Rheum. Dis.* **1995**, *54* (5), 429–432. https://doi.org/10.1136/ARD.54.5.429.

(84) Lee, J. Y.; Spicer, A. P. Hyaluronan: A Multifunctional, MegaDalton, Stealth Molecule. *Curr. Opin. Cell Biol.* **2000**, *12* (5), 581–586. https://doi.org/10.1016/S0955-0674(00)00135-6.

(85) R, S.; AA, A.; KN, S. Hyaluronan Fragments: An Information-Rich System. *Eur. J. Cell Biol.* **2006**, *85* (8), 699–715. https://doi.org/10.1016/J.EJCB.2006.05.009.

(86) M, L.; A, K.; MS, S.; AR, G.; T, G. Hyaluronic Acid in Inflammation and Tissue Regeneration. *Wounds a Compend. Clin. Res. Pract.* **2016**, *28* (3), 78–88.

(87) G, T.; RF, T.; CM, I. Chemotaxis towards Hyaluronan Is Dependent on CD44 Expression and Modulated by Cell Type Variation in CD44-Hyaluronan Binding. *J. Cell Sci.* **2005**, *118* (Pt 21), 5119–5128. https://doi.org/10.1242/JCS.02629.

(88) WY, C.; G, A. Functions of Hyaluronan in Wound Repair. *Wound Repair Regen.* **1999**, *7* (2), 79–89. https://doi.org/10.1046/J.1524-475X.1999.00079.X.

(89) G, A.; V, V.; G, A.; L, P.; P, B. Hyaluronic Acid: Redefining Its Role. *Cells* **2020**, *9* (7).

https://doi.org/10.3390/CELLS9071743.

(90) Kumar, M.; Muzzarelli, R.; … C. M.-C.; 2004, undefined. Chitosan Chemistry and Pharmaceutical Perspectives. *ACS Publ.* **2004**, *104* (12), 6017–6084. https://doi.org/10.1021/cr030441b.

(91) Li, Q.; Dunn, E. T.; Grandmaison, E. W.; Goosen, M. F. A. Applications and Properties of Chitosan. *J. Bioact. Compat. Polym.* **1992**, *7* (4), 370–397. https://doi.org/10.1177/088391159200700406.

(92) Shepherd, R.; Reader, S.; Falshaw, A. Chitosan Functional Properties. *Glycoconjugate J. 1997 144* **1997**, *14* (4), 535–542. https://doi.org/10.1023/A:1018524207224.

(93) Fei Liu, X.; Lin Guan, Y.; Zhi Yang, D.; Yao, K. DE. Antibacterial Action of Chitosan and Carboxymethylated Chitosan. **2000**. https://doi.org/10.1002/1097-4628(20010214)79:7.

(94) Baino, F.; Novajra, G.; Vitale-Brovarone, C. Bioceramics and Scaffolds: A Winning Combination for Tissue Engineering. *Front. Bioeng. Biotechnol.* **2015**, *0*, 202. https://doi.org/10.3389/FBIOE.2015.00202.

(95) Kopeček, J. Hydrogel Biomaterials: A Smart Future? *Biomaterials* **2007**, *28* (34), 5185–5192. https://doi.org/10.1016/J.BIOMATERIALS.2007.07.044.

(96) Hoffman, A. S. Hydrogels for Biomedical Applications. *Adv. Drug Deliv. Rev.* **2012**, *64* (SUPPL.), 18–23. https://doi.org/10.1016/J.ADDR.2012.09.010.

(97) Chhibber, T.; Shinde, R.; Lahooti, B.; Bagchi, S.; Varahachalam, S. P.; Gaddam, A.; Jaiswal, A. K.; Gracia, E.; Chand, H. S.; Kaushik, A.; Jayant, R. D. Hydrogels in Tissue Engineering. In *Intelligent Hydrogels in Diagnostics and Therapeutics*; 2020; pp 105–122. https://doi.org/10.1201/9781003036050-8.

(98) Sgambato, A.; Cipolla, L.; Russo, L. Bioresponsive Hydrogels: Chemical Strategies and Perspectives in Tissue Engineering. *Gels* **2016**, *2* (4), 28. https://doi.org/10.3390/gels2040028.

(99) Hoare, T. R.; Kohane, D. S. Hydrogels in Drug Delivery: Progress and Challenges. *Polymer*. Elsevier April 15, 2008, pp 1993–2007. https://doi.org/10.1016/j.polymer.2008.01.027.

(100) Laftah, W. A.; Hashim, S.; Ibrahim, A. N. Polymer Hydrogels: A Review. *Polymer - Plastics Technology and Engineering*. Taylor & Francis Group October 2011, pp 1475–

1486. https://doi.org/10.1080/03602559.2011.593082.

(101) JM, B.; DW, G.; PJ, D.; CA, van B.; J, F. A Controlled Release System for Proteins Based on Poly(Ether Ester) Block-Copolymers: Polymer Network Characterization. *J. Control. Release* **1999**, *62* (3), 393–405. https://doi.org/10.1016/S0168-3659(99)00170-4.

(102) GJ, B.; CA, van B.; D, B.; M, P. Cell-Seeding and in Vitro Biocompatibility Evaluation of Polymeric Matrices of PEO/PBT Copolymers and PLLA. *Biomaterials* **1993**, *14* (8), 598–604. https://doi.org/10.1016/0142-9612(93)90178-5.

(103) Perin, F.; Motta, A.; Maniglio, D. Amphiphilic Copolymers in Biomedical Applications: Synthesis Routes and Property Control. *Mater. Sci. Eng. C* **2021**, *123*, 111952. https://doi.org/10.1016/J.MSEC.2021.111952.

(104) M, B.; A, M. Fabrication of Patterned Calcium Cross-Linked Alginate Hydrogel Films and Coatings through Reductive Cation Exchange. *Carbohydr. Polym.* **2015**, *131*, 57–64. https://doi.org/10.1016/J.CARBPOL.2015.05.021.

(105) Higham, A. K.; Bonino, C. A.; Raghavan, S. R.; Khan, S. A. Photo-Activated Ionic Gelation of Alginate Hydrogel: Real-Time Rheological Monitoring of the Two-Step Crosslinking Mechanism. *Soft Matter* **2014**, *10* (27), 4990–5002. https://doi.org/10.1039/c4sm00411f.

(106) Shi, Y.; Zhang, X.; Li, J.; Wang, Z.; Cheng, S.; Chen, L.; Qiang, Y.; Li, H.; Ni, J. Preparation and Pharmacokinetics of an Injectable Thermosensitive Hydrogel of Diminazene Aceturate. *J. Drug Deliv. Sci. Technol.* **2013**, *23* (6), 531–535. https://doi.org/10.1016/S1773-2247(13)50081-5.

(107) Akhtar, M. F.; Hanif, M.; Ranjha, N. M. Methods of Synthesis of Hydrogels … A Review. *Saudi Pharmaceutical Journal*. Elsevier September 1, 2016, pp 554–559. https://doi.org/10.1016/j.jsps.2015.03.022.

(108) Kim, M. H.; Park, W. H. Chemically Cross-Linked Silk Fibroin Hydrogel with Enhanced Elastic Properties, Biodegradability, and Biocompatibility. *Int. J. Nanomedicine* **2016**, *11*, 2967–2978. https://doi.org/10.2147/IJN.S106467.

(109) Lopérgolo, L. C.; Lugão, A. B.; Catalani, L. H. Direct UV Photocrosslinking of Poly(N-Vinyl-2-Pyrrolidone) (PVP) to Produce Hydrogels. *Polymer (Guildf).* **2003**, *44* (20), 6217–6222. https://doi.org/10.1016/S0032-3861(03)00686-4.

(110) Pereira, R. F.; Bártolo, P. J. 3D Bioprinting of Photocrosslinkable Hydrogel Constructs. *J. Appl. Polym. Sci.* **2015**, *132* (48). https://doi.org/10.1002/APP.42458.

(111) Kuckling, D.; Harmon, M.; Macromolecules, C. F.-; 2002, undefined. Photo-Cross-Linkable PNIPAAm Copolymers. 1. Synthesis and Characterization of Constrained Temperature-Responsive Hydrogel Layers. *ACS Publ.* **2002**, *35* (16), 6377–6383. https://doi.org/10.1021/ma0203041.

(112) Miyamoto, K.; Sasaki, M.; Minamisawa, Y.; Kurahashi, Y.; Kano, H.; Ishikawa, S. I. Evaluation of in Vivo Biocompatibility and Biodegradation of Photocrosslinked Hyaluronate Hydrogels (HADgels). *J. Biomed. Mater. Res. - Part A* **2004**, *70* (4), 550–559. https://doi.org/10.1002/jbm.a.30112.

(113) Mohd Amin, M. C. I.; Ahmad, N.; Halib, N.; Ahmad, I. Synthesis and Characterization of Thermo- and PH-Responsive Bacterial Cellulose/Acrylic Acid Hydrogels for Drug Delivery. *Carbohydr. Polym.* **2012**, *88* (2), 465–473. https://doi.org/10.1016/J.CARBPOL.2011.12.022.

(114) N, M.; MCI, M. A.; M, P.; N, A.; NF, R. Bacterial Cellulose/Acrylic Acid Hydrogel Synthesized via Electron Beam Irradiation: Accelerated Burn Wound Healing in an Animal Model. *Carbohydr. Polym.* **2014**, *114*, 312–320. https://doi.org/10.1016/J.CARBPOL.2014.08.025.

(115) Yue, K.; Trujillo-de Santiago, G.; Alvarez, M. M.; Tamayol, A.; Annabi, N.; Khademhosseini, A. Synthesis, Properties, and Biomedical Applications of Gelatin Methacryloyl (GelMA) Hydrogels. *Biomaterials*. Elsevier December 1, 2015, pp 254–271. https://doi.org/10.1016/j.biomaterials.2015.08.045.

(116) F, L.; KH, B.; M, K. Injectable Hydrogel Systems Crosslinked by Horseradish Peroxidase. *Biomed. Mater.* **2015**, *11* (1). https://doi.org/10.1088/1748-6041/11/1/014101.

(117) Hu, W.; Wang, Z.; Xiao, Y.; Zhang, S.; Wang, J. Advances in Crosslinking Strategies of Biomedical Hydrogels. *Biomaterials Science*. Royal Society of Chemistry March 2019, pp 843–855. https://doi.org/10.1039/c8bm01246f.

(118) Kolb, H. C.; Finn, M. G.; Sharpless, K. B. Click Chemistry: Diverse Chemical Function from a Few Good Reactions. *Angewandte Chemie - International Edition*. 2001, pp 2004–2021. https://doi.org/10.1002/1521-3773(20010601)40:11<2004::AID-ANIE2004>3.0.CO;2-5.

(119) Gregoritza, M.; Brandl, F. P. The Diels-Alder Reaction: A Powerful Tool for the Design of Drug Delivery Systems and Biomaterials. *Eur. J. Pharm. Biopharm.* **2015**, *97* (Pt B), 438–453. https://doi.org/10.1016/j.ejpb.2015.06.007.

(120) Kolb, H. C.; Sharpless, K. B. The Growing Impact of Click Chemistry on Drug Discovery. *Drug Discov. Today* **2003**, *8* (24), 1128–1137. https://doi.org/10.1016/S1359-6446(03)02933-7.

(121) Mather, B. D.; Viswanathan, K.; Miller, K. M.; Long, T. E. Michael Addition Reactions in Macromolecular Design for Emerging Technologies. *Prog. Polym. Sci.* **2006**, *31* (5), 487–531. https://doi.org/https://doi.org/10.1016/j.progpolymsci.2006.03.001.

(122) Metters, A.; Biomacromolecules, J. H.-; 2005, undefined. Network Formation and Degradation Behavior of Hydrogels Formed by Michael-Type Addition Reactions. *ACS Publ.* **2005**, *6* (1), 290–301. https://doi.org/10.1021/bm049607o.

(123) Censi, R.; Fieten, P.; Martino, P. di; … W. H.-; 2010, undefined. In Situ Forming Hydrogels by Tandem Thermal Gelling and Michael Addition Reaction between Thermosensitive Triblock Copolymers and Thiolated Hyaluronan. *ACS Publ.* **2010**, *43* (13), 5771–5778. https://doi.org/10.1021/ma100606a.

(124) Lutolf, M.; Biomacromolecules, J. H.-; 2003, undefined. Synthesis and Physicochemical Characterization of End-Linked Poly(Ethylene Glycol)-Co-Peptide Hydrogels Formed by Michael-Type Addition. *ACS Publ.* **2003**, *4* (3), 713–722. https://doi.org/10.1021/bm025744e.

(125) Baur, D. A.; Toney, H. R.; Saunders, M. J.; Baur, K. G.; Luden, N. D.; Womack, C. J. Carbohydrate Hydrogel Beverage Provides No Additional Cycling Performance Benefit versus Carbohydrate Alone. *Eur. J. Appl. Physiol.* **2019**, *119* (11–12), 2599–2608. https://doi.org/10.1007/S00421-019-04240-4.

(126) Liu, Z.; Lin, Q.; Sun, Y.; Liu, T.; Bao, C.; Li, F.; Zhu, L. Spatiotemporally Controllable and Cytocompatible Approach Builds 3D Cell Culture Matrix by Photo-Uncaged-Thiol Michael Addition Reaction. *Adv. Mater.* **2014**, *26* (23), 3912–3917. https://doi.org/10.1002/ADMA.201306061.

(127) Nair, D. P.; Podgórski, M.; Chatani, S.; Gong, T.; Xi, W.; Fenoli, C. R.; Bowman, C. N. The Thiol-Michael Addition Click Reaction: A Powerful and Widely Used Tool in Materials Chemistry. *Chem. Mater.* **2014**, *26* (1), 724–744. https://doi.org/10.1021/cm402180t.

(128) Y, Z.; W, N.; J, Z.; X, Y. Rapidly in Situ Forming Adhesive Hydrogel Based on a PEG-Maleimide Modified Polypeptide through Michael Addition. *J. Mater. Sci. Mater. Med.* **2013**, *24* (10), 2277–2286. https://doi.org/10.1007/S10856-013-4987-1.

(129) Smith, L. J.; Taimoory, S. M.; Tam, R. Y.; Baker, A. E. G.; Binth Mohammad, N.; Trant,

J. F.; Shoichet, M. S. Diels-Alder Click-Cross-Linked Hydrogels with Increased Reactivity Enable 3D Cell Encapsulation. *Biomacromolecules* **2018**, *19* (3), 926–935. https://doi.org/10.1021/acs.biomac.7b01715.

(130) Nicolas, J.; Magli, S.; Rabbachin, L.; Sampaolesi, S.; Nicotra, F.; Russo, L. 3D Extracellular Matrix Mimics: Fundamental Concepts and Role of Materials Chemistry to Influence Stem Cell Fate. *Biomacromolecules* **2020**, *21* (6), 1968–1994. https://doi.org/10.1021/acs.biomac.0c00045.

(131) Murphy, S. V.; Atala, A. 3D Bioprinting of Tissues and Organs. *Nature Biotechnology*. Nature Publishing Group August 5, 2014, pp 773–785. https://doi.org/10.1038/nbt.2958.

(132) Moroni, L.; Boland, T.; Burdick, J. A.; Maria, C. De; Derby, B.; Forgacs, G.; Groll, J.; Li, Q.; Malda, J.; Mironov, V. A.; Mota, C.; Nakamura, M.; Shu, W.; Takeuchi, S.; Woodfield, T. B. F.; Xu, T.; Yoo, J. J.; Vozzi, G. Biofabrication: A Guide to Technology and Terminology. *Trends Biotechnol.* **2018**, *36* (4), 384–402. https://doi.org/10.1016/J.TIBTECH.2017.10.015.

(133) Mota, C.; Camarero-Espinosa, S.; Baker, M. B.; Wieringa, P.; Moroni, L. Bioprinting: From Tissue and Organ Development to in Vitro Models. *Chemical Reviews*. American Chemical Society 2020, pp 10547–10607. https://doi.org/10.1021/acs.chemrev.9b00789.

(134) Fonseca, A. C.; Melchels, F. P. W.; Ferreira, M. J. S.; Moxon, S. R.; Potjewyd, G.; Dargaville, T. R.; Kimber, S. J.; Domingos, M. Emulating Human Tissues and Organs: A Bioprinting Perspective Toward Personalized Medicine. *Chem. Rev.* **2020**, *120* (19), 11128–11174. https://doi.org/10.1021/ACS.CHEMREV.0C00342.

(135) Malda, J.; Visser, J.; Melchels, F. P.; Jüngst, T.; Hennink, W. E.; Dhert, W. J. A.; Groll, J.; Hutmacher, D. W. 25th Anniversary Article: Engineering Hydrogels for Biofabrication. *Adv. Mater.* **2013**, *25* (36), 5011–5028. https://doi.org/10.1002/ADMA.201302042.

(136) Gungor-Ozkerim, P.; Inci, I.; … Y. Z.-B.; 2018, undefined. Bioinks for 3D Bioprinting: An Overview. *pubs.rsc.org*.

(137) Seol, Y.; Kang, H.; Lee, S.; … A. A.-E. J. of; 2014, undefined. Bioprinting Technology and Its Applications. *academic.oup.com*.

(138) Mironov, V.; Reis, N.; engineering, B. D.-T.; 2006, undefined. Bioprinting: A Beginning. *liebertpub.com* **2006**, *12* (4), 631–634. https://doi.org/10.1089/ten.2006.12.631.

(139) Murphy, S. V; Atala, A. 3D Bioprinting of Tissues and Organs. *Nat. Biotechnol. 2014 328* **2014**, *32* (8), 773–785. https://doi.org/10.1038/nbt.2958.

(140) Murphy, S.; biotechnology, A. A.-N.; 2014, undefined. 3D Bioprinting of Tissues and Organs. *nature.com*.

(141) Zhang, L. G.; Fisher, J. P.; Leong, K. W. *3D Bioprinting and Nanotechnology in Tissue Engineering and Regenerative Medicine*; Elsevier Inc., 2015. https://doi.org/10.1016/C2013-0-18595-9.

(142) Papaioannou, T. G.; Manolesou, D.; Dimakakos, E.; Tsoucalas, G.; Vavuranakis, M.; Tousoulis, D. 3D Bioprinting Methods and Techniques: Applications on Artificial Vessel Fabrication. *Acta Cardiol. Sin.* **2019**, *35* (3), 284. https://doi.org/10.6515/ACS.201905_35(3).20181115A.

(143) Guillotin, B.; Souquet, A.; Catros, S.; Duocastella, M.; Pippenger, B.; Bellance, S.; Bareille, R.; Rémy, M.; Bordenave, L.; Amédée j, J.; Guillemot, F. Laser Assisted Bioprinting of Engineered Tissue with High Cell Density and Microscale Organization. *Biomaterials* **2010**, *31* (28), 7250–7256. https://doi.org/10.1016/J.BIOMATERIALS.2010.05.055.

(144) Donderwinkel, I.; van Hest, J. C. M.; Cameron, N. R. Bio-Inks for 3D Bioprinting: Recent Advances and Future Prospects. *Polym. Chem.* **2017**, *8* (31), 4451–4471. https://doi.org/10.1039/C7PY00826K.

(145) Datta, P.; Ayan, B.; Ozbolat, I. T. Bioprinting for Vascular and Vascularized Tissue Biofabrication. *Acta Biomater.* **2017**, *51*, 1–20. https://doi.org/10.1016/J.ACTBIO.2017.01.035.

(146) Datta, P.; Ayan, B.; Ozbolat, I. T. Bioprinting for Vascular and Vascularized Tissue Biofabrication. *Acta Biomaterialia*. 2017, pp 1–20. https://doi.org/10.1016/j.actbio.2017.01.035.

(147) Bakhshinejad, A.; D'Souza, R. M. A Brief Comparison between Available Bio-Printing Methods. In *2015 IEEE Great Lakes Biomedical Conference, GLBC 2015 - Proceedings*; Institute of Electrical and Electronics Engineers Inc., 2015. https://doi.org/10.1109/GLBC.2015.7158294.

(148) Boularaoui, S.; Al Hussein, G.; Khan, K. A.; Christoforou, N.; Stefanini, C. An Overview of Extrusion-Based Bioprinting with a Focus on Induced Shear Stress and Its Effect on Cell Viability. *Bioprinting*. 2020. https://doi.org/10.1016/j.bprint.2020.e00093.

(149) Vijayavenkataraman, S.; Yan, W. C.; Lu, W. F.; Wang, C. H.; Fuh, J. Y. H. 3D

Bioprinting of Tissues and Organs for Regenerative Medicine. *Adv. Drug Deliv. Rev.* **2018**, *132*, 296–332. https://doi.org/10.1016/j.addr.2018.07.004.

(150) Unagolla, J. M.; Jayasuriya, A. C. Hydrogel-Based 3D Bioprinting: A Comprehensive Review on Cell-Laden Hydrogels, Bioink Formulations, and Future Perspectives. *Applied Materials Today*. NIH Public Access March 1, 2020. https://doi.org/10.1016/j.apmt.2019.100479.

(151) Mahinroosta, M.; Jomeh Farsangi, Z.; Allahverdi, A.; Shakoori, Z. Hydrogels as Intelligent Materials: A Brief Review of Synthesis, Properties and Applications. *Materials Today Chemistry*. Elsevier Ltd June 1, 2018, pp 42–55. https://doi.org/10.1016/j.mtchem.2018.02.004.

(152) Noh, I.; Kim, N.; Tran, H. N.; Lee, J.; Lee, C. 3D Printable Hyaluronic Acid-Based Hydrogel for Its Potential Application as a Bioink in Tissue Engineering. *Biomater. Res. 2019 231* **2019**, *23* (1), 1–9. https://doi.org/10.1186/S40824-018-0152-8.

(153) Law, N.; Doney, B.; Glover, H.; Qin, Y.; Aman, Z. M.; Sercombe, T. B.; Liew, L. J.; Dilley, R. J.; Doyle, B. J. Characterisation of Hyaluronic Acid Methylcellulose Hydrogels for 3D Bioprinting. *J. Mech. Behav. Biomed. Mater.* **2018**, *77*, 389–399. https://doi.org/10.1016/j.jmbbm.2017.09.031.

(154) Poldervaart, M. T.; Goversen, B.; de Ruijter, M.; Abbadessa, A.; Melchels, F. P. W.; Oner, F. C.; Dhert, W. J. A.; Vermonden, T.; Alblas, J. 3D Bioprinting of Methacrylated Hyaluronic Acid (MeHA) Hydrogel with Intrinsic Osteogenicity. *PLoS One* **2017**, *12* (6), e0177628. https://doi.org/10.1371/journal.pone.0177628.

(155) GhavamiNejad, A.; Ashammakhi, N.; Wu, X. Y.; Khademhosseini, A. Crosslinking Strategies for 3D Bioprinting of Polymeric Hydrogels. *Small*. Wiley-VCH Verlag September 1, 2020. https://doi.org/10.1002/smll.202002931.

(156) Pierce, B. F.; Pittermann, E.; Ma, N.; Gebauer, T.; Neffe, A. T.; Hölscher, M.; Jung, F.; Lendlein, A. Viability of Human Mesenchymal Stem Cells Seeded on Crosslinked Entropy-Elastic Gelatin-Based Hydrogels. *Macromol. Biosci.* **2012**, *12* (3), 312–321. https://doi.org/10.1002/mabi.201100237.

(157) Buhus, G.; Peptu, C.; Popa, M.; Desbrières, J. Controlled Release of Water Soluble Antibiotics by Carboxymethylcellulose- And Gelatin-Based Hydrogels Crosslinked with Epichlorohydrin. *Cellul. Chem. Technol.* **2009**, *43* (4–6), 141–151.

(158) Echave, M. C.; Burgo, L. S.; Pedraz, J. L.; Orive, G. Gelatin as Biomaterial for Tissue Engineering. *Curr. Pharm. Des.* **2017**, *23* (24).

https://doi.org/10.2174/092986732466617051112310l.

(159) Bello, A. B.; Kim, D.; Kim, D.; Park, H.; Lee, S.-H. Engineering and Functionalization of Gelatin Biomaterials: From Cell Culture to Medical Applications. *Tissue Eng. Part B Rev.* **2020**, *26* (2), 164–180. https://doi.org/10.1089/ten.teb.2019.0256.

(160) Chen, M. B.; Srigunapalan, S.; Wheeler, A. R.; Simmons, C. A. A 3D Microfluidic Platform Incorporating Methacrylated Gelatin Hydrogels to Study Physiological Cardiovascular Cell-Cell Interactions. *Lab Chip* **2013**, *13* (13), 2591–2598. https://doi.org/10.1039/c3lc00051f.

(161) Jiang, T.; James, R.; Kumbar, S. G.; Laurencin, C. T. Chitosan as a Biomaterial: Structure, Properties, and Applications in Tissue Engineering and Drug Delivery. In *Natural and Synthetic Biomedical Polymers*; Elsevier, 2014; pp 91–113. https://doi.org/10.1016/B978-0-12-396983-5.00005-3.

(162) Cheng, Y. H.; Ko, Y. C.; Chang, Y. F.; Huang, S. H.; Liu, C. J. ling. Thermosensitive Chitosan-Gelatin-Based Hydrogel Containing Curcumin-Loaded Nanoparticles and Latanoprost as a Dual-Drug Delivery System for Glaucoma Treatment. *Exp. Eye Res.* **2019**, *179*, 179–187. https://doi.org/10.1016/j.exer.2018.11.017.

(163) Ren, Y.; Zhao, X.; Liang, X.; Ma, P. X.; Guo, B. Injectable Hydrogel Based on Quaternized Chitosan, Gelatin and Dopamine as Localized Drug Delivery System to Treat Parkinson's Disease. *Int. J. Biol. Macromol.* **2017**, *105*, 1079–1087. https://doi.org/10.1016/j.ijbiomac.2017.07.130.

(164) Mao, J. S.; Zhao, L. G.; Yin, Y. J.; Yao, K. De. Structure and Properties of Bilayer Chitosan-Gelatin Scaffolds. *Biomaterials* **2003**, *24* (6), 1067–1074. https://doi.org/10.1016/S0142-9612(02)00442-8.

(165) Shi, X. Y.; Tan, T. W. New Contact Lens Based on Chitosan/Gelatin Composites. *J. Bioact. Compat. Polym.* **2004**, *19* (6), 467–479. https://doi.org/10.1177/0883911504048410.

(166) Afewerki, S.; Sheikhi, A.; Kannan, S.; Ahadian, S.; Khademhosseini, A. Gelatin-Polysaccharide Composite Scaffolds for 3D Cell Culture and Tissue Engineering: Towards Natural Therapeutics. *Bioeng. Transl. Med.* **2019**. https://doi.org/10.1002/btm2.10124.

(167) Rodríguez-Rodríguez, R.; Espinosa-Andrews, H.; Velasquillo-Martínez, C.; García-Carvajal, Z. Y. Composite Hydrogels Based on Gelatin, Chitosan and Polyvinyl Alcohol to Biomedical Applications: A Review. *Int. J. Polym. Mater. Polym. Biomater.* **2020**.

https://doi.org/10.1080/00914037.2019.1581780.

(168) Caron, I.; Rossi, F.; Papa, S.; Aloe, R.; Sculco, M.; Mauri, E.; Sacchetti, A.; Erba, E.; Panini, N.; Parazzi, V.; Barilani, M.; Forloni, G.; Perale, G.; Lazzari, L.; Veglianese, P. A New Three Dimensional Biomimetic Hydrogel to Deliver Factors Secreted by Human Mesenchymal Stem Cells in Spinal Cord Injury. *Biomaterials* **2016**, *75*, 135–147. https://doi.org/10.1016/j.biomaterials.2015.10.024.

(169) Bagher, Z.; Atoufi, Z.; Alizadeh, R.; Farhadi, M.; Zarrintaj, P.; Moroni, L.; Setayeshmehr, M.; Komeili, A.; Kamrava, S. K. Conductive Hydrogel Based on Chitosan-Aniline Pentamer/Gelatin/Agarose Significantly Promoted Motor Neuron-like Cells Differentiation of Human Olfactory Ecto-Mesenchymal Stem Cells. *Mater. Sci. Eng. C. Mater. Biol. Appl.* **2019**, *101*, 243–253. https://doi.org/10.1016/j.msec.2019.03.068.

(170) Sorkio, A.; Koch, L.; Koivusalo, L.; Deiwick, A.; Miettinen, S.; Chichkov, B.; Skottman, H. Human Stem Cell Based Corneal Tissue Mimicking Structures Using Laser-Assisted 3D Bioprinting and Functional Bioinks. *Biomaterials* **2018**, *171*, 57–71. https://doi.org/10.1016/j.biomaterials.2018.04.034.

(171) Luo, X.; Liu, Y.; Pang, J.; Bi, S.; Zhou, Z.; Lu, Z.; Feng, C.; Chen, X.; Kong, M. Thermo/Photo Dual-Crosslinking Chitosan-Gelatin Methacrylate Hydrogel with Controlled Shrinking Property for Contraction Fabrication. *Carbohydr. Polym.* **2020**, *236*, 116067. https://doi.org/10.1016/j.carbpol.2020.116067.

(172) Saraiva, S. M.; Miguel, S. P.; Ribeiro, M. P.; Coutinho, P.; Correia, I. J. Synthesis and Characterization of a Photocrosslinkable Chitosan-Gelatin Hydrogel Aimed for Tissue Regeneration. *RSC Adv.* **2015**, 63478–63488. https://doi.org/10.1039/c5ra10638a.

(173) Liu, Y.; An, M.; Wang, L.; Qiu, H. Preparation and Characterization of Chitosan-Gelatin/Glutaraldehyde Scaffolds. *J. Macromol. Sci. Part B Phys.* **2014**. https://doi.org/10.1080/00222348.2013.837290.

(174) Jiang, Y.; Chen, J.; Deng, C.; Suuronen, E. J.; Zhong, Z. Click Hydrogels, Microgels and Nanogels: Emerging Platforms for Drug Delivery and Tissue Engineering. *Biomaterials* **2014**, *35* (18), 4969–4985. https://doi.org/10.1016/j.biomaterials.2014.03.001.

(175) Smith, L. J.; Taimoory, S. M.; Tam, R. Y.; Baker, A. E. G.; Binth Mohammad, N.; Trant, J. F.; Shoichet, M. S. Diels-Alder Click-Cross-Linked Hydrogels with Increased Reactivity Enable 3D Cell Encapsulation. *Biomacromolecules* **2018**, *19* (3), 926–935.

https://doi.org/10.1021/acs.biomac.7b01715.

(176) Tan, H.; Rubin, J. P.; Marra, K. G. Direct Synthesis of Biodegradable Polysaccharide Derivative Hydrogels Through Aqueous Diels-Alder Chemistry. *Macromol. Rapid Commun.* **2011**, *32* (12), 905–911. https://doi.org/10.1002/MARC.201100125.

(177) Magli, S.; Rossi, G. B.; Risi, G.; Bertini, S.; Cosentino, C.; Crippa, L.; Ballarini, E.; Cavaletti, G.; Piazza, L.; Masseroni, E.; Nicotra, F.; Russo, L. Design and Synthesis of Chitosan—Gelatin Hybrid Hydrogels for 3D Printable in Vitro Models. *Front. Chem.* **2020**, *8*, 524. https://doi.org/10.3389/fchem.2020.00524.

(178) Magli, S.; Rossi, L.; Consentino, C.; Bertini, S.; Nicotra, F.; Russo, L. Combined Analytical Approaches to Standardize and Characterize Biomaterials Formulations: Application to Chitosan-Gelatin Cross-Linked Hydrogels. *Biomol. 2021, Vol. 11, Page 683* **2021**, *11* (5), 683. https://doi.org/10.3390/BIOM11050683.

(179) Claaßen, C.; Claaßen, M. H.; Truffault, V.; Sewald, L.; Tovar, G. E. M.; Borchers, K.; Southan, A. Quantification of Substitution of Gelatin Methacryloyl: Best Practice and Current Pitfalls. *Biomacromolecules* **2018**, *19* (1), 42–52. https://doi.org/10.1021/acs.biomac.7b01221.

(180) Gupta, D.; Tator, C. H.; Shoichet, M. S. Fast-Gelling Injectable Blend of Hyaluronan and Methylcellulose for Intrathecal, Localized Delivery to the Injured Spinal Cord. *Biomaterials* **2006**, *27* (11), 2370–2379. https://doi.org/10.1016/j.biomaterials.2005.11.015.

(181) Varaprasad, K.; Reddy, N. N.; Ravindra, S.; Vimala, K.; Raju, K. M. Synthesis and Characterizations of Macroporous Poly(Acrylamide-2- Acrylamido-2-Methyl-1-Propanesulfonic Acid) Hydrogels for in Vitro Drug Release of Ranitidine Hydrochloride. *Int. J. Polym. Mater. Polym. Biomater.* **2011**, *60* (7), 490–503. https://doi.org/10.1080/00914037.2010.531816.

(182) Gandini, A. The Furan/Maleimide Diels-Alder Reaction: A Versatile Click-Unclick Tool in Macromolecular Synthesis. *Prog. Polym. Sci.* **2013**, *38* (1), 1–29. https://doi.org/10.1016/j.progpolymsci.2012.04.002.

(183) C, L.; D, L. M.; B, C.; KE, L.; GD, L. Hybrid Collagen Alginate Hydrogel as a Platform for 3D Tumor Spheroid Invasion. *Acta Biomater.* **2018**, *75*, 213–225. https://doi.org/10.1016/J.ACTBIO.2018.06.003.

(184) Bertini, S.; Bisio, A.; Torri, G.; Bensi, D.; Terbojevich, M. Molecular Weight Determination of Heparin and Dermatan Sulfate by Size Exclusion Chromatography

with a Triple Detector Array. *Biomacromolecules* **2005**, *6* (1), 168–173. https://doi.org/10.1021/bm049693s.

(185) Bowman, W. A.; Rubinstein, M.; Tan, J. S. Polyelectrolyte-Gelatin Complexation: Light-Scattering Study. *Macromolecules* **1997**, *30* (11), 3262–3270. https://doi.org/10.1021/ma961915u.

(186) Rinaudo, M.; Milas, M.; Dung, P. Le. Characterization of Chitosan. Influence of Ionic Strength and Degree of Acetylation on Chain Expansion. *Int. J. Biol. Macromol.* **1993**, *15* (5), 281–285. https://doi.org/10.1016/0141-8130(93)90027-J.

(187) Zhao, W.; Glavas, L.; Odelius, K.; Edlund, U.; Albertsson, A. C. A Robust Pathway to Electrically Conductive Hemicellulose Hydrogels with High and Controllable Swelling Behavior. *Polymer (Guildf).* **2014**. https://doi.org/10.1016/j.polymer.2014.05.003.

(188) Moroni, L.; Burdick, J. A.; Highley, C.; Lee, S. J.; Morimoto, Y.; Takeuchi, S.; Yoo, J. J. Biofabrication Strategies for 3D in Vitro Models and Regenerative Medicine. *Nat. Rev. Mater.* **2018**, *3* (5), 21–37. https://doi.org/10.1038/s41578-018-0006-y.

(189) Ooi, H. W.; Hafeez, S.; van Blitterswijk, C. A.; Moroni, L.; Baker, M. B. Hydrogels That Listen to Cells: A Review of Cell-Responsive Strategies in Biomaterial Design for Tissue Regeneration. *Mater. Horizons* **2017**, *4* (6), 1020–1040. https://doi.org/10.1039/C7MH00373K.

(190) Schindelin, J.; Arganda-Carreras, I.; Frise, E.; Kaynig, V.; Longair, M.; Pietzsch, T.; Preibisch, S.; Rueden, C.; Saalfeld, S.; Schmid, B.; Tinevez, J.-Y.; White, D. J.; Hartenstein, V.; Eliceiri, K.; Tomancak, P.; Cardona, A. Fiji: An Open-Source Platform for Biological-Image Analysis. *Nat. Methods 2012 97* **2012**, *9* (7), 676–682. https://doi.org/10.1038/nmeth.2019.

(191) Pina, S.; Ribeiro, V.; Marques, C.; Maia, F.; Materials, T. S.-; 2019, undefined. Scaffolding Strategies for Tissue Engineering and Regenerative Medicine Applications. *mdpi.com* **2019**. https://doi.org/10.3390/ma12111824.

(192) Ruprai, H.; Romanazzo, S.; Ireland, J.; Kilian, K.; Mawad, D.; George, L.; Wuhrer, R.; Houang, J.; Ta, D.; Myers, S.; Lauto, A. Porous Chitosan Films Support Stem Cells and Facilitate Sutureless Tissue Repair. *ACS Appl. Mater. Interfaces* **2019**, *11* (36), 32613–32622. https://doi.org/10.1021/acsami.9b09123.

(193) Xu, K.; Ganapathy, K.; Andl, T.; Wang, Z.; Copland, J. A.; Chakrabarti, R.; Florczyk, S. J. 3D Porous Chitosan-Alginate Scaffold Stiffness Promotes Differential Responses in Prostate Cancer Cell Lines. *Biomaterials* **2019**, *217*, 119311.

https://doi.org/10.1016/j.biomaterials.2019.119311.

(194) Yang, S.; Leong, K.-F.; Du, Z.; Chua, C.-K. The Design of Scaffolds for Use in Tissue Engineering. Part I. Traditional Factors. *https://home.liebertpub.com/ten* **2004**, *7* (6), 679–689. https://doi.org/10.1089/107632701753337645.

(195) Klawitter, J. J.; Hulbert, S. F. Application of Porous Ceramics for the Attachment of Load Bearing Internal Orthopedic Applications. *J. Biomed. Mater. Res.* **1971**, *5* (6), 161–229. https://doi.org/10.1002/JBM.820050613.

(196) Whang, K.; Healy, K. E.; Elenz, D. R.; Nam, E. K.; Tsai, D. C.; Thomas, C. H.; Nuber, G. W.; Glorieux, F. H.; Travers, R.; Sprague, S. M. Engineering Bone Regeneration with Bioabsorbable Scaffolds with Novel Microarchitecture. *https://home.liebertpub.com/ten* **2007**, *5* (1), 35–51. https://doi.org/10.1089/TEN.1999.5.35.

(197) Podhorská, B.; Vetrík, M.; Chylíková-Krumbholcová, E.; Kománková, L.; Banafshehvaragh, N. R.; Šlouf, M.; Dušková-Smrčková, M.; Janoušková, O. Revealing the True Morphological Structure of Macroporous Soft Hydrogels for Tissue Engineering. *Appl. Sci. 2020, Vol. 10, Page 6672* **2020**, *10* (19), 6672. https://doi.org/10.3390/APP10196672.

(198) Zong, X.; Bien, H.; Chung, C. Y.; Yin, L.; Fang, D.; Hsiao, B. S.; Chu, B.; Entcheva, E. Electrospun Fine-Textured Scaffolds for Heart Tissue Constructs. *Biomaterials* **2005**, *26* (26), 5330–5338. https://doi.org/10.1016/J.BIOMATERIALS.2005.01.052.

(199) WangLimin; LuSteven; LamJohnny; Kurtis, K.; G., M. Fabrication of Cell-Laden Macroporous Biodegradable Hydrogels with Tunable Porosities and Pore Sizes. *https://home.liebertpub.com/tec* **2014**, *21* (3), 263–273. https://doi.org/10.1089/TEN.TEC.2014.0224.

(200) Dehghani, F.; Annabi, N. Engineering Porous Scaffolds Using Gas-Based Techniques. *Curr. Opin. Biotechnol.* **2011**, *22* (5), 661–666. https://doi.org/10.1016/J.COPBIO.2011.04.005.

(201) Lebourg, M.; Sabater Serra, R.; Más Estellés, J.; Hernández Sánchez, F.; Gómez Ribelles, J. L.; Suay Antón, J. Biodegradable Polycaprolactone Scaffold with Controlled Porosity Obtained by Modified Particle-Leaching Technique. *J. Mater. Sci. Mater. Med. 2007 195* **2007**, *19* (5), 2047–2053. https://doi.org/10.1007/S10856-007-3282-4.

(202) Yeh, Y.; Feeney, R. E. Antifreeze Proteins: Structures and Mechanisms of Function.

Chem. Rev. **1996**, *96* (2). https://doi.org/10.1021/cr950260c.

(203) Sun, X.; Griffith, M.; Pasternak, J. J.; Glick, B. R. Low Temperature Growth, Freezing Survival, and Production of Antifreeze Protein by the Plant Growth Promoting Rhizobacterium Pseudomonas Putida GR12-2. *https://doi.org/10.1139/m95-107* **2011**, *41* (9), 776–784. https://doi.org/10.1139/M95-107.

(204) Mangiagalli, M.; Sarusi, G.; Kaleda, A.; Bar Dolev, M.; Nardone, V.; Vena, V. F.; Braslavsky, I.; Lotti, M.; Nardini, M. Structure of a Bacterial Ice Binding Protein with Two Faces of Interaction with Ice. *FEBS J.* **2018**, *285* (9), 1653–1666. https://doi.org/10.1111/FEBS.14434.

(205) Mangiagalli, M.; Bar-Dolev, M.; … P. T.-T. F.; 2017, undefined. Cryo-protective Effect of an Ice-binding Protein Derived from Antarctic Bacteria. *Wiley Online Libr.* **2017**, *284* (1), 163–177. https://doi.org/10.1111/febs.13965.

(206) Loh, Q. L.; Choong, C. Three-Dimensional Scaffolds for Tissue Engineering Applications: Role of Porosity and Pore Size. *Tissue Engineering - Part B: Reviews*. Mary Ann Liebert, Inc. December 1, 2013, pp 485–502. https://doi.org/10.1089/ten.teb.2012.0437.

(207) Marsico, G.; Jin, C.; Abbah, S. A.; Brauchle, E. M.; Thomas, D.; Rebelo, A. L.; Orbanić, D.; Chantepie, S.; Contessotto, P.; Papy-Garcia, D.; Rodriguez-Cabello, C.; Kilcoyne, M.; Schenke-Layland, K.; Karlsson, N. G.; McCullagh, K. J. A.; Pandit, A. Elastin-like Hydrogel Stimulates Angiogenesis in a Severe Model of Critical Limb Ischemia (CLI): An Insight into the Glyco-Host Response. *Biomaterials* **2021**, *269*. https://doi.org/10.1016/j.biomaterials.2020.120641.

(208) Laurent, G. J. The Molecular Biology and Pathology of Elastic Tissue. *Thorax* **1996**, *51* (8), 874–874. https://doi.org/10.1136/thx.51.8.874-a.

(209) Spelat, R.; Ferro, F.; Contessotto, P.; Warren, N. J.; Marsico, G.; Armes, S. P.; Pandit, A. A Worm Gel-Based 3D Model to Elucidate the Paracrine Interaction between Multiple Myeloma and Mesenchymal Stem Cells. *Mater. Today Bio* **2020**, *5*. https://doi.org/10.1016/j.mtbio.2019.100040.

(210) Xu, C.; Dai, G.; Hong, Y. Recent Advances in High-Strength and Elastic Hydrogels for 3D Printing in Biomedical Applications. *Acta Biomater.* **2019**, *95*, 50–59. https://doi.org/10.1016/j.actbio.2019.05.032.

(211) Coenen, A. M. J.; Bernaerts, K. V.; Harings, J. A. W.; Jockenhoevel, S.; Ghazanfari, S. Elastic Materials for Tissue Engineering Applications: Natural, Synthetic, and Hybrid

Polymers. *Acta Biomaterialia*. Acta Materialia Inc October 1, 2018, pp 60–82. https://doi.org/10.1016/j.actbio.2018.08.027.

(212) Kristensen, J. H.; Karsdal, M. A. *Chapter 30 - Elastin*; 2016. https://doi.org/10.1016/B978-0-12-809847-9.00030-1.

(213) Wise, S. G.; Mithieux, S. M.; Weiss, A. S. Engineered Tropoelastin and Elastin-Based Biomaterials. *Advances in protein chemistry and structural biology*. 2009. https://doi.org/10.1016/s1876-1623(08)78001-5.

(214) Arribas, S. M.; Hinek, A.; González, M. C. Elastic Fibres and Vascular Structure in Hypertension. *Pharmacology and Therapeutics*. 2006. https://doi.org/10.1016/j.pharmthera.2005.12.003.

(215) Daamen, W. F.; Veerkamp, J. H.; van Hest, J. C. M.; van Kuppevelt, T. H. Elastin as a Biomaterial for Tissue Engineering. *Biomaterials*. 2007. https://doi.org/10.1016/j.biomaterials.2007.06.025.

(216) Mbundi, L.; González-Pérez, M.; González-Pérez, F.; Juanes-Gusano, D.; Rodríguez-Cabello, J. C. Trends in the Development of Tailored Elastin-Like Recombinamer–Based Porous Biomaterials for Soft and Hard Tissue Applications. *Front. Mater.* **2021**, *7*. https://doi.org/10.3389/FMATS.2020.601795/FULL.

(217) Yeo, G. C.; Mithieux, S. M.; Weiss, A. S. The Elastin Matrix in Tissue Engineering and Regeneration. *Curr. Opin. Biomed. Eng.* **2018**, *6*, 27–32. https://doi.org/10.1016/j.cobme.2018.02.007.

(218) Wen, Q.; Mithieux, S. M.; Weiss, A. S. Elastin Biomaterials in Dermal Repair. *Trends Biotechnol.* **2020**, *38* (3), 280–291. https://doi.org/10.1016/j.tibtech.2019.08.005.

(219) Xiao, Y.; Chinoy, Z. S.; Pecastaings, G.; Bathany, K.; Garanger, E.; Lecommandoux, S. Design of Polysaccharide-b-Elastin-Like Polypeptide Bioconjugates and Their Thermoresponsive Self-Assembly. *Biomacromolecules* **2020**, *21* (1), 114–125. https://doi.org/10.1021/acs.biomac.9b01058.

(220) Varanko, A. K.; Su, J. C.; Chilkoti, A. Elastin-Like Polypeptides for Biomedical Applications. *https://doi.org/10.1146/annurev-bioeng-092419-061127* **2020**, *22*, 343–369. https://doi.org/10.1146/ANNUREV-BIOENG-092419-061127.

(221) Pérez, L. A.; Hernández, R.; Alonso, J. M.; Pérez-González, R.; Sáez-Martínez, V. Hyaluronic Acid Hydrogels Crosslinked in Physiological Conditions: Synthesis and Biomedical Applications. *Biomed. 2021, Vol. 9, Page 1113* **2021**, *9* (9), 1113. https://doi.org/10.3390/BIOMEDICINES9091113.

(222) Rucker, R. B.; Dubick, M. A. Elastin Metabolism and Chemistry: Potential Roles in Lung Development and Structure. *Environ. Health Perspect.* **1984**, *VOL. 55*, 179–191. https://doi.org/10.1289/ehp.8455179.

(223) Ragnoni, E.; Palombo, F.; Green, E.; Winlove, C. P.; Donato, M. Di; Lapini, A. Coacervation of α-Elastin Studied by Ultrafast Nonlinear Infrared Spectroscopy. *Phys. Chem. Chem. Phys.* **2016**, *18* (40), 27981–27990. https://doi.org/10.1039/C6CP04049G.

(224) Durand, P.-L.; Grau, E.; Cramail, H. Bio-Based Thermo-Reversible Aliphatic Polycarbonate Network. *Molecules* **2019**, *25* (1), 74. https://doi.org/10.3390/molecules25010074.

(225) Zhang, H.; Dong, Y.; Wang, L.; Wang, G.; Wu, J.; Zheng, Y.; Yang, H.; Zhu, S. Low Swelling Hyperbranched Poly(Amine-Ester) Hydrogels for PH-Modulated Differential Release of Anticancer Drugs. *J. Mater. Chem.* **2011**, *21* (35), 13530–13537. https://doi.org/10.1039/c1jm11823d.

(226) Li, Z.; He, G.; Hua, J.; Wu, M.; Guo, W.; Gong, J.; Zhang, J.; Qiao, C. Preparation of γ-PGA Hydrogels and Swelling Behaviors in Salt Solutions with Different Ionic Valence Numbers. *RSC Adv.* **2017**. https://doi.org/10.1039/c6ra26419k.

(227) Chavda, H.; Patel, C. Effect of Crosslinker Concentration on Characteristics of Superporous Hydrogel. *Int. J. Pharm. Investig.* **2011**, *1* (1), 17. https://doi.org/10.4103/2230-973x.76724.

(228) Dokukin, M. E.; Sokolov, I. On the Measurements of Rigidity Modulus of Soft Materials in Nanoindentation Experiments at Small Depth. *Macromolecules* **2012**, *45* (10), 4277–4288. https://doi.org/10.1021/ma202600b.

(229) Alonso, J. L.; Goldmann, W. H. Feeling the Forces: Atomic Force Microscopy in Cell Biology. *Life Sciences*. Pergamon April 25, 2003, pp 2553–2560. https://doi.org/10.1016/S0024-3205(03)00165-6.

(230) Lekka, M.; Laidler, P.; Gil, D.; Lekki, J.; Stachura, Z.; Hrynkiewicz, A. Z. Elasticity of Normal and Cancerous Human Bladder Cells Studied by Scanning Force Microscopy. *Eur. Biophys. J.* **1999**, *28* (4), 312–316. https://doi.org/10.1007/s002490050213.

(231) Budday, S.; Ovaert, T. C.; Holzapfel, G. A.; Steinmann, P.; Kuhl, E. Fifty Shades of Brain: A Review on the Mechanical Testing and Modeling of Brain Tissue. *Arch. Comput. Methods Eng.* **2019**, *27* (4), 1187–1230. https://doi.org/10.1007/s11831-019-09352-w.

(232) Guimarães, C.; Gasperini, L.; … A. M.-N. R.; 2020, undefined. The Stiffness of Living Tissues and Its Implications for Tissue Engineering. *nature.com*.

(233) Booth, A. J.; Hadley, R.; Cornett, A. M.; Dreffs, A. A.; Matthes, S. A.; Tsui, J. L.; Weiss, K.; Horowitz, J. C.; Fiore, V. F.; Barker, T. H.; Moore, B. B.; Martinez, F. J.; Niklason, L. E.; White, E. S. Acellular Normal and Fibrotic Human Lung Matrices as a Culture System for in Vitro Investigation. *Am. J. Respir. Crit. Care Med.* **2012**, *186* (9), 866–876. https://doi.org/10.1164/rccm.201204-0754OC.

(234) Koch, M.; Włodarczyk-Biegun, M. K. Faithful Scanning Electron Microscopic (SEM) Visualization of 3D Printed Alginate-Based Scaffolds. *bioRxiv* **2020**, 2020.03.18.997668. https://doi.org/10.1101/2020.03.18.997668.

(235) De Moor, L.; Fernandez, S.; Vercruysse, C.; Tytgat, L.; Asadian, M.; De Geyter, N.; Van Vlierberghe, S.; Dubruel, P.; Declercq, H. Hybrid Bioprinting of Chondrogenically Induced Human Mesenchymal Stem Cell Spheroids. *Front. Bioeng. Biotechnol.* **2020**, *8*, 484. https://doi.org/10.3389/fbioe.2020.00484.

(236) Zeynali Thesis Supervisor, A.; Chirico, G.; Ferraro, P.; Cerullo, G.; di Milano Paolo Radaelli, P.; Andreani, C. "Two-Photon Assisted Direct Laser Writing of Proteinaceous Microarchitectures Containing Plasmonic Nanoparticles; Characterization and Optimization." **2020**.

(237) Sneddon, I. N. The Relation between Load and Penetration in the Axisymmetric Boussinesq Problem for a Punch of Arbitrary Profile. *Int. J. Eng. Sci.* **1965**, *3* (1), 47–57. https://doi.org/10.1016/0020-7225(65)90019-4.

(238) Butt, H.-J.; Cappella, B.; Kappl, M. Force Measurements with the Atomic Force Microscope: Technique, Interpretation and Applications. *SurSR* **2005**, *59* (1), 1–152. https://doi.org/10.1016/J.SURFREP.2005.08.003.

(239) Gladson, C. L.; Prayson, R. A.; Liu, W. M. The Pathobiology of Glioma Tumors. *Annual Review of Pathology: Mechanisms of Disease*. Annual Reviews January 15, 2010, pp 33–50. https://doi.org/10.1146/annurev-pathol-121808-102109.

(240) Delgado-López, P. D.; Corrales-García, E. M. Survival in Glioblastoma: A Review on the Impact of Treatment Modalities. *Clinical and Translational Oncology*. Springer March 10, 2016, pp 1062–1071. https://doi.org/10.1007/s12094-016-1497-x.

(241) Putavet, D. A.; de Keizer, P. L. J. Residual Disease in Glioma Recurrence: A Dangerous Liaison with Senescence. *Cancers*. MDPI March 2021, p 1560. https://doi.org/10.3390/cancers13071560.

(242) Schmidt, M. C.; Antweiler, S.; Urban, N.; Mueller, W.; Kuklik, A.; Meyer-Puttlitz, B.; Wiestler, O. D.; Louis, D. N.; Fimmers, R.; Von Deimling, A. Impact of Genotype and Morphology on the Prognosis of Glioblastoma. *J. Neuropathol. Exp. Neurol.* **2002**, *61* (4), 321–328. https://doi.org/10.1093/jnen/61.4.321.

(243) Davis, M. E. Glioblastoma: Overview of Disease and Treatment. *Clin. J. Oncol. Nurs.* **2016**, *20* (5), S2. https://doi.org/10.1188/16.CJON.S1.2-8.

(244) Olivier, C.; Oliver, L.; Lalier, L.; Vallette, F. M. Drug Resistance in Glioblastoma: The Two Faces of Oxidative Stress. *Frontiers in Molecular Biosciences*. Frontiers January 27, 2021, p 468. https://doi.org/10.3389/fmolb.2020.620677.

(245) Papi, A.; Bartolini, G.; Ammar, K.; Guerra, F.; Ferreri, A. M.; Rocchi, P.; Orlandi, M. Inhibitory Effects of Retinoic Acid and IIF on Growth, Migration and Invasiveness in the U87MG Human Glioblastoma Cell Line. *Oncol. Rep.* **2007**, *18* (4), 1015–1021. https://doi.org/10.3892/or.18.4.1015.

(246) Serra, R. Matrix Metalloproteinases in Health and Disease. *Biomolecules*. 2020, pp 1–3. https://doi.org/10.3390/biom10081138.

(247) Singh, D.; Srivastava, S. K.; Chaudhuri, T. K.; Upadhyay, G. Multifaceted Role of Matrix Metalloproteinases (MMPs). *Frontiers in Molecular Biosciences*. Frontiers May 13, 2015, p 19. https://doi.org/10.3389/fmolb.2015.00019.

(248) Cai, H.; Wang, J.; Xi, S.; Ni, X.; Chen, Y.; Yu, Y.; Cen, Z.; Yu, Z.; Chen, F.; Guo, C.; Zhang, J.; Ke, C.; Wang, J.; Chen, Z. Tenascin-c Mediated Vasculogenic Mimicry Formation via Regulation of MMP2/MMP9 in Glioma. *Cell Death Dis. 2019 1012* **2019**, *10* (12), 1–14. https://doi.org/10.1038/s41419-019-2102-3.

(249) Hu, F.; Ku, M.-C.; Markovic, D.; Dzaye, O.; Lehnardt, S.; Synowitz, M.; Wolf, S. A.; Kettenmann, H. Glioma-Associated Microglial MMP9 Expression Is Upregulated by TLR2 Signaling and Sensitive to Minocycline. *Int. J. Cancer* **2014**, *135* (11), 2569–2578. https://doi.org/10.1002/IJC.28908.

(250) Lakka, S. S.; Gondi, C. S.; Yanamandra, N.; Olivero, W. C.; Dinh, D. H.; Gujrati, M.; Rao, J. S. Inhibition of Cathepsin B and MMP-9 Gene Expression in Glioblastoma Cell Line via RNA Interference Reduces Tumor Cell Invasion, Tumor Growth and Angiogenesis. *Oncogene 2004 2327* **2004**, *23* (27), 4681–4689. https://doi.org/10.1038/sj.onc.1207616.

(251) Lakka, S. S.; Gondi, C. S.; Rao, J. S. Proteases and Glioma Angiogenesis. *Brain Pathol.* **2005**, *15* (4), 327–341. https://doi.org/10.1111/J.1750-3639.2005.TB00118.X.

(252) Liu, Y.; Zhou, Y.; Zhang, X. S.; Shen, B. Z. Expression of VEGF and MMP-9 and MRI Imaging Changes in Cerebral Glioma. *Oncol. Lett.* **2011**, *2* (6), 1171–1175. https://doi.org/10.3892/ol.2011.384.

(253) Munaut, C.; Noël, A.; Hougrand, O.; Foidart, J. M.; Boniver, J.; Deprez, M. Vascular Endothelial Growth Factor Expression Correlates with Matrix Metalloproteinases MT1-MMP, MMP-2 and MMP-9 in Human Glioblastomas. *Int. J. Cancer* **2003**, *106* (6), 848–855. https://doi.org/10.1002/ijc.11313.

(254) Ma, C.; Li, Y.; Zhang, X.; Zhao, G.; Xu, H. Levels of Vascular Endothelial Growth Factor and Matrix Metalloproteinase-9 Proteins in Patients with Glioma. *J. Int. Med. Res.* **2014**, *42* (1), 198–204. https://doi.org/10.1177/0300060513481924.

(255) Ramachandran, R. K.; Sørensen, M. D.; Aaberg-Jessen, C.; Hermansen, S. K.; Kristensen, B. W. Expression and Prognostic Impact of Matrix Metalloproteinase-2 (MMP-2) in Astrocytomas. *PLoS One* **2017**, *12* (2), e0172234. https://doi.org/10.1371/journal.pone.0172234.

(256) Nagase, H. Activation Mechanisms of Matrix Metalloproteinases. *Biological Chemistry*. March 1, 1997, pp 151–160.

(257) Hur, J. H.; Park, M. J.; Park, I. C.; Yi, D. H.; Rhee, C. H.; Hong, S. Il; Lee, S. H. Matrix Metalloproteinases in Human Gliomas : Activation of Matrix Metalloproteinase-2 (MMP-2) May Be Correlated with Membrane-Type-1 Matrix Metalloproteinase (MT1-MMP) Expression. *J. Korean Med. Sci.* **2000**, *15* (3), 309–314. https://doi.org/10.3346/jkms.2000.15.3.309.

(258) Fingleton, B. MMP Inhibitor Clinical Trials - The Past, Present, and Future. In *The Cancer Degradome: Proteases and Cancer Biology*; Springer, New York, NY, 2008; pp 759–785. https://doi.org/10.1007/978-0-387-69057-5_36.

(259) Leone, G.; Pepi, S.; Consumi, M.; Lamponi, S.; Fragai, M.; Martinucci, M.; Baldoneschi, V.; Francesconi, O.; Nativi, C.; Magnani, A. Sodium Hyaluronate-g-2-((N-(6-Aminohexyl)-4-Methoxyphenyl)Sulfonamido)-N-Hydroxyacetamide with Enhanced Affinity towards MMP12 Catalytic Domain to Be Used as Visco-Supplement with Increased Degradation Resistance. *Carbohydr. Polym.* **2021**, *271*, 118452. https://doi.org/10.1016/j.carbpol.2021.118452.

(260) Breschi, L.; Martin, P.; Mazzoni, A.; Nato, F.; Carrilho, M.; Tjäderhane, L.; Visintini, E.; Cadenaro, M.; Tay, F. R.; Dorigo, E. D. S.; Pashley, D. H. Use of a Specific MMP-Inhibitor (Galardin) for Preservation of Hybrid Layer. *Dent. Mater.* **2010**, *26* (6), 571–

578. https://doi.org/10.1016/j.dental.2010.02.007.

(261) Oh, J.; Takahashi, R.; Kondo, S.; Mizoguchi, A.; Adachi, E.; Sasahara, R. M.; Nishimura, S.; Imamura, Y.; Kitayama, H.; Alexander, D. B.; Ide, C.; Horan, T. P.; Arakawa, T.; Yoshida, H.; Nishikawa, S. I.; Itoh, Y.; Seiki, M.; Itohara, S.; Takahashi, C.; Noda, M. M. The Membrane-Anchored MMP Inhibitor RECK Is a Key Regulator of Extracellular Matrix Integrity and Angiogenesis. *Cell* **2001**, *107* (6), 789–800. https://doi.org/10.1016/S0092-8674(01)00597-9.

(262) Failes, T. W.; Cullinane, C.; Diakos, C. I.; Yamamoto, N.; Lyons, J. G.; Hambley, T. W. Studies of a Cobalt(III) Complex of the MMP Inhibitor Marimastat: A Potential Hypoxia-Activated Prodrug. *Chem. - A Eur. J.* **2007**, *13* (10), 2974–2982. https://doi.org/10.1002/chem.200601137.

(263) Shalinsky, D. R.; Brekken, J.; Zou, H.; McDermott, C. D.; Forsyth, P.; Edwards, D.; Margosiak, S.; Bender, S.; Truitt, G.; Wood, A.; Varki, N. M.; Appelt, K. Broad Antitumor and Antiangiogenic Activities of AG3340, a Potent and Selective MMP Inhibitor Undergoing Advanced Oncology Clinical Trials. In *Annals of the New York Academy of Sciences*; New York Academy of Sciences, 1999; Vol. 878, pp 236–270. https://doi.org/10.1111/j.1749-6632.1999.tb07689.x.

(264) Guo, M. S.; Wu, Y. Y.; Liang, Z. B. Hyaluronic Acid Increases MMP-2 and MMP-9 Expressions in Cultured Trabecular Meshwork Cells from Patients with Primary Open-Angle Glaucoma. *Mol. Vis.* **2012**, *18*, 1175–1181.

(265) Hong, S. I.; Park, M. J.; Kim, M. S.; Rhee, C. H.; Lee, S. H. PTEN Suppresses Hyaluronic Acid-Induced Matrix Metalloproteinase-9 Expression in U87MG Glioblastoma Cells through Focal Adhesion Kinase Dephosphorylation. *Cancer Res.* **2002**, *62* (21), 6318–6322. https://doi.org/10.1016/S0959-8049(02)80906-6.